

Proposed American National Standard

Guide to Reference and Standard Ionosphere Models

DRAFT December 2013

Sponsored by

American Institute of Aeronautics and Astronautics

Approved **TBD**

American National Standards Institute

Abstract

This guide assists in the selection of ionospheric models for engineering design or scientific research. It describes the content of the models, uncertainties and limitations, technical basis, databases from which the models are formed, publication references, and sources of computer codes for 46 ionospheric models. The models cover the altitude range from the Earth's surface to approximately 10,000 kilometers. This guide is intended to assist communication and space system designers and developers, geophysicists, space physicists, and climatologists in understanding available models, comparing sources of data, and interpreting engineering and scientific results based on different ionospheric models.

**American
National
Standard**

Approval of an American National Standard requires verification by ANSI that the requirements for due process, consensus, and other criteria have been met by the standards developer.

Consensus is established when, in the judgment of the ANSI Board of Standards Review, substantial agreement has been reached by directly and materially affected interests. Substantial agreement means much more than a simple majority, but not necessarily unanimity. Consensus requires that all views and objections be considered, and that a concerted effort be made toward their resolution.

The use of American National Standards is completely voluntary; their existence does not in any respect preclude anyone, whether he has approved the standards or not, from manufacturing, marketing, purchasing, or using products, processes, or procedures not conforming to the standards.

The American National Standards Institute does not develop standards and will in no circumstances give an interpretation of any American National Standard. Moreover, no person shall have the right or authority to issue an interpretation of an American National Standard in the name of the American National Standards Institute. Requests for interpretations should be addressed to the secretariat or sponsor whose name appears on the title page of this standard.

CAUTION NOTICE: This American National Standard may be revised or withdrawn at any time. The procedures of the American National Standards Institute require that action be taken to affirm, revise, or withdraw this standard no later than five years from the date of approval. Purchasers of American National Standards may receive current information on all standards by calling or writing the American National Standards Institute.

Published by
American Institute of Aeronautics and Astronautics
1801 Alexander Bell Drive, Reston, VA 20191

Copyright © 201X American Institute of Aeronautics and
Astronautics
All rights reserved

No part of this publication may be reproduced in any form, in an electronic retrieval system or otherwise, without prior written permission of the publisher.

Printed in the United States of America

ISBN xx-x-xxxxx-xxx-x

Contents

Foreword.....	v
1 Scope.....	1
3 NCAR Thermosphere-Ionosphere-Electrodynamics General Circulation Model (TIE-GCM)	7
4 Coupled Thermosphere-Ionosphere Model (CTIM)	10
5 Coupled Thermosphere-Ionosphere-Plasmasphere Model (CTIP)	12
6 AFRL Global Theoretical Ionospheric Model (GTIM).....	13
7 Parameterized Ionospheric Model (PIM)	15
8 International Reference Ionosphere (IRI), 1996.....	17
9 Empirical Model of the Ionosphere (EMI).....	20
10 The Sheffield University Plasmasphere-Ionosphere Model (SUPIM)	22
11 The Field Line Interhemispheric Plasma Model.....	25
12 Global Assimilation of Ionospheric Measurements–Full Physics (GAIM-FP)	28
13 Global Assimilation of Ionospheric Measurements–Gauss-Markov (GAIM-GM).....	30
14 JPL/USC GAIM: The Jet Propulsion Laboratory/University of Southern California Global Assimilative Ionospheric Model.....	33
15 Ionosphere Forecast Model (IFM).....	35
16 Ionosphere-Plasmasphere Model (IPM)	37
17 Ionosphere–Polar Wind Model (IPWM)	39
18 Ionosphere–Polar Wind–PIC (IPW-PIC) Model	41
19 Thermosphere-Ionosphere Forecast Model (TIFM).....	43
20 NRL SAMI2/SAMI3 Models.....	45
21 Texas Reconfigurable Ionosphere-Plasmasphere Logarithmic Data Assimilator (TRIPL-DA)	46
22 Ionospheric Data Assimilation Four-Dimensional (IDA4D)	48
23 Incoherent Scatter Radar Ionospheric Models (ISRIMs)	51
24 Probabilistic Topside Ionosphere Model	54
25 Algebraic Model	56
26 Numerical Model of D-Region Ion Chemistry, 1995.....	58
27 Solar EUV and Chemistry Model	62
28 AFRL Boltzmann-Fokker-Planck Model for the Daytime Lower Ionosphere.....	65
29 AFRL Transport Model for the Electron-Proton-Hydrogen Atom Aurora	67
30 Two-Cell Ionospheric Convections Model.....	70
31 Heppner-Maynard Electric Field Models	72
32 Millstone Hill Empirical Electric Field Model, 1986.....	75
33 APL High-Latitude Convection Model	77
34 Weimer Electric Potential, Current, and Joule Heating Models	80

35	The Assimilative Mapping of Ionospheric Electrodynamics (AMIE).....	83
36	HWM Empirical Wind Model	86
37	Global Empirical Models of T_e	88
38	Empirical Model of the Ionospheric Electron and Ion Temperatures	90
39	Photochemical Equilibrium Model for Ionospheric Conductivity	93
40	Empirical Model of Conductivities	94
41	Auroral Electron and Ion Fluxes.....	96
42	WBMOD Ionospheric Scintillation Model (NWRA), 1995.....	98
43	PBMOD Time-Dependent Model of the Global Low-Latitude Ionosphere and Radio Scintillation	101
44	FIRST: Forecasting Ionospheric Real-Time Scintillation Tool (NOAA, CIRES).....	104
45	Model of the Trough in the High-Latitude F-Layer	106
46	GPS Eight-Coefficient TEC Model	108
47	The CPI TEC Model.....	110

List of Tables

Table 1 – Summary of reference and standard ionospheres.....	1
Table 2 – Model uncertainties.....	17
Table 3 – Local climatology for the ISR sites.....	51

Foreword

This *Guide to Reference and Standard Ionosphere Models* is sponsored by the American Institute of Aeronautics and Astronautics (AIAA) as part of its Standards Program.

The proliferation of ionospheric models and the lack of documentation have hindered general knowledge of their availability as well as their relative strengths, weaknesses, and limitations. The intent of this guide is to compile, in one reference, practical information about known and available ionospheric models—those that describe the physical properties and practical effects of the ionosphere as a function of altitude, latitude, and other key parameters. At this writing, the included models are those intended for general-purpose, scientific, or aerospace applications and therefore extend to heights ranging from 50 to 10,000 km. Dynamical models of the ionosphere are included in this guide, as the dynamics are essential to many applications.

The guide summarizes the principal features of the models:

- Model content
- Model uncertainties and limitations
- Basis of the model
- Database or model input parameters
- Publication references
- Dates of development, authors, and sponsors
- Model codes and sources.

The models are grouped according to whether they describe primarily global, regional, or special properties.

There is limited information on standard deviations from the mean values or frequencies of occurrence of some of the variables described by these models. This limits quantitative assessments of uncertainties. Correlation distances for electron densities, and statistics on scintillation are well defined. These and other statistics are discussed in the body of the guide. Candidates for inclusion in this guide have been solicited by means of advertisements in publications including announcements at national and international meetings of URSI, IAGA, AGU, COSPAR, AIAA, and scientific community newsletters. This collection of models is not exhaustive. It is hoped that future editions will include additional models from the international community.

We are indebted to those authors who submitted their models for inclusion, to those who offered valuable advice, to Jared Fulgham for notable assistance, and to the editors/reviewers: W. Kent Tobiska (Editor), Herbert C. Carlson, Robert W. Schunk, and Ludger Scherliess.

The first revision was prepared and approved in 1998. The second revision was initiated in 2010 and approved in 201X by the AIAA Atmospheric and Space Environments Committee on Standards (ASE CoS). At the time of this revision, the AIAA Atmospheric and Space Environments CoS included the following members:

W. Kent Tobiska, Chair	Space Environment Technologies
Harold E. Addy	NASA Glenn Research Center
Bill Atwell	The Boeing Company
William H. Bauman	ENSCO
Andy Broeren	NASA Glenn Research Center

Donald Cook	The Boeing Company
Jack E. Ehernberger	Consultant
Dale C. Ferguson	Air Force Research Laboratory
Craig D. Fry	Exploration Physics International Inc.
Henry B. Garrett	Jet Propulsion Laboratory
Glynn Germany	Ball Aerospace
Nelson W. Green	Jet Propulsion Laboratory
Hassan A. Hassan	North Carolina State University
Dale L. Johnson	NASA Marshall Space Flight Center, Retired
Delores J. Knipp	Space Environment Technologies
Shu T. Lai	Air Force Research Laboratory
Christopher Mertens	NASA Langley Research Center
Joseph Minow	NASA Marshall Space Flight Center
John J. Murray	NASA Langley Research Center
Mike Newchurch	University of Alabama in Huntsville
Jerry Owens	NASA Marshall Space Flight Center
Fred Proctor	NASA Langley Research Center
Ludger Scherliess	Utah State University
Robert Schunk	Utah State University
Andrew Shapiro*	Jet Propulsion Laboratory
Fred Slane	Space Environment Technologies
William W. Vaughan	University of Alabama in Huntsville
John Wise	Air Force Research Laboratory
David J. Youker	General Electric Aviation

This 201X revision of *Guide to Reference and Standard Ionosphere Models* contains updated information on several models relative to information on references, sources, and so forth. In addition, a few of the models in the previous edition that are now obsolete have been replaced with updated versions. The model for which updated information is provided is the NCAR Thermosphere-Ionosphere-Electrodynamics General Circulation Model (TIE-GCM).

Some new models that have been added include the following:

1. The Assimilative Mapping of Ionospheric Electrodynamics (AMIE)
2. Global Assimilation of Ionospheric Measurements—Full Physics (GAIM-FP)
3. Global Assimilation of Ionospheric Measurements—Gauss-Markov (GAIM-GM)
4. JPL/USC GAIM: The Jet Propulsion Laboratory/University of Southern California Global Assimilative Ionospheric Model

5. Ionosphere Forecast Model (IFM)
6. Ionosphere-Plasmasphere Model (IPM)
7. Ionosphere-Polar Wind Model (IPWM)
8. Ionosphere-Polar Wind-PIC (IPW-PIC)
9. Thermosphere-Ionosphere Forecast Model (TIFM)
10. NRL SAMI2/SAMI3 Models
11. Texas Reconfigurable Ionosphere-Plasmasphere-Logarithmic Data Assimilator (TIPL-DA)
12. Weimer Electric Potential, Current, and Joule Heating Models
13. Incoherent Scatter Radar Ionospheric Models (ISRIMs)
14. Probabilistic Topside Ionosphere Model
15. PBMOD Time-Dependent Model of the Global Low-Latitude Ionosphere and Radio Scintillation

NOTE The cooperation of all those who provided input, both for the updates and new entries, is sincerely appreciated. Without their contributions, this significant revision of the *AIAA Guide to Reference and Standard Ionosphere Models* would not have been possible.

The AIAA Atmospheric and Space Environments Committee on Standards (W. Kent Tobiska, Chairperson) approved this document for publication in 201X.

The AIAA Standards Executive Council (NAME, Chairperson) accepted this document for publication in TBD.

The AIAA Standards Procedures provide that all approved Standards, Recommended Practices, and Guides are advisory only. Their use by anyone engaged in industry or trade is entirely voluntary. There is no agreement to adhere to any AIAA standards publication and no commitment to conform to or be guided by a standards report. In formulating, revising, and approving standards publications, the Committees on Standards will not consider patents, which may apply to the subject matter. Prospective users of the publications are responsible for protecting themselves against liability for infringement of patents or copyrights, or both.

1 Scope

This guide describes the content of the models, uncertainties and limitations, technical basis, databases from which the models are formed, publication references, and sources of computer codes for 46 ionospheric models (see Table 1). The models cover the altitude range from the Earth's surface to approximately 10,000 km. It is intended to assist communication and space system designers and developers, geophysicists, space physicists, and climatologists in understanding available models and comparing sources of data, and interpreting engineering and scientific results based on different ionospheric models.

Table 1 — Summary of reference and standard ionospheres

Model (Page No.)	Geographic Region	Altitude Range (km)	Parameters	Species Included	Temporal Variation	Output Data Presentation	Principal Application
USU (5)	global	90–1000	$N_e, N_i, T_e, T_{ij}, T_{i_s}, u_e, u_i$	$NO^+, O_2^+, N_2^+, N^+, O^+, H^+$	10–100 sec	3D grid	scientific studies
NCAR/TIE-GCM (7)	global	97–500	$T_n, T_i, T_e, \text{neutrals } U, V, W$	$CO_2, O, O_2, N(^1S), N(^2D), O^+, O_2^+, NO^+, N_e(\text{cm}^{-3})$	120 sec	tables, plots	scientific studies
CTIM (10)	global	80–10,000	$N_e, N_i, \text{neutrals } U, V, W, T_n, T_e, T_i$	$O^+, H^+, NO^+, O_2N_2^+, N^+, O, O_2^+, N_2, NO, N(^2D), N(^1S)$	1–6 min	tables, plots	scientific studies
CTIP (12)	global	80–10,000	$N_e, N_i, \text{neutrals } U, V, W, T_n, T_e, T_i, T_e$	$O^+, H^+, NO^+, O_2^+, N_2^+, N^+, O, O_2, N_2, NO, N(2D), N(4S)$	1–15 min	tables, plots	scientific studies
GTIM (13)	global	90–22,000	N_e, N_i	$NO^+, O_2^+, O^+, H^+, He^+$	diurnal with resolution of 15 min	tables, plots	theoretical climatology and development of parametric models such as PIM
PIM (15)	global	90–22,000	$N_e, TEC, f_oF_2, h_mF_2, f_oE, h_mE$	O^+, NO^+, O_2	diurnal with resolution of 30 min	tables	theoretical climatology, systems design
IRI (17)	global	$N_e: 50\text{--}2000$ $T: 120\text{--}3000$ $N_i: 100\text{--}2000$	N_e, T_e, T_i, N_i	$O^-, H^+, He^-, NO, O_2^-, N_2^-$ cluster	diurnal (LT, UT, solar zenith angle), seasonal solar cycle	tables, interactive on WWW	spacecraft instrument design, satellite tracking, radio wave propagation, altimeter data analysis ray-tracing, education, etc.
EMI (20)	global coverage (lat)	50–4000	H^+, He^+, N_2^+, NO^+	N^+, O^+, O_2^+, N_e	diurnal seasonal solar activity	figures, tables	scientific studies
SUPIM (22)	global	90–22,000	N_e, N_i, T_e, T_i	$O^+, O_2^+, NO^+, H^+, He^+$	diurnal with resolution of 15 min	tables	theoretical studies and climatology
FLIP (25)	mid-lat	90–22,000	N_e, N_i, T_e, T_i	$H^+, He^+, O^+, N^+, NO^+, O_2^+, (^2D), O^+(^2P), N(^2D), N(S^4), NO, O(^1D), N_2(\text{vib})$	diurnal 1–30 min resolution	tables, plots	mid-latitude ionosphere-plasmasphere single ground comparison

Table 1 — Summary of reference and standard ionospheres (*cont.*)

Model (Page No.)	Geographic Region	Altitude Range (km)	Parameters	Species Included	Temporal Variation	Output Data Pre- sentation	Principal Application
GAIM-FP (28)	global	90–30,000	N_mE , h_mE , N_mF_2 , h_mF_2 , N_i , E_i , U_n , O/N_2 , TEC	NO^+ , O_2^+ , N_2^+ , O^+ , H^+ , He^+	1-15 min	3D grid	scientific studies
GAIM-GM (30)	global	90–1400	N_mE , h_mE , N_mF_2 , h_mF_2 , N_e , TEC	NO^+ , O_2^+ , N_2^+ , O^+ , H^+	15 min	3D grid	scientific studies
JPL/USC GAIM (33)	global	40–80	H_mF_2 , N_mF_2	O^+ , H^+ , He^+	5–12 min	3D grid	scientific studies
IFM (35)	global	90–1500	N_mE , h_mE , N_mF_2 , h_mF_2 , N_i	NO^+ , O_2^+ , N_2^+ , O^+ , H^+	1 min	3D grid	scientific studies
IPM (37)	global	90–30,000	N_mE , h_mE , N_mF_2 , h_mF_2 , N_i , TEC	NO^+ , O_2^+ , N_2^+ , O^+ , He^+ , H^+	1 min	3D grid	scientific studies
IPWM (39)	global	90–9000	T_e , T_i , N_i	NO^+ , O_2^+ , N_2^+ , O^+ , H^+	1 min	3D grid	scientific studies
IPW-PIC (41)	global	90–1200	N_i , T_e , T_i	NO^+ , O_2^+ , N_2^+ , O^+ , H^+	1 min	3D grid	scientific studies
TIFM (43)	global	90–500	N_n , U_n , T_n	N_2 , O_2 , O	1 min	3D grid	scientific studies
SAMI2/ SAMI3 (45)	global/ mid-lat	85-20,000	N_e , N_i , TEC, U_i , T_e , T_i	H^+ , He^+ , N^+ , O^+ , N_2^+ , NO^+ , O_2^+	30 sec–15 min	3D plotting	scientific studies
TRIPL-DA (46)	global	user specified, 100–22,000	N_e at every grid point	ions only	user specified, > input data stream	3D mapping	scientific studies
IDA4D (48)	global	100–20,000 user selectable; often only E- and F- regions used	N_e		~5 min	graphical or data files of 3D distribution	scientific studies, radio propagation applications, concept of operations tool for mission planning applications
ISRIMs (51)	≈35–55° sub-auroral	100–500	N_e , T_e , T_i		1–3 hr	tables, plots	scientific studies
PTIM (54)	global, single altitude of 800 km +/- 1 scale height	830–860	mode, median, and mean densities, probability of reaching a given density	electrons only	climate model only	probability of observing a given electron density level	Estimating both typical and extreme electron density values at a common LEO orbit
Algebraic (56)	global	60–90		21 positive ions 8 negative ions	diurnal	tables, plots	scientific studies
Numerical Chem. (58)	global	60–90		36 positive ions 19 negative ions	diurnal	tables, plots	scientific studies

Table 1 — Summary of reference and standard ionospheres (*cont.*)

Model (Page No.)	Geographic Region	Altitude Range (km)	Parameters	Species Included	Temporal Variation	Output Data Pre- sentation	Principal Application
Solar EUV and Chemistry (62)	global	90–120	N_i^+ , N_i^- , N_e neutrals	5 negative ions 4 positive ions	steady state	global	90–120
AFRL B-F-P (65)	mid-lat	100–250	N_e , N_i , T_e	O^+ , N_2^+ , O_2^+ , O , N_2 , O_2	steady state	tables, plots	mid-latitude daytime E- and F1-regions of ionosphere
Electron- Proton Aurora (67)	high lat >60°	90–600	N_e , N_i , N_2^+ (3914Å) N_2 (3371Å) LBH (1325, 1354, 1383, 1493Å) OI (1356 Å) $L\alpha$ (1216Å) $H\beta$ (4861Å) $H\alpha$ (6563Å)	H^+ , H, O, N_2 , O_2	steady state	tables, plots	auroral ionosphere: ionization of emission yields
Two-cell convection (70)	high lat	150–2000	electrostatic potential	N/A	directly IMF input driven	tables	ionosphere convection flow applications
Heppner- Maynard (72)	high lat >45° geo- magnetic	100–150	electric potential	N/A	statistical k_p - dependent	point values, plots	modeling
Millstone Hill (75)	high lat	150–2000	electrostatic potential	N/A	either of 3 indices: precipitation, K_p or IMF B_y/B_z	tables	ionosphere convection flow
APL (77)	global	100–500	V_i (electric potential)	N/A	2 min	velocity maps	scientific modeling studies
Weimer (80)	high-lat	300-1000	V (electric potential), Ψ (mag- netic scalar potential)	N/A	diurnal and polar tilt angle, at epic	tables, plots, mapping	scientific studies
AMIE (83)	global high lat	mapped to 110	V_i , E , I , J , Σ_p , Σ_H , JH	N/A	indices or IMF	plots, mapping	ionosphere convection, input to ionospheric models, scientific studies
HWM (86)	global	7–500	neutral atm wind	horizontal neutral wind	diurnal seasonal solar and magnetic activity	tables	wind climatology
Empirical T_e (88)	global	140–4000	T_e (N_e dependent)	T_e , N_e	latitude local time	tables	climatological model testing
Empirical T_e , T_i (90)	global coverage (lat)	50–4000	T_e , T_i	T_e , T_i	diurnal seasonal solar activity	figures, tables	scientific studies
PEMIC (92)	high lat	85–220	N_e , N_i , σ_p , σ_H , Σ_p , Σ_H	NO^+ , O_2^+ , N_2^+ , O^+	sec	tables, plots	scientific studies

Table 1 — Summary of reference and standard ionospheres (*cont.*)

Model (Page #)	Geographic Region	Altitude Range (km)	Parameters	Species Included	Temporal Variation	Output Data Presentation	Principal Application
EMC (93)	high-lat >50° geomagnetic	110	Σ_p, Σ_H	e^- ions	hr	tables, figures	input to ionospheric models, scientific studies
AEIF (95)	high-lat >50° geomagnetic	110	Σ_p, Σ_H	e^- ions	hr	tables, figures	input to ionospheric models, scientific studies
WBMOD (97)	global	150–1000	plasma irregularity strength & spectrum	N_e	diurnal seasonal solar cycle	tables, plots	eng specs, climatology of scintillation at VHF and above
PBMOD (100)	low-lat	90–2000	S4 scintillation	$O^+, H^+, NO^+, O_2^+, N_2^+$	at epic	tables, plots	scientific studies
FIRST (103)	global		S4 scintillation				forecasting
HF/VHF (105)	high-lat	F-layer maximum	foF ₂ MLAT/MLT boundaries	N_e	15 min to several hr	graphs, formulae	input to global ionospheric models
GPS TEC (107)	global	N/A	TEC, ionospheric delay at GPS frequencies	N/A	diurnal	tables	single frequency GPS users
CPI TEC (109)	global	N/A	TEC, ionosphere delay at GPS frequencies	$O^+, H^+, He^+, NO^+, O_2^+$	diurnal	tables	single frequency GPS users, TEC climatology, TEC variability studies

2 USU Time-Dependent Model of the Global Ionosphere

2.1 Model Content

The USU ionospheric model describes the three-dimensional, time-dependent evolution of the global ionosphere at altitudes between 90 and 1000 km. The numerical model yields density distributions for electrons and six ion species (NO^+ , O_2^+ , N_2^+ , O^+ , N^+ , H^+) as a function of latitude, longitude, and altitude on a prespecified spatial grid. The model also calculates the isotropic electron temperature and the ion temperatures both parallel and perpendicular to the geomagnetic field on the same spatial grid. The model outputs the global density and temperature distributions at specified times.

Numerous physical and chemical processes are contained in the model, including field-aligned diffusion, cross-field electrodynamic drifts, thermospheric winds, polar wind escape, energy-dependent chemical reactions, neutral composition changes, ion production due to EUV radiation and auroral electron precipitation, thermal conduction, diffusion-thermal heat flow, and a host of local heating and cooling mechanisms. The model also takes account of the offset between the geomagnetic and geographic poles.

Depending on the inputs, the global ionospheric model can describe different solar cycle, seasonal, and daily variations. It can describe different levels of sustained geomagnetic activity, as well as storm and substorm dynamics.

2.2 Model Uncertainties and Limitations

2.2.1 To a large extent, the reliability of the calculated ionospheric parameters depends on the accuracy to which the global inputs can be specified. The ionospheric model is most sensitive to the magnetospheric electric field and particle precipitation inputs at high latitudes, the thermospheric winds at mid-latitudes, and the equatorial (dynamo) electric fields at low latitudes.

2.2.2 The topside plasma scale heights can be significantly affected by the downward electron heat flux through the upper boundary, but this input is virtually unknown on a global scale.

2.2.3 Steep spatial gradients can lead to plasma instabilities and scintillations, but the ionospheric model does not take instabilities into account.

2.2.4 A supercomputer is needed for global simulations.

2.3 Basis of the Model

2.3.1 The USU model of the global ionosphere is based on a Euler-Lagrange hybrid numerical scheme. For the mid-high latitude region, the ion continuity, momentum, and energy equations are solved as a function of altitude using a fixed spatial grid, whereas for the equatorial region the ion equations are solved along the magnetic field (B) from one hemisphere to the conjugate hemisphere on a fixed spatial grid. In all latitudinal domains, the plasma flux tubes are allowed to convect through a moving neutral atmosphere in a direction perpendicular to B due to magnetospheric, co-rotational, and dynamo electric fields. The three-dimensional nature of the model is obtained by following many flux tubes of plasma while keeping track of their positions at all times. This approach has the advantage over a purely Eulerian scheme, which requires fixed grid points in latitude and longitude, because more flux tubes can be placed in the high-latitude regions where sharp horizontal gradients are expected, such as near the auroral oval and main trough.

2.3.2 The continuity, momentum, and energy equations correspond to a set of nonlinear, second-order, partial differential equations. The equations are first linearized in time, and then finite differences are used for the spatial and temporal derivatives. The resulting coupled algebraic equations are solved with standard matrix inversion techniques.

2.3.3 At the lower boundary (90 km), the different ion species are assumed to be in chemical equilibrium, and hence the boundary ion densities are obtained simply by equating local sources and sinks. Likewise, the ion and electron temperatures at the lower boundary are obtained by equating local heating and cooling rates.

2.3.4 At the upper boundary (1000 km), a protonospheric exchange flux is specified for O^+ , and the fluxes of the other ion species are assumed to be negligibly small. The upper boundary conditions on the ion and electron temperatures are specifications of the downward heat fluxes through this boundary.

2.3.5 A 4 km spatial step is used in the vertical direction, and the time step typically varies from 10 to 100 sec as a given flux tube follows a specified trajectory. The high-latitude region, above $50^\circ N$, is usually modeled with 500 flux tubes of plasma, if empirical plasma convection and particle precipitation patterns are used (climatology modeling). For storm and high-resolution studies, 1000–3000 flux tubes are used.

2.4 Model Input Parameters

The ionospheric model requires several inputs. The main global inputs are the neutral densities, temperatures, and winds; the magnetospheric and equatorial electric field distributions; the auroral electron precipitation pattern; the downward electron heat flux through the upper boundary; and the protonospheric exchange flux. Typically, empirical or statistical models are used for the required atmospheric and magnetospheric inputs, but in this case the calculated ionospheric parameters pertain to the climatology of the region. For storm and substorm simulations, the temporal variation of the magnetospheric and atmospheric inputs must be specified.

2.5 Publication References

2.5.1 Schunk, R.W. (1988), A mathematical model of the middle and high latitude ionosphere, *Pure Appl. Geophys.* 127, 255–303.

2.5.2 Sojka, J.J. (1989), Global scale, physical models of the F region ionosphere, *Rev. Geophys.* 27, 371–403.

2.6 Dates of Development

1973 Original one-dimensional, mid-latitude, multi-ion (NO^+ , O_2^+ , N_2^+ , O^+) model.

1975 High-latitude effects due to plasma convection and particle precipitation added for single plasma flux tubes.

1980 Updated chemical scheme and new ions (N^+ and H^+) are added.

1981 Plasma convection and particle precipitation patterns added so that multiple flux tubes can be followed.

1982 A more complete ion energy equation is added.

1983 Time-dependent plasma convection and particle precipitation patterns are included so that geomagnetic storms and substorms can be modeled.

1985 An equatorial ionospheric model is added so that the entire globe can be modeled.

1986 The complete electron energy equation is added.

1992 A grid system that allows for a high spatial resolution in a specified region is developed.

2.7 Model Codes and Sources

The model is in the form of a large Fortran code, but it is not user-friendly and is not available. However, the authors frequently run the model in collaborative studies with both experimentalists and other modelers.

3 NCAR Thermosphere-Ionosphere-Electrodynamics General Circulation Model (TIE-GCM)

3.1 Model Developers

R. G. Roble et al.
High Altitude Observatory
National Center for Atmospheric Research

3.2 Model Description

The National Center for Atmospheric Research (NCAR) Thermosphere-Ionosphere-Electrodynamics General Circulation Model (TIE-GCM) is a comprehensive, first-principles, three-dimensional, non-linear representation of the coupled thermosphere and ionosphere system that includes a self-consistent solution of the low-latitude electric field. The model solves the three-dimensional momentum, energy, and continuity equations for neutral and ion species at each time step, using a semi-implicit, fourth-order, centered, finite difference scheme on each pressure surface in a staggered vertical grid. It has 29 constant pressure levels in the vertical, extending from approximately 97 km to 500 km in intervals of one-half scale height, and a $5^\circ \times 5^\circ$ latitude-longitude grid, in its base configuration. The time step is 120 s.

3.3 Model Assumptions, Uncertainties, and Limitations

Hydrostatic equilibrium, constant gravity, steady-state ion and electron energy equations, and incompressibility on a constant pressure surface are assumed. Ion velocities are derived from the potential field created by combining the imposed magnetospheric potential with the low-latitude dynamo potential, then calculating ion velocities from $\mathbf{E} \times \mathbf{B}$ drifts, rather than solving the ion momentum equations explicitly. Some minor species are not currently included in the model, including H and He, their ions, and Ar. Several parameterizations are used in the TIE-GCM: an empirical model is used to specify photoelectron heating; the production of secondary electrons is included using an empirical model derived from two-stream calculations; the effects of mixing by gravity waves are included using an eddy diffusion formulation; and CO_2 is included by specifying a lower boundary condition, assuming that it is in diffusive equilibrium. The upper boundary conditions for electron heat transfer and electron number flux are empirical formulations. At the lower boundary, atmospheric tides are specified using the Global Scale Wave Model (GSWM).

3.4 Model Inputs

- Solar EUV inputs:
F_{10.7} (current daily F_{10.7} solar index) and F_{10.7A} (81-day center-averaged F_{10.7} solar index)
- Particle precipitation:
Hemispheric Power in GW, obtained from 3-hour K_p index
- Ionospheric electric fields at high latitudes:
Provided by Heelis model (or Weimer model, in the future)
- Inputs for Heelis model:
Cross-polar cap potential in kV, obtained from 3-hour K_p index
Hemispheric Power in GW, obtained from 3-hour K_p index
Optional (not implemented): y-component of the interplanetary magnetic field (B_y) in nT
- Inputs for Weimer model:
Interplanetary magnetic field, B_y and B_z, in nT
Solar wind density and speed, n and v , in cm^{-3} and km s^{-1}

- Inputs for lower boundary:

Diurnal and semi-diurnal migrating tides, specified by the GSWM

3.5 Model Outputs

Primary time-dependent output fields, specified in latitude, longitude, and pressure level:

Geopotential height: Height of pressure surfaces (cm)

Temperatures: Neutral, ion, electron (K)

Neutral winds: zonal, meridional (cm^{-3}), vertical (s^{-1})

Composition: O, O₂, NO, N(⁴S), N(²D) (mass mixing ratios—dimensionless)

Ion and electron densities: O⁺, O₂⁺, Ne (cm^{-3}) (*NO⁺ is calculated from $N_e - (O^+ + O_2^+)$*)

Electric potential: (V)

NOTE Other fields are available as secondary histories, which can be set as needed.

3.6 Additional Information

The TIE-GCM is a community model that can be run on a variety of computational platforms. The model source code is provided under the auspices of an open-source academic research license. Standard runs are available from the HAO/NCAR web site, and runs-on-request can also be generated at the NASA Community Coordinated Modeling Center (CCMC). For additional information, see these web pages:

TIE-GCM web page: <http://www.hao.ucar.edu/modeling/tgcm>

User Guide: <http://www.hao.ucar.edu/modeling/tgcm/doc/userguide>

Documentation: http://www.hao.ucar.edu/modeling/tgcm/doc/tiegcm_modeldes.pdf

Release Notes: http://www.hao.ucar.edu/modeling/tgcm/download/files/tiegcm1.9x_release.html

Post-Processing: http://www.hao.ucar.edu/modeling/tgcm/download/files/tgcmproc29_idl.tar.gz

NOTE Registration at the main web page is required in order to access the /tgcm/download area.

3.7 References

3.7.1 Dickinson, R.E., E.C. Ridley, and R.G. Roble (1981), A three-dimensional general circulation model of the thermosphere, *J. Geophys. Res.* 86, 1499–1512.

3.7.2 Dickinson, R.E., E.C. Ridley, and R.G. Roble (1984), Thermospheric general circulation with coupled dynamics and composition, *J. Atmos. Sci.* 41, 205–219.

3.7.3 Hagan, M.E., M.D. Burrage, J.M. Forbes, J. Hackney, W.J. Randel, and X. Zhang (1999), GSWM-98: Results for migrating solar tides, *J. Geophys. Res.* 104, 6813–6827.

3.7.4 Qian, L., S.C. Solomon, and T.J. Kane (2009), Seasonal variation of thermospheric density and composition, *J. Geophys. Res.* 114, A01312, doi:10.1029/2008JA013643.

3.7.5 Richmond, A.D. (1995), Ionospheric electrodynamics using magnetic apex coordinates, *J. Geomag. Geoelectr.* 47, 191–212.

3.7.6 Richmond, A.D., E.C. Ridley, and R.G. Roble (1992), A thermosphere/ionosphere general circulation model with coupled electrodynamics, *Geophys. Res. Lett.* 6, 601–604.

3.7.7 Roble, R.G. (1995), Energetics of the mesosphere and thermosphere, *AGU, Geophysical Monographs*, eds. R.M. Johnson and T.L. Killeen, 87, 1–22.

3.7.8 Roble, R.G., and E.C. Ridley (1987), An auroral model for the NCAR thermospheric general circulation model (TGCM), *Annales Geophys.* 5A, 369–382.

- 3.7.9** Roble, R.G., R.E. Dickinson, and E.C. Ridley (1982), Global circulation and temperature structure of the thermosphere with high-latitude plasma convection, *J. Geophys. Res.* 87, 1599–1614.
- 3.7.10** Roble, R.G., R.E. Dickinson, and E.C. Ridley (1977), Seasonal and solar-cycle variations of zonal mean circulation in the thermosphere, *J. Geophys. Res.* 82, 5493–5504.
- 3.7.11** Roble, R.G., E.C. Ridley, A.D. Richmond, and R.E. Dickinson (1988), A coupled thermosphere/ionosphere general circulation model, *Geophys. Res. Lett.* 15, 1325–1328.
- 3.7.12** Roble, R.G., E.C. Ridley, and R.E. Dickinson (1987), On the global mean structure of the thermosphere, *J. Geophys. Res.* 92, 8745–8758.
- 3.7.13** Solomon, S.C., and L. Qian (2005), Solar extreme ultraviolet irradiance for general circulation models, *J. Geophys. Res.* 110, A10306, doi: 10.1029/2005JA011160.
- 3.7.14** Wang, W., T.L. Killeen, A.G. Burns, and R.G. Roble (1999), A high-resolution, three-dimensional, time-dependent, nested grid model of the coupled thermosphere-ionosphere, *J. Atmos. Sol.-Terr. Phys.* 61, 385–397.
- 3.7.15** Wang, W., M. Wiltberger, A.G. Burns, S. Solomon, T.L. Killeen, N. Maruyama, and J. Lyon (2004), Initial results from the CISM coupled magnetosphere-ionosphere-thermosphere (CMIT) model: thermosphere ionosphere responses, *J. Atmos. Sol.-Terr. Phys.* 66, 1425–1442, doi:10.1016/j.jastp.2004.04.008.
- 3.7.16** Wiltberger, M., W. Wang, A. Burns, S. Solomon, J.G. Lyon, and C.C. Goodrich (2004), Initial results from the coupled magnetosphere ionosphere thermosphere model: magnetospheric and ionospheric responses, *J. Atmos. Sol.-Terr. Phys.* 66, 1411–1444, doi:10.1016/j.jastp.2004.03.026.

3.8 Developer Contacts

Stan Solomon
303-497-2179
stans@ucar.edu

Ben Foster
303-497-1595
foster@ucar.edu

4 Coupled Thermosphere-Ionosphere Model (CTIM)

The Coupled Thermosphere-Ionosphere Model (CTIM) has evolved from an integration of a neutral thermospheric code and a high- and mid-latitude ionosphere model. The neutral thermospheric model was originally developed by Fuller-Rowell and Rees (1980) at University College London (UCL); the ionospheric model originated from Sheffield University (Quegan et al., 1982). A complete description is provided in Fuller-Rowell et al. (1996). A recent upgrade of this model, including a self-consistent plasmasphere and low-latitude ionosphere, is described in the section on CTIP.

4.1 Thermosphere Model

The thermospheric code simulates the time-dependent structure of the wind vector, temperature, and density of the neutral thermosphere by numerically solving the non-linear primitive equations of momentum, energy, and continuity. The global atmosphere is divided into a series of elements in geographic latitude, longitude, and pressure. Each grid point rotates with Earth to define a non-inertial frame of reference in a spherical polar coordinate system. Latitude resolution is 2° and longitude is 18° . Each longitude slice sweeps through local time with a 1 min time step. In the vertical direction, the atmosphere is divided into 15 levels in logarithm of pressure, from a lower boundary of 1 Pa at 80 km altitude, to an altitude above 500 km.

The momentum equation is nonlinear and the solution describes the horizontal and vertical advection, curvature and Coriolis effects, pressure gradients, horizontal and vertical viscosity, and ion drag. The nonlinear energy equation is solved self-consistently with the momentum equation; it describes three-dimensional advection and the exchange between internal, kinetic, and potential energy. The solutions also describe horizontal and vertical heat conduction by both molecular and turbulent diffusion, heating by solar UV and EUV radiation, cooling by infrared radiation, and Joule heating.

Time-dependent major species composition equations are solved including the evolution of O, O₂, and N₂, under chemistry, transport, and mutual diffusion (Fuller-Rowell et al., 1994). The time-dependent variables of southward and eastward wind, total energy density, and concentrations of O, O₂, and N₂ are evaluated at each grid point by an explicit, time-stepping numerical technique. After each iteration the vertical wind, the temperature, the density, and the heights of pressure surfaces are derived. The parameters can be interpolated to fixed heights for comparison with experimental data.

4.2 Ionosphere Model

The equations for the neutral thermosphere are solved self-consistently with a high- and mid-latitude ionospheric convection model (Quegan et al., 1982). The ionosphere is computed self-consistently with the thermosphere poleward of 23° latitude in both hemispheres. In this coupled model, the ionospheric Lagrangian frame has been modified to be more compatible with the Eulerian frame by the use of semi-Lagrangian technique (Fuller-Rowell et al., 1987, 1988).

Transport under the influence of the magnetospheric electric field is explicitly treated, assuming $\mathbf{E} \times \mathbf{B}$ drifts and collisions with the neutral particles. The densities of atomic ions H⁺ and O⁺ and the ion temperature are evaluated over the height range from 100 to 10,000 km, including horizontal transport, vertical diffusion, and the ion-ion and ion-neutral chemical processes. Below 400 km, the additional contribution from the molecular ion species N₂⁺, O₂⁺, and NO⁺, and atomic ion N⁺ are included. The ion temperature is calculated under the assumption of thermal balance between heat gained from the electron gas, ion-neutral frictional heating, and heat lost to the neutral gas.

4.3 Common Inputs

The magnetospheric input to the model is based on the statistical models of auroral precipitation and electric fields described by Fuller-Rowell and Evans (1987) and Foster et al. (1986), respectively. Both inputs are keyed to a hemispheric power index (PI), based on the TIROS/NOAA auroral particle measurements, and are mutually consistent in this respect. The PI index runs from 1 to 10 to cover various levels of geomagnetic activity; the relationship between PI and K_p can be found in Foster et al. (1986). Alternative electric field and auroral precipitation models can easily be incorporated into the model.

The (2,2), (2,3), (2,4), (2,5), and (1,1) propagating tidal modes are imposed at 97 km altitude (Fuller-Rowell et al., 1991); amplitude and phase can be prescribed. Ionization rates from the EUV flux are evaluated from reference spectra for high and low solar activity on the basis of the Atmospheric Explorer (AE) measurements.

4.4 Publication References

- 4.4.1 Foster, J.C., J.M. Holt, R.G. Musgrove, and D.S. Evans (1986), Ionospheric convection associated with discrete levels of particle precipitation, *Geophys. Res. Lett.* 13, 656–659.
- 4.4.2 Fuller-Rowell, T.J., and D.S. Evans (1987), Height-integrated Pedersen and Hall conductivity patterns inferred from the TIROS-NOAA satellite data, *J. Geophys. Res.* 92, 7606–7618.
- 4.4.3 Fuller-Rowell, T.J., and D. Rees (1980), A Three-Dimensional Time-Dependent Global Model of the Thermosphere, *J. Atmos. Sci.* 37, 2545–2567.
- 4.4.4 Fuller-Rowell, T.J., S. Quegan, D. Rees, R.J. Moffett, and G.J. Bailey (1987), Interactions between neutral thermospheric composition and the polar ionosphere using a coupled ionosphere-thermosphere model, *J. Geophys. Res.* 92, 7744–7748.
- 4.4.5 Fuller-Rowell, T.J., S. Quegan, D. Rees, R.J. Moffett, and G.J. Bailey (1988), Simulations of the seasonal and universal time variations of the high-latitude thermosphere and ionosphere using a coupled, three-dimensional, model, *Pure Appl. Geophys.* 127, 189–217.
- 4.4.6 Fuller-Rowell, T.J., D. Rees, H.F. Parish, T.S. Virdi, P.J.S. Williams, and R.G. Johnson (1991), Lower Thermosphere Coupling Study: Comparison of observations with predictions of the University College London-Sheffield Thermosphere-Ionosphere Model, *J. Geophys. Res.* 96, 1181–1202.
- 4.4.7 Fuller-Rowell, T.J., M.V. Codrescu, R.J. Moffett, and S. Quegan (1994), Response of the thermosphere and ionosphere to geomagnetic storms, *J. Geophys. Res.* 99, 3893–3914.
- 4.4.8 Fuller-Rowell, T.J., D. Rees, S. Quegan, R.J. Moffett, M.V. Codrescu, and G.H. Millward (1996), A Coupled Thermosphere-Ionosphere Model (CTIM), *STEP Handbook of Ionospheric Models*, edited by R.W. Schunk, SCOSTEP and Utah State University, 217.
- 4.4.9 Quegan, S., G.J. Bailey, R.J. Moffett, R.A. Heelis, T.J. Fuller-Rowell, D. Rees, and R.W. Spiro (1982), A theoretical study of the distribution of ionization in the high-latitude ionosphere and the plasmasphere: first results on the mid-latitude trough and the light-ion trough, *J. Atmos. Terr. Phys.* 44, 619–640.

4.5 Contacts

The model is available for collaborations. Please contact Tim Fuller-Rowell, Space Environment Center, 325 Broadway, Boulder, CO 80303; tel. 303-497-5764; e-mail: Tim.Fuller-Rowell@noaa.gov; or Mihail Codrescu, Space Environment Center, 325 Broadway, Boulder, CO 80303; tel. 303-497-6763; e-mail: Mihail.Codrescu@noaa.gov.

5 Coupled Thermosphere-Ionosphere-Plasmasphere Model (CTIP)

5.1 Model content

The Coupled Thermosphere-Ionosphere-Plasmasphere model (CTIP) is an enhanced version of the CTIM model described elsewhere in this guide. The new enhanced version is identical to CTIM, but includes a fully coupled model of the Earth's mid- and low-latitude ionosphere and plasmasphere, where CTIM relies on an empirical description.

5.2 Basis of the Model

The new ionosphere-plasmasphere component of CTIP solves the coupled equations of continuity, momentum, and energy to calculate the densities, field-aligned velocities, and temperatures of the ions O^+ and H^+ and the electrons along a total of 800 independent flux-tubes arranged in magnetic longitude and L value (20 longitudes and 40 L values). The effects of $\mathbf{E} \times \mathbf{B}$ drift at lower latitudes are incorporated by the inclusion of an empirical low-latitude electric field model. Full three-dimensional routines are used to interpolate parameters between the thermosphere and ionosphere-plasmasphere grids.

Recent developments of the CTIP model have included changing the mid- and low-latitude ionosphere/plasmasphere component such that the basic equations are now solved in a Eulerian (rather than Lagrangian) framework. This is a subtle change that allows ionospheric $\mathbf{E} \times \mathbf{B}$ convection to take any form. (Previous incarnations required flux-tubes to return to their geographic starting positions during a 24 hr simulation.) In addition the resolution of the ionosphere, in the height-latitude plane, has been significantly increased, such that the equatorial ionosphere, between altitudes of 200 and 1300 km, is modeled with a vertical resolution of 20 km. The new resolution represents a threefold increase in the number of individual flux-tubes solved within the model, necessary in order to correctly simulate (in particular) the dusk sector ionospheric response to the "pre-reversal enhancement" low-latitude electric field.

The CTIP model is thus a fully dynamic coupled model of the global thermosphere and ionosphere and has recently been used to study the mid-latitude ionospheric F2-layer annual and semi-annual variations (Millward et al., 1996a). A full description of the mathematical basis of the model has been given by Millward et al. (1996b).

5.3 Publication References

5.3.1 Millward, G.H., H. Rishbeth, T.J. Fuller-Rowell, A.D. Aylward, S. Quegan, and R.J. Moffett (1996a), Ionospheric F2-layer annual and semi-annual variations, *J. Geophys. Res.* 101(3).

5.3.2 Millward, G.H., R.J. Moffett, S. Quegan, and T.J. Fuller-Rowell (1996b), A coupled thermosphere-ionosphere-plasmasphere model, CTIP, *STEP Handbook of Ionospheric Models*, edited by R.W. Schunk, SCOSTEP and Utah State University, 217.

5.4 Model Codes and Sources

The model consists of a large and tortuous Fortran code, requires a powerful workstation or supercomputer to run, and is not particularly user-friendly. However, it is suitable for collaborative studies. Contact either Tim Fuller-Rowell (at the address given in the CTIM report) or George Millward, Space Environment Center, 325 Broadway, Boulder, CO 80303, tel. 303-497-7754 (email: gmillward@sel.noaa.gov).

6 AFRL Global Theoretical Ionospheric Model (GTIM)

6.1 Model Content

The Air Force Research Laboratory (AFRL) Global Theoretical Ionospheric Model (GTIM) is a time-dependent, ionospheric model that calculates ion (NO^+ , O_2^+ , O^+ , He^+ , H^+) densities as a function of altitude, latitude, longitude, and local time, globally. The output from GTIM covers the height range from 90 to 1600 km on a pre-specified grid of latitudes and longitudes, depending on the scale of the phenomenon under investigation. Nominally, the output ion and electron densities are calculated every 2° dip latitude, every 5° longitude, and every 0.5 hr local time.

The model calculates O^+ , He^+ , and H^+ densities by solving the coupled ion momentum and continuity equations numerically using a Crank-Nicholson implicit finite differencing technique. The model includes the effects of production by solar EUV radiation and energetic particle precipitation, loss through charge exchange with the neutral atmosphere and transport by $\mathbf{E} \times \mathbf{B}$ drift, ambipolar diffusion, and collisions with neutral atmosphere. The offset between the geographic poles and geomagnetic poles is taken into account. The molecular ions NO^+ and O_2^+ are calculated under the chemical equilibrium assumption that production equals loss and no transport effects are included.

6.2 Model Uncertainties and Limitations

In calculating global ion and electron density distributions, the model uncertainties relate to how well the required inputs to GTIM can be specified. A number of studies have established that, if these can be realistically specified, then excellent agreement between calculated and observed electron density profiles is achieved. At low and high latitudes, the most important transport mechanism is $\mathbf{E} \times \mathbf{B}$ drift, whereas at mid latitudes, it is neutral winds that are critical in determining realistic ion and electron densities.

The major limitation of the model is that it is not coupled to the neutral atmosphere, the electrodynamics, or the energetics of the plasma, so that neither temperatures nor electric fields are self-consistently calculated.

6.3. Basis of the Model

GTIM solves the coupled ion (O^+ , He^+ , and H^+) momentum and continuity equations in a frame of reference that drifts with the $\mathbf{E} \times \mathbf{B}$ drift velocity (Eulerian frame of reference) of the ion and electrons. The r , θ , ϕ coordinate system is transformed to an α , β , γ coordinate system, where α and β are perpendicular to the geomagnetic field line direction, and γ is parallel to \mathbf{B} . A number of transformations are carried out that facilitate the solving of the linear, second-order, partial differential equation. At low and mid latitudes, the solution is carried out along the entire field line from one hemisphere (90 km N) to the other (90 km S), and the boundary conditions at both ends assume $[\text{O}^+] = 0$. At high latitudes (above about $\pm 60^\circ$ dip latitude), the upper boundary condition at 1600 km provides flux values (Nv_γ) parallel to \mathbf{B} .

6.4 Model Input Parameters

Inputs to GTIM include a neutral atmosphere model, a solar production rate model, $\mathbf{E} \times \mathbf{B}$ drift pattern, a model for precipitating energetic electrons and protons, a horizontal neutral wind model, and a model for electron and ion temperatures. All of these inputs come from well-established references and observations and will not be detailed here.

6.5 Publication References

6.5.1 Anderson, D.N. (1973), A theoretical study of the ionospheric F-region equatorial anomaly, I; theory, *Planetary Space Sci.* 21, 409–420.

6.5.2 Decker, D.T., C.E. Valladares, R. Sheehan, S. Basu, D.N. Anderson, and R.A. Heelis (1994), Modeling daytime F-layer patches over Sondrestrom, *Radio Sci.* 29, 249–268.

6.6 Dates of Development and Authors

6.6.1 Dates:

1973 Development of the low-latitude portion of GTIM.

1976 Development of the mid-latitude portion of GTIM.

1994 Development of the high-latitude portion of GTIM.

1995–97 Addition of light ions (He^+ and H^+) to low- and mid-latitude portion of GTIM.

6.6.2 Authors: D.N. Anderson, D.T. Decker, M.W. Fox, R.E. Daniell, and R.W. Simon.

6.7 Model Codes and Sources

The model consists of a large number of Fortran coded subroutines that provide the GTIM output, but in no way is it well documented, user-friendly, or available to outside users. However, many collaborative studies have been carried out using GTIM.

DRAFT--For Public Review Only--Dec 2013

7 Parameterized Ionospheric Model (PIM)

7.1 Model Content

The Parameterized Ionospheric Model (PIM) is a global model of the *theoretical* climatology of the ionosphere. That is, PIM is a parameterization of the output from an amalgamation of theoretical ionospheric models, including the USU Time Dependent Ionospheric Model (TDIM) for high latitudes and the Global Theoretical Ionospheric Model (GTIM) for low and mid latitudes, augmented by the empirical plasmasphere model of Gallagher (1988). An earlier version of PIM has been described by Daniell et al. (1995).

The output from all of these models has been parameterized in terms of solar activity ($F_{10.7}$), geomagnetic activity (K_p), and season (Equinox, June Solstice, December Solstice). The format of the output of PIM is user selectable, and includes electron density profiles and/or profile parameters (TEC, N_mF_2 , h_mF_2 , N_mE , h_mE , etc.) on user-specified grids in latitude/longitude/altitude (geographic or geomagnetic) or azimuth/elevation/range.

7.2 Model Uncertainties and Limitations

PIM is a climatological model based on diurnally reproducible runs of physics-based models. As such, it cannot accurately reproduce specific situations, especially the storm time ionosphere. It is intended to represent typical (rather than average) ionospheric conditions.

Because the model is based on seasonal runs, it does not represent the complete annual variation of the ionosphere and is most inaccurate between equinoxes and solstices.

7.3 Basis of the Model

PIM consists of two major components: (1) a large set of coefficient files, from which the electron density profile may be derived at any specified latitude, longitude, season, and solar geophysical condition, and (2) an algorithm for reconstructing the electron density profiles from these coefficients.

PIM is based on diurnally reproducible runs of its parent physics-based models for specified solar/geophysical conditions and seasons. That is, the physics-based models are run with constant or steady state forcing functions until the steady-state response of the ionosphere is obtained. This usually occurs after a few hours of solar illumination. The output of the physics-based models consists of altitude profiles of the densities of the three dominant ions of the E- and F-regions (O^+ , N_2^+ , and O_2^+) on a latitude/longitude grid at regular intervals of local time or UT, depending on the model.

The ion density profiles are then represented as linear combinations of Empirical Orthonormal Functions (EOFs), which are derived from the complete set of profiles for a given set of solar/geophysical conditions. Depending on latitude region, the coefficients of the EOFs are fit by orthogonal functions in latitude, longitude, and/or UT.

The resulting coefficients are stored in files and constitute one of the two major constituents of PIM. The other component, the Fortran code itself, reconstructs the ion density profiles at the times and places specified by the user and sums the ion densities to obtain the electron density. If the user has asked for profile parameters, the height and density of the E- and F-layer peaks are found, and the profile is integrated to produce TEC.

The structures of the coefficient files differ for the various ionospheric regions. Merging between regions is accomplished by averaging between profiles in overlapping regions. Interpolation for solar/geophysical conditions between the values of the model runs is also accomplished by operating on profiles (rather than coefficients). This is because the EOFs were derived separately from each block of runs; that is, the basis functions are different for different sets of solar/geophysical conditions and different ionospheric regions.

This will probably change in PIM version 2, which will be based on a universal set of EOFs so that all interpolation can be done in “coefficient space.” It will also be based on a single, unified ionospheric model, GTIM.

7.4 Model Input Parameters

The user inputs are the date and time (UT) of the run, the solar/geophysical conditions ($F_{10.7}$ and K_p), choice of coordinates (geomagnetic or geographic), choice of output grid (latitude/longitude/altitude or azimuth/elevation/range), and the specifics of the output grid.

7.5 Publication References

7.5.1 Daniell, R.E., L.D. Brown, D.N. Anderson, M.W. Fox, P.H. Doherty, D.T. Decker, J.J. Sojka, and R.W. Schunk (1995), Parameterized ionospheric model: a global ionospheric parameterization based on first principles models, *Radio Sci.* 30, 1499–1510.

7.5.2 Gallagher, D.L., P.D. Craven, and R.H. Comfort (1988), An empirical model of the earth’s plasmasphere, *Adv. Space Res.* 8, 15–24.

7.6 Dates of Development, Authors, and Sponsors

7.6.1 Dates:

1987–90 Development of the high-latitude portion of the model.

1990 Development of the low- and mid-latitude portion.

1993 Version 1 of PIM.

1997 Most recent version of the code (1.6).

7.6.2 Authors: R.E. Daniell, L.D. Brown, W.G. Whartenby, J.J. Sojka, P.H. Doherty, D.T. Decker, and D.N. Anderson.

7.6.3 Sponsor: Air Force Research Laboratory.

7.7 Model Codes and Sources

The model may be obtained by contacting Lincoln Brown at CPI, tel. 781-487-2250 (email: brown@cpiboston.com). The source code and associated coefficient files are available free of charge from either of two FTP sites on the Internet. They are also available on CD-ROM for a nominal charge. (Contact Mr. Brown for specific information.) The source code is Fortran, and each version is verified to run under MS-DOS, DEC-VMS, and Sun-UNIX operating systems. (With minor modifications, the code has been successfully run under other UNIX “flavors.”) There are approximately 40–50 registered PIM users around the world.

8 International Reference Ionosphere (IRI), 1996

8.1 Model Content

The International Reference Ionosphere is the standard ionospheric model recommended for international use by the scientific union's Committee on Space Research (COSPAR) and International Union of Radio Science (URSI). A joint working group of COSPAR and URSI is in charge of developing and improving the model. By charter, IRI, like other international standard models (e.g., CIRA, MSIS, IGRF), is an empirical model, thus avoiding the uncertainties of the evolving theoretical understanding. Annual IRI Workshops are the forum for progress/status reports of ongoing IRI projects, for comparisons with new data sources, for resolving issues of conflicting data sources, and for decisions about improvements and additions for the next release of the model. The presentations from these workshops are published in *Advances in Space Research*, Vols.(Nos.) 4(1), 5(7), 5(10), 7(6), 8(4), 10(8), 10(11), 11(10), 13(3), 14(12), 15(2), and 16(1).

IRI provides monthly averages of the electron density, the ion composition (O^+ , H^+ , He^+ , NO^+ , O_2^+ , N_2^+ , and cluster ions), the electron temperature, and the ion temperature for magnetically quiet conditions. Efforts are underway to include models for ionospheric storm effects and models for the ion drift and spread-F.

The IRI model, its background, database, and mathematical formulas are explained in detail in special reports published by URSI (Rawer et al., 1978), by the WDC-A-STP (Rawer et al., 1981), and by the NSSDC (Bilitza, 1990).

8.2 Model Uncertainties and Limitations

Like any empirical model, IRI is as good and representative as the data that are available for developing/improving the model. Since most of the ionospheric data have been accumulated at European and North American latitudes, these regions are also the ones that are best represented in IRI. The Northern hemisphere and the continents in general are better represented than the Southern hemisphere and the oceans, again because of obvious differences in data volume. The IRI model should be primarily used for subauroral latitudes. At auroral and polar latitudes, the model has to rely on data from just a few stations and satellites, clearly not enough to fully describe this highly variable region. At these high latitudes, IRI should be considered as a first estimate for describing the background ionosphere.

The uncertainties are typically as follows in Table 2:

Table 2 — IRI Model uncertainties for D, E, and F region parameters

Region	Peak height	Peak density	Temperatures	Ion composition
F region	±15%	±30%	±20%	±50%
E region	±5%	±10%	±10%	±50%
D region	±10%	±70%	(undetermined)	(undetermined)

Improvements in the accuracy of the electron density values can be obtained by introducing measured values for the F peak height and density; IRI supports this option. In addition, IRI provides an option to use measured electron densities to obtain more accurate electron temperatures by employing the well-known anti-correlation between electron temperature and density.

8.3 Basis of the Model

The IRI electron density model uses the CCIR world maps for the F and E peak parameters. A special formula was developed by the IRI team to convert the CCIR-given M3000 propagation factor to the F peak height. For the F peak density an additional choice is given with the URSI-88 maps. These were developed by a special URSI Working Group (C. Rush, Chair) and have shown better results than CCIR in the ocean areas. In addition, a user can enter measured peak parameters into IRI, if available. The CCIR formulas for the F1 ledge and the E peak densities were modified for IRI to better agree with more recent measurements. The IRI topside is based on an analytical representation of Bent's compilation of Alouette and ISIS topside sounder data. Incoherent scatter data from Jicamarca and Arecibo and AEROS and AE-C *in situ* measurements have been used to improve the formula at low latitudes. The representation of the region between E and F peaks is based on ionosonde real-height profiles and on incoherent scatter data (valley). The D-region model assumes an inflection point at 80 to 88 km; this height is correlated to the transition from molecular to cluster ions. The global and temporal variation of the density at that point was modeled with the help of all available (reliable) rocket data.

The electron and ion temperature models are based largely on AEROS RPA and AE-C, ISIS-1, ISIS-2 Langmuir probe data. These data provide a global mapping of temperatures at several altitudes. The whole profile was then established with the help of incoherent scatter data from Jicamarca, Arecibo, and Millstone Hill. At 120 km, the plasma temperatures coincide with the value given by the COSPAR International Reference Atmosphere (CIRA); this was one of the COSPAR requirements. Through all altitudes the temperatures are such that $T_n < T_i < T_e$.

The IRI ion composition model assumes charge neutrality. IRI primarily models the global and temporal variation of atomic and molecular oxygen ions (O^+ , O_2^+) and then fills up to 100% with light ions (H^+ , He^+) above the F peak and with NO^+ ions below. The model is based on a compilation of rocket and satellite RPA and IMS data. The rather limited database makes the ion composition model the weakest part of the IRI. Problems with instrument calibrations have made it difficult to use IMS data from several of the early satellites. Discrepancies were also found between satellite and incoherent scatter measurements. Efforts are now focusing on using the transition heights (light ions to O^+ , O^+ to molecular ions, molecular to cluster, cluster to negative ions) as the characteristic parameters of the composition profiles.

8.4 Database

Electron density: ionosonde (E-, F-peak, bottomside), incoherent scatter radar (h_mF_2 , E-valley, topside), absorption (D-region), rockets (D-, E-region), Alouette, ISIS topside sounder (topside), AEROS, AE-C, DE-2 *in situ* (topside); ion composition: RPA and IMS measurements from satellites (AE-C, AEROS-B, S3-1, OGO-6, Electron 2, 4, Cosmos 274, Sputnik 3) and rockets; temperatures: Langmuir probe and RPA measurements from AEROS-A,B, ISIS-1,-2, AE-C, -E, DE-2, incoherent scatter data from Jicamarca, Arecibo, Millstone Hill, St. Santin, Malvern.

8.5 Publication References

8.5.1 Bilitza, D. (1990), International reference ionosphere 1990, NSSDC/WDC-A-R&S 90-22, Greenbelt, MD.

8.5.2 Bilitza, D., K., and E.G. Rawer, eds. (1994), Ionospheric models, *Adv. Space Res.* 14(12).

8.5.3 Rawer, K., S. Ramakrishnan, and D. Bilitza (1978), International reference ionosphere 1978, URSI Special Rept., Brussels, Belgium.

8.5.4 Rawer, K., D. Bilitza, and S. Ramakrishnan (1978), Goals and status of the international reference ionosphere, *Rev. Geophys.* 16, 177–181.

8.5.5 Rawer, K., J.V. Lincoln, and R.O. Conkright (1981), International reference ionosphere IRI-79, WDC-A-STP Rept. UAG-82, Boulder, CO.

8.5.6 Rawer, K., and W.R. Piggott (1990), Development of IRI-90, *Adv. Space Res.* 10(11).

8.5.7 Rawer, K., and W.R. Piggott (1991), Enlarged space and ground data base for ionospheric modeling, *Adv. Space Res.* 11(10).

8.5.8 Rawer, K., W.R. Piggott, and A.K. Paul (1993), Advances in global/regional descriptions of ionospheric parameters, *Adv. Space Res.* 13(3).

8.5.9 Rawer, K., W.R. Piggott, and A.K. Paul, eds. (1995), Off median phenomena and IRI, *Adv. Space Res.* 15(2).

8.5.10 Rawer, K., D. Bilitza, and W. Singer, eds. (1995), The high latitudes in the IRI, *Adv. Space Res.* 16(1).

8.5.11 Rawer, K., D. Bilitza, K. Mahajan, and A. Mitra, eds. (1996), Low and equatorial latitudes in the IRI, *Adv. Space Res.* 18(6).

8.6 Dates of Development and Authors

8.6.1 Dates:

- 1968 Working Group established.
- 1972 First set of preliminary tables.
- 1978 IRI-78, URSI Special Report.
- 1981 IRI-80, WDC-A-STP Report UAG-82.
- 1986 IRI-86 (also on diskette for use on PCs).
- 1990 IRI-90, NSSDC Report 90-22.
- 1995 IRI-95, anonymous FTP and WWW.

8.6.2 Authors: COSPAR/URSI Working Group (K. Rawer, L. Bossy, and D. Bilitza, Chairs).

8.7 Model Codes and Sources

The model codes can be retrieved from the anonymous FTP site at nssdca.gsfc.nasa.gov in directory `pub/models/IRI`; an ASCII version of the model coefficients can be found in `directorypub/models/IRI90ASCII`. The software package also can be obtained on diskette from NSSDC's request coordination office (CRUSO), National Space Science Data Center, NASA/GSFC, Code 633.4, Greenbelt, MD 20771, tel. 301-286-6695, FAX 301-286-1771 (email: request@nssdca.gsfc.nasa.gov). The model can also be accessed and run interactively online at <http://nssdc.gsfc.nasa.gov/space/model>. There are also web pages describing the model and listing the Working Group composition and the IRI Workshops that have been held so far.

9 Empirical Model of the Ionosphere (EMI)

9.1 Model Content

The empirical model of the ionosphere provides number densities (cm^{-3}) of

Atomic ions:	$\text{H}^+, \text{He}^+, \text{N}^+, \text{O}^+$
Molecular ions:	$\text{N}_2^+, \text{NO}^+, \text{O}_2^+$
Electrons:	N_e

as a function of

Altitude:	50–4000 km
Latitude:	dipole latitude, N_2 , O_2 , O , NO
Time:	day count d (annual variation) magnetic local time τ
Solar activity:	solar flux $f_{10.7}$ for quiet geophysical conditions ($K_p \leq 3$)

The number densities n of the ion species and the electrons are obtained from the appropriate figures (Köhnlein, 1989a and 1989b). At $F_{10.7} = 84 \times 10^{-22} \text{ Wm}^{-2} \text{ Hz}^{-1}$ and $K_p \leq 3$:

Average density (time independent):
see Köhnlein (1989a and 1989b, Figs. 3–6),
 $\log_{10}n$ vs. altitude;

Time-independent density (latitudinal):
see Köhnlein (1989a and 1989b, Figs. 7–18),
 $\log_{10}n$ vs. altitude at $\phi = 90^\circ, 45^\circ, 0^\circ, -90^\circ$;
 $\log_{10}n$ vs. dipole latitude at discrete heights;

Annual variation:
see Köhnlein (1989a and 1989b, Figs. 19–30),
 $\log_{10}n$ vs. altitude at equinox and solstice conditions ($d = 80, 173, 266, 356$);
comparison with data: $\log_{10}n$ vs. day count at discrete heights;

$\Delta \log_{10}n$ (relative):
dipole latitude vs. day count at discrete heights;

Diurnal variation:
see Köhnlein (1989a, Figs. 31–46), and Köhnlein (1989b, Figs. 31–48),
 $\log_{10}n$ vs. altitude at $\phi = 0^\circ, 45^\circ$, and $\tau = 0\text{h}, 6\text{h}, 12\text{h}, 18\text{h}$;
comparison with data:

$\log_{10}n$ vs. magnetic local time at discrete heights and $\phi = 0^\circ, 45^\circ$;
 $\Delta \log_{10}n$ (relative):
dipole latitude vs. magnetic local time at discrete heights;

And superpositions thereof, i.e.,
diurnal variation + relative annual variation
 \Rightarrow diurnal variation at a selected day of the year;
annual variation + relative diurnal variation
 \Rightarrow diurnal variation at a selected magnetic local time.

9.2 Model Uncertainties and Limitations

The discrepancies between the model and the observations (used) are shown for the annual and diurnal variations in Köhnlein (1989a and 1989b, Figs. 20, 23, 26, 29, 32, 33, 36, 37, 40, 41, 44, 45), and in Köhnlein (1989b, Figs. 46 and 47). In general, the model agrees well with the observations.

The uncertainties of the model are mainly due to the uneven data coverage and the simplicity of the analytical approach (e.g., linearity, no longitudinal terms, no disturbed conditions).

Data from epochs not used in the database may show greater deviations from the model. This is especially true for disturbed geophysical conditions that are not considered in the model (also see Köhnlein, 1993).

9.3 Basis of the Model

The vertical and horizontal structures of the model are treated on an equal footing.

The plasma parameters are expanded into spherical harmonics (Köhnlein, 1989a, Eqs. 2.1–2.10), wherein the model coefficients depend on altitude, solar flux $F_{10.7}$, and the geomagnetic index K_p .

Restricting the model to quiet geophysical conditions ($K_p \leq 3$), the above coefficients depend linearly on $F_{10.7}$, whereas their height variations are expressed by cubic spline functions.

9.4 Database

The database of the model consists of observations by satellites, incoherent scatter stations, and rocket profiles covering the time interval 1964–1979 (Köhnlein, 1989a, Table1 therein; and Köhnlein, 1989b, Table1 and Figs.1 and 2 therein).

9.5 Publication References

9.5.1 Köhnlein, W. (1989a), A model of the terrestrial ionosphere in the altitude interval 50–4000 km: I. atomic ions (H^+ , He^+ , N^+ , O^+), *Earth Moon Planets*. 45, 53–100.

9.5.2 Köhnlein, W. (1989b), A model of the terrestrial ionosphere in the altitude interval 50–4000 km: II. molecular ions (N_2^+ , NO^+ , O_2^+) and electron density, *Earth Moon Planets*. 47, 109–163.

9.5.3 Köhnlein, W. (1993), Comparison of the ion composition data with empirical models (comment), *Adv. Space Res.* 13(3), 85–86, 125–132.

9.6 Dates of Development, Authors, and Sponsors

9.6.1 Date: 1983.

9.6.2 Author: W. Köhnlein.

9.6.3 Sponsors: Deutsche Forschungsgemeinschaft and University of Bonn.

9.7 Model Codes and Sources

The model was developed in Fortran code specifically adapted to a CDC computer.

Because of the detailed graphical representation, Köhnlein (1989a and 1989b) can be used as a quick reference for ion and electron densities at low solar fluxes ($F_{10.7} \approx 84$) and quiet geophysical conditions ($K_p \leq 3$) in the altitude interval 50–4000 km.

10 The Sheffield University Plasmasphere-Ionosphere Model (SUPIM)

10.1 Model Content

The Sheffield University Plasmasphere-Ionosphere Model (SUPIM) is a mathematical model that describes the distribution of ionization within the Earth's mid- and equatorial latitude ionosphere. In the model, time-dependent equations of continuity, momentum, and energy balance for the O^+ , H^+ , He^+ , N_2^+ , O_2^+ , and NO^+ ions, and the electrons are solved along magnetic field lines for the ion and electron concentrations, field-aligned velocities, and temperatures. The magnetic field is an eccentric-dipole representation of the Earth's magnetic field, the offset between the magnetic and geographic poles being determined from the first eight non-zero terms of the usual spherical harmonic expansion of the geomagnetic scalar potential used in the International Geomagnetic Reference Field (IGRF). Particular cases of the eccentric dipole are the tilted-centered dipole and the axial-centered dipole. These cases are obtained by truncating the spherical harmonic expansion after the first three non-zero terms and the first term, respectively.

Included in the model are numerous physical and chemical processes. The principal processes include ion production due to solar EUV radiation, ion production and loss due to chemical reactions between the constituent ions and with the neutral gases, ambipolar and thermal diffusion, ion-ion and ion-neutral collisions, thermospheric meridional and zonal winds, electrodynamic drift, thermal conduction, photo-electron heating, frictional heating, and a host of local heating and cooling mechanisms.

Enhancements/modifications have been made to the "standard" model for specific studies. For example, inclusion of sub-auroral ion drifts (SAIDs), a self-consistent, low-latitude atmospheric dynamo model, anisotropic ion temperatures, vibrational excitation of N_2 , the separation of O^+ into its 4S , 2D , and 2P states, and vertical neutral winds.

Depending upon the inputs, the model can describe different solar cycle, seasonal, daily, and magnetic activity variations. It can also provide descriptions of the diurnal, altitude, latitude, and longitudinal variations.

10.2. Model Uncertainties and Limitations

10.2.1 To a large extent, the reliability of the calculated ionospheric parameters depends upon the accuracy to which the model inputs can be specified.

10.2.2 Except for a few locations, the model inputs of thermospheric wind and the vertical $\mathbf{E} \times \mathbf{B}$ drift are poorly known. Some adjustments to these parameters may be needed.

10.3 Basis of the Model

10.3.1 The model is a mathematical formulation of the known physical and chemical processes of the Earth's ionosphere and plasmasphere. The motion of the plasma is considered to be due to ambipolar diffusion parallel to the magnetic field with an additional $\mathbf{E} \times \mathbf{B}$ drift perpendicular to the magnetic field.

10.3.2 The model equations are solved at a discrete set of points along an eccentric dipole magnetic field line from a base altitude of around 120 km in the northern hemisphere to a base altitude of around 120 km in the southern hemisphere. There are switches in the model code to make the magnetic field a tilted-centered or axial-centered dipole.

10.3.3 At mid-latitudes, the vertical $\mathbf{E} \times \mathbf{B}$ drift velocity has little effect on the model results and is usually taken to be zero. For many applications, only one field line needs to be considered.

10.3.4 At equatorial latitudes, inclusion of the vertical $\mathbf{E} \times \mathbf{B}$ drift is essential as this drift gives rise to the equatorial anomaly. Under the influence of a vertical $\mathbf{E} \times \mathbf{B}$ drift the plasma associated with a particular magnetic field line is associated with a different magnetic field line at later times. Thus, in order to provide

reasonable 24 hr coverage of the modeled parameters within a specified altitude and latitude region, the model equations have to be solved for many magnetic field lines.

10.3.5 The continuity, momentum, and energy balance equations for each constituent ion and the electrons form a set of highly nonlinear, second-order partial parabolic equations. The equations are first linearized in them, and then finite differences are used for the spatial and temporal derivatives. The resulting coupled tri-diagonal systems of linear algebraic equations are solved by a standard technique.

10.3.6 At the lower boundary of each hemisphere ($z = 120$ km), the ions and electrons are taken to be in chemical equilibrium, and the densities are obtained by equating the local sources and sinks. Likewise, the ion and electron temperatures are obtained by equating local heating and cooling rates.

10.3.7 The time step is usually taken to be 15 min. The spatial step along the magnetic field line varies along the field line, and the number of points increases with increasing apex altitude. A mathematical formulation is used to give the point distribution. The points are arranged to give a spatial step of about 5 km at F-region altitudes.

10.4 Model Input Parameters

10.4.1 Latitude and longitude of ground station, day, and year.

10.4.2 An IGRF (presently IGRF85) for the determination of the magnetic field.

10.4.3 A solar EUV flux spectrum (presently from EUV94).

10.4.4 A thermosphere model (presently MSIS-86) for the determination of the neutral densities and temperatures.

10.4.5 A thermospheric wind model (presently HWM-90) for the determination of the meridional and zonal winds.

10.4.6 A vertical $\mathbf{E} \times \mathbf{B}$ drift model.

The model inputs described in section 4.1 are read into the model from an input file. The model inputs described in sections 4.2–4.6 are incorporated into the model code as sets of subroutines. The subroutines permit easy modification as improved values become available and for the modifications/changes made in applications of the model to particular studies.

10.5 Publication References

10.5.1 Bailey, G.J., and R. Sellek (1990), A mathematical model of the earth's plasmasphere and its application in a study of He^+ at $L=3.0$, *Ann. Geophys.* 8, 171–190.

10.5.2 Bailey, G.J., R. Sellek, and Y. Rippeth (1993), A modeling study of the equatorial topside ionosphere, *Ann. Geophys.* 11, 263–272.

10.6 Dates of Development, Authors, and Sponsors

10.6.1 Dates

1975 One-hemisphere model—ions O^+ and H^+

1978 Extended to two hemispheres.

1979 He^+ added to one-hemisphere model.

1980 Major revision—two-hemisphere model, axial-centered dipole magnetic field, energy balance equations, new numerical procedures for solving model equations, ions O^+ and H^+ .

1983 $\mathbf{E} \times \mathbf{B}$ drift added.

- 1990 Major revision—the ions He^+ , N_2^+ , O_2^+ , and NO^+ added.
- 1993 Major revision—magnetic field represented by an eccentric dipole.
- 1994 Two-stream approximation method used to determine photoelectron-heating rates.
- 1995 Changes made to numerical procedures to improve numerical stability.

10.6.2 Author (principal): Graham J. Bailey, School of Mathematics and Statistics, Applied Mathematics Section, The University of Sheffield, Sheffield S3 7RH, UK.

10.6.3 Sponsors: Plasma Physics and Astronomy Research Council (PPARC), UK.

10.7 Model Codes and Sources

The model is not user-friendly, and collaboration, in the first instance, is required between the user and the author (Graham Bailey). The author would be happy to discuss collaborations with interested groups. The author would consider enhancing/modifying the model and model codes to meet specific requests. The model codes are written in Fortran and have been developed for use on a high-performance PC. It is straightforward to modify the codes for use on workstations and mainframes.

11 The Field Line Interhemispheric Plasma Model

11.1 Model Content

The Field Line Interhemispheric Plasma (FLIP) Model is a first-principles, one-dimensional, time-dependent, chemical and physical model of the ionosphere and plasmasphere. It couples the local ionosphere to the overlying plasmasphere and conjugate ionosphere by solving the ion continuity and momentum, ion and electron energy, and photoelectron equations along entire magnetic flux tubes. The interhemispheric solutions yield densities and fluxes of H^+ , O^+ , He^+ , and N^+ , as well as the electron and ion temperatures. In addition, continuity and momentum equations are solved to provide the densities of minor neutral species [$N(^2D)$, $N(^4S)$, NO] and the first six vibrational levels of N_2 in both hemispheres. A large number of other minor ion and neutral densities are calculated from chemical equilibrium between 80 and 600 km in the northern and southern hemispheres. Other outputs from the model include particle and heat fluxes, electron heating and cooling rates, photoelectron fluxes, chemical production and loss rates, and, most significantly, airglow emission rates. Major neutral densities are supplied by the MSIS model. A three-dimensional version of the model is obtained by simulating several hundred corotating flux tubes.

11.2 Model Uncertainties and Limitations

11.2.1 In several recent studies, the FLIP model typically produces F2 peak electron densities within 30% of the measured densities during the daytime, despite the potential for large errors in several key inputs. At night, discrepancies between measured and modeled densities can often be as much as a factor of 2.

11.2.2 During quiet times, the error in the inputs for the solar EUV flux, MSIS neutral densities, reaction rates, and cross-sections are typically about 20%. During magnetic storms, uncertainties in the MSIS neutral densities may be much larger, resulting in similar errors in calculated electron densities.

11.2.3 The largest uncertainty for ionospheric modeling at mid latitudes is the neutral wind magnitude. However, when measurements of $h_m F_2$ are available, the uncertainty is reduced to about 20% by using the algorithm that we have developed.

11.2.4 The current FLIP model is basically a mid-latitude model because it neglects convection electric fields, which are important at equatorial and auroral latitudes.

11.2.5 The uncertainty of the plasma content of plasmaspheric flux tubes is not important during the daytime but can produce about a 50% error in calculated $N_m F_2$ at night.

11.2.6 The FLIP model is a low-speed model that is not applicable in the plasmasphere for ion densities below about 100 cm^{-3} .

11.3 Basis of the Model

11.3.1 The FLIP model calculates the plasma densities and temperatures along complete magnetic flux tubes, from 80 km in the northern hemisphere, through the plasmasphere, to 80 km in the southern hemisphere, as a function of time. A tilted dipole approximation is used for the Earth's magnetic field.

11.3.2 The set of nonlinear, second-order, partial differential equations for continuity, momentum, and energy is transformed into finite difference equations and solved by a Newton-Raphson iterative scheme. The scheme is stable and time steps are generally 0.5 hr except near twilight, where 10 min or less are used.

11.3.3 A variable spatial grid is set up along the magnetic field line. There are approximately 200 grid points distributed in such a way as to give a grid spacing of less than 10 km in the ionosphere and less than one scale height of H^+ in the plasmasphere.

11.3.4 The boundary conditions imposed at the feet of the flux tube near 100 km are chemical equilibrium for ions and thermal equilibrium for temperatures. The initial plasmaspheric H^+ density must also be specified.

11.3.5 A unique feature of the FLIP model is the option to employ measurements of h_mF_2 , N_mF_2 , and topside T_e as additional constraints for different types of studies.

11.4 Model Input Parameters

11.4.1 The standard model can be run by simply specifying the date and the geographic location, but there are a large number of other options.

11.4.2 Activity indices K_p , daily $F_{10.7}$, and average $F_{10.7}$ for the MSIS neutral density, HWM-93 wind, and solar EUV flux models are read from a file but can also be specified.

11.4.3 Measured h_mF_2 , N_mF_2 , and topside T_e can be input from a file. The h_mF_2 is automatically turned into a neutral wind so that the model h_mF_2 follows the observed values.

11.4.4 There are a large number of adjustable parameters, such as time step and length of the run, which control the action of the model.

11.5 Publication References

11.5.1 Torr, M.R., D.G. Torr, P.G. Richards, and S.P. Yung (1990), Mid- and low-latitude model of thermospheric emissions, 1, $O^+(^2P)$ 7320 and $N_2(^2P)$ 3371, *J. Geophys. Res.* 95(21), 147.

11.5.2 Richards, P.G. (1991), An improved algorithm for determining neutral winds from the height of the F2 peak electron density, *J. Geophys. Res.* 96(17), 839.

11.5.3 Richards, P.G., D.G. Torr, B.W. Reinisch, R.R. Gamache, and P.J. Wilkinson (1994), F2 peak electron density at Millstone Hill and Hobart: comparison of theory and measurement at solar maximum, *J. Geophys. Res.* 99(15), 5.

11.5.4 Richards, P.G., D.G. Torr, M.J. Buonsanto, and D.P. Sipler (1994), Ionospheric effects of the March 1990 magnetic storm: comparison of theory and measurement, *J. Geophys. Res.* 99(23), 359.

11.5.5 Richards, P.G., J.A. Fennelly, and D.G. Torr (1994), EUVAC: A solar EUV flux model for aeronomic calculations, *J. Geophys. Res.* 99, 8981.

11.5.6 Richards, P.G., D.G. Torr, M.E. Hagan, and M.J. Buonsanto (1995), A new algorithm for improved ionospheric electron density modeling, *Geophys. Res. Letters* 22, 1385.

11.5.7 Richards, P.G. (1996), The field line interhemispheric plasma model, *Solar-Terrestrial Energy Program: Handbook of Ionospheric Models*, edited by R.W. Schunk, p. 207.

11.6 Dates of Development, Authors, and Sponsors

11.6.1 Dates

1979 Development of interhemispheric solutions for $[O^+]$, $[H^+]$, T_e , and T_i .

1980 Interhemispheric solutions for photoelectron flux and solutions for minor ion and neutral densities added.

1981 Diffusion equations for vibrationally excited N_2 effects included.

1982 Improvements to the photoelectron flux model to reproduce observed flux.

1986 Developed original algorithm for obtaining winds from h_mF_2 .

1991 Improved algorithm for getting winds from h_mF_2 .

- 1992 Added energetic electron precipitation for auroral studies.
- 1993 Developed algorithm to cause model to reproduce both $h_m F_2$ and $N_m F_2$.
- 1994 Developed EUVAC solar EUV flux model.
- 1995 Developed algorithm to reproduce observed topside ionosphere.

11.6.2 Author (principal): Phil Richards, Computer Science Department, The University of Alabama in Huntsville, Huntsville, AL 35899, USA.

11.6.3 Sponsors: National Aeronautics and Space Agency, National Science Foundation.

11.7 Model Codes and Sources

A VAX version of the model is available to be installed at the user's institution. A UNIX version is also under development. The model runs from DEC command files that are well documented. There is also an interface that helps the user understand the model and aids in the setting up of the DEC command files. Some previous users with a good knowledge of the ionosphere have been able to run the model with little additional help. The author also runs the model for collaborative studies. Contact person: Phil Richards, Computer Science Department, The University of Alabama in Huntsville, Huntsville, AL 35899, USA (email: pgrichds@gmail.com).

DRAFT--For Public Review Only--DEC 2013

12 Global Assimilation of Ionospheric Measurements—Full Physics (GAIM-FP)

12.1 Model Content

The GAIM-FP model was developed at Utah State University (Schunk et al., 2004; Scherliess et al., 2004, 2009, 2010). The model uses a physics-based model of the ionosphere-plasmasphere system and a Kalman filter as a basis for assimilating a diverse set of real-time (or near real-time) measurements. The physics-based model is the Ionosphere Plasmasphere Model (IPM), which is global and covers the E-region, F-region, topside ionosphere, and plasmasphere from 90 to 30,000 km. It takes account of six ion species (NO^+ , O_2^+ , N_2^+ , O^+ , H^+ , He^+). The primary output of the GAIM-FP model is a time-dependent, three-dimensional plasma density distribution at user-specified times. However, the model also provides quantitative estimates of the accuracy of the reconstructed plasma densities, as well as the self-consistent drivers of the ionosphere-plasmasphere system (e.g., neutral winds and electric fields). In addition, auxiliary parameters are provided, including N_mE , h_mE , N_mF_2 , h_mF_2 , slant, and vertical TEC. The GAIM-FP model assimilates bottomside N_e profiles from a variable number of ionosondes, slant TEC from a variable number of ground-based GPS/TEC stations, *in situ* N_e from the DMSP satellites, occultation data, and line-of-sight UV emissions measured by satellites. The model can be run in a global, regional, or local mode. Forecasting is accomplished by running the IPM forward in time from a given GAIM-FP specification using predictions for the IPM inputs.

12.2 Model Uncertainties and Limitations

12.2.1 The accuracy of the reconstructed ionosphere depends on the amount of data assimilated, the diversity of the data types, and the quality of the data.

12.2.2 When very little data are assimilated, the output of GAIM-FP is primarily from the physics-based model (IPM).

12.2.3 Plasma instabilities and bubbles are not taken into account in the physics-based model (IPM).

12.2.4 GAIM-FP only assimilates data between $\pm 60^\circ$ geomagnetic latitudes. The plasma density distribution at high latitudes is provided by the physics-based model, which is currently only driven by the geophysical conditions.

12.3 Basis of the Model

The GAIM-FP model rigorously evolves the ionosphere and plasmasphere electron density field and its associated errors using the full physical model. Advantages of this rigorous approach are expected to be most significant in data-sparse regions and during times of severe weather. Necessary approximations to make the model computationally tractable capitalize on the newest developments in oceanographic data assimilation. The model is based on a new physics-based model that is composed of an Ionosphere-Plasmasphere Model (IPM) that covers low and mid-latitudes. The new physics-based model includes six ion species (NO^+ , O_2^+ , N_2^+ , O^+ , He^+ , H^+), ion and electron temperatures, and plasma drifts parallel and perpendicular to the geomagnetic field. These models use the International Geomagnetic Reference Field, which accurately describes the relative positions of the geographic and geomagnetic equators and the declination of the magnetic field lines. The physics-based model covers the altitude range from 90 to 30,000 km, which includes the E-region, F-region, topside ionosphere, and plasmasphere. Different data sources are assimilated via an ensemble Kalman filter technique and quality control algorithms are provided as an integral part of the model. The outputs of the GAIM-FP model are provided on user-specified altitude, latitude, and longitude grids; local horizontal grids as small as 25×25 km are also possible.

In practice, the resolution adopted depends on the data distribution, and runs are frequently conducted with a 7.5° longitudinal resolution and a $1\text{--}2^\circ$ latitudinal resolution in the global mode. In the regional mode, spatial resolution can be 3.75° in longitude and 1° in latitude if there are sufficient data to warrant such a resolution. In altitude, the spatial resolution of the output is currently 4 km in the E-region and 10

km in the F-region. Above the F-region, the altitude spacing in the filter increases, taking advantage of the increasing scale length in the topside ionosphere. Data are currently assimilated in GAIM-FP at a 15-min interval.

12.4 Model Input Parameters

The GAIM-FP model requires the start date (year, day of the year). The IPM model uses $F_{10.7}$, average $F_{10.7}$, daily A_p and K_p indices. The IPM also uses empirical inputs for the neutral atmosphere, e.g., neutral composition and wind, low-latitude electric field, solar EUV and UV radiation, and resonantly scattered radiation.

The GAIM-FP model accepts data from multiple sources, including slant TEC from GPS ground stations via RINEX files, *a priori* bias information for GPS satellites and ground stations, true-height electron density profiles from DISS ionosondes via SAO formatted files, SSULI and SSUSI UV radiances via SDF2 files, DMSP IES *in situ* electron densities via EDR files, and occultation data from multiple satellites.

12.5 Publication References

12.5.1 Scherliess, L., R.W. Schunk, J.J. Sojka, and D.C. Thompson (2004), Development of a physics-based reduced state Kalman filter for the ionosphere, *Radio Sci.* 39, RS1S04, doi:10.1029/2002RS002797.

12.5.2 Scherliess, L., D.C. Thompson, and R.W. Schunk (2009), Ionospheric dynamics and drivers obtained from a physics-based data assimilation model, *Radio Sci.* 44, RS0A32, doi:10.1029/2008RS004068.

2.5.3 Scherliess, L., D.C. Thompson, and R.W. Schunk (2010), Data assimilation models: A “new” tool for ionospheric science and applications, in IAGA Book, *The Dynamic Magnetosphere*.

12.5.4 Schunk, R.W., et al. (2004), Global assimilation of ionospheric measurements (GAIM), *Radio Sci.* 39, RS1S02, doi:10.1029/2002RS002794.

12.6 Dates of Development and Authors

12.6.1 Dates

- 2004 Initial version of GAIM-FP completed.
- 2005 Multiple data sources are included.
- 2010 Further improvements/modifications are in progress.

12.6.2 Developers/authors: L. Scherliess, R. W. Schunk, and D. C. Thompson.

12.7 Model Codes and Sources

The code is not available, but collaborative studies with other scientists are possible.

13 Global Assimilation of Ionospheric Measurements–Gauss-Markov (GAIM-GM)

13.1 Model Content

The GAIM-GM model was developed at Utah State University (Schunk et al., 2004a, b; 2005a, b; Scherliess et al., 2004, 2006, 2010). The model uses a physics-based model of the ionosphere and a Kalman filter as a basis for assimilating a diverse set of real-time (or near real-time) measurements. The physics-based model is the Ionosphere Forecast Model (IFM), which is global and covers the E-region, F-region, and topside from 90 to 1400 km. It takes account of five ion species (NO^+ , O_2^+ , N_2^+ , O^+ , H^+). The main output of the model is a three-dimensional electron density distribution at user-specified times. In addition, auxiliary parameters are also provided, including N_mE , h_mE , N_mF_2 , h_mF_2 , slant, and vertical TEC. The GAIM-GM model assimilates bottomside N_e profiles from a variable number of ionosondes, slant TEC from a variable number of ground-based GPS/TEC stations, *in situ* N_e from the DMSP satellites, occultation data, and line-of-sight UV emissions measured by satellites. Quality control algorithms for all of the data types are provided as an integral part of the model. The GAIM-GM model takes account of latent data (up to 3 hours) and provides a 24-hour forecast. The model can be run in a global, regional, or nested grid mode. The primary output from GAIM-GM is a time-dependent, three-dimensional global electron density distribution.

13.2 Model Uncertainties and Limitations

13.2.1 The accuracy of the reconstructed ionosphere depends on the amount of data assimilated, the diversity of the data types, and the quality of the data.

13.2.2 When very little data are assimilated, the output of GAIM-GM is primarily from the physics-based model (IFM).

13.2.3 Plasma instabilities and bubbles are not taken into account in the physics-based model (IFM).

13.2.4 The GAIM-GM model only assimilates data between $\pm 60^\circ$ geographic latitude. The plasma density distribution at high latitude is provided by the IFM and is currently only driven by the geophysical conditions.

13.3 Basis of the Model

The GAIM-GM model is based on the Ionosphere Forecast Model (IFM), which covers the E-region, F-region, and topside ionosphere up to 1400 km and takes account of five ion species (NO^+ , O_2^+ , N_2^+ , O^+ , H^+). In GAIM-GM the ionosphere densities obtained from the IFM constitute the background ionosphere density field on which perturbations are superimposed based on the available data and their errors. To reduce the computational requirements, these perturbations and the associated errors evolve over time with a statistical model (Gauss-Markov process) and not rigorously with the physical model. As a result, GAIM-GM can be executed on a limited number of CPUs. Like all assimilation techniques, the GAIM-GM uses the errors on the observations and models in the analysis, and computes the errors in the match. The resolution adopted depends on the data distribution, and frequently, runs are conducted with a 15° longitudinal resolution and a 4° latitudinal resolution in the global mode. In the regional mode, the spatial resolutions can be 3.75° in longitude and 1° in latitude if there are sufficient data to warrant such a resolution. In altitude, the spatial resolution is currently 4 km in the E-region and 20 km in the F-region. Above the F-region, the altitude spacing in the filter increases, taking advantage of the increasing scale length in the topside ionosphere. Data are currently assimilated in GAIM-GM at a 15-min interval. Note that the spatial and temporal resolutions used in the filter for data assimilation are not the same as those used in the Ionosphere Forecast Model, where the resolutions are much finer.

To date, numerous simulations have been conducted with several different data types, including simulations with GPS/TEC data from up to 1000 ground receivers, *in situ* N_e from 4 DMSP satellites, bottomside N_e profiles from 80 ionosondes, occultation data from various satellites (IOX, CHAMP, SAC-

C), and UV emission data from satellites (Scherliess et al., 2006; Sojka et al., 2007; Thompson et al., 2006, 2009; Zhu et al., 2006; Jee et al., 2008).

The GAIM-GM model is an operational model at the Air Force Weather Agency.

13.4 Model Input Parameters

For a run, the GAIM-GM model requires the start date (year, day of the year) and the duration of the run in days (currently, from 1 day up to many years). The IFM model uses $F_{10.7}$, average $F_{10.7}$, daily A_p , and eight 3-hour K_p indices. The IFM also uses empirical inputs for the neutral atmosphere and magnetosphere parameters needed by the model, e.g., neutral composition and wind, low and high latitude electric fields, and auroral precipitation.

The GAIM-GM model accepts data from multiple sources, including slant TEC from GPS ground stations via RINEX files, *a priori* bias information for GPS satellites and ground stations, true-height electron density profiles from DISS ionosondes via SAO formatted files, SSULI and SSUSI UV radiances via SDF2 files, occultation data, and DMSP IES *in situ* electron densities via EDR files.

13.5. Publication References

13.5.1 Jee, G., A.G. Burns, W. Wang, S.C. Solomon, R.W. Schunk, L. Scherliess, D.C. Thompson, J.J. Sojka, and L. Zhu (2008), Driving the TING model with GAIM electron densities: ionospheric effects on the thermosphere, *J. Geophys. Res.* 113, A03305, doi:10.1029/2007JA012580.

13.5.2 Scherliess, L., R.W. Schunk, J.J. Sojka, and D.C. Thompson (2004), Development of a physics-based reduced state Kalman filter for the ionosphere, *Radio Sci.* 39, RS1S04, doi:10.1029/2002RS002797.

13.5.3 Scherliess, L., R.W. Schunk, J.J. Sojka, D.C. Thompson, and L. Zhu (2006), The USU GAIM Gauss-Markov Kalman filter model of the ionosphere: Model description and validation, *J. Geophys. Res.* 111, A11315, doi:10.1029/2006JA011712.

13.5.4 Scherliess, L., D.C. Thompson, and R.W. Schunk (2010), Data assimilation models: A “new” tool for ionospheric science and applications, in IAGA Book, *The Dynamic Magnetosphere*, 2010.

13.5.5 Schunk, R.W., et al. (2004a), Global assimilation of ionospheric measurements (GAIM), *Radio Sci.*, 39, RS1S02, doi:10.1029/2002RS002794.

13.5.6 Schunk, R.W., L. Scherliess, J.J. Sojka, and D.C. Thompson (2004b), USU global ionospheric data assimilation models, *Proc. SPIE.* 5548, doi:10.1117/12.562448, 327–336.

13.5.7 Schunk, R.W., L. Scherliess, J.J. Sojka, D.C. Thompson, and L. Zhu (2005a), An operational data assimilation model of the global ionosphere, *2005 Ionospheric Effects Symposium*, edited by J. M. Goodman, JMG Associates Ltd., 512–518.

13.5.8 Schunk, R.W., L. Scherliess, J.J. Sojka, D.C. Thompson, and L. Zhu (2005b), Ionospheric weather forecasting on the horizon, *Space Weath.* 3, S08007, doi:10.1029/2004SW000138.

13.5.9 Sojka, J.J., D.C. Thompson, L. Scherliess, and R.W. Schunk (2007), Accessing USU-GAIM ionospheric weather specification over Australia during the 2004 CAWSES campaign, *J. Geophys. Res.* 112, A09306, doi:10.1029/2006JA012048.

13.5.10 Thompson, D.C., L. Scherliess, J.J. Sojka, and R.W. Schunk (2006), The Utah State University Gauss-Markov Kalman filter in the ionosphere: the effect of slant TEC and electron density profile data on model fidelity, *J. Atmos. Solar-Terr. Phys.* 68, 947–958.

13.5.11 Thompson, D.C., L. Scherliess, J.J. Sojka, and R.W. Schunk (2009), Plasmasphere and upper ionosphere contributions and corrections during the assimilation of GPS slant TEC, *Radio Sci.* 44, RS0A02, doi:10.1029/2008RS004016.

13.5.12 Zhu, L., G. Jee, L. Scherliess, R.W. Schunk, J.J. Sojka, and D.C. Thompson (2006), Validation study of the Ionosphere Forecast Model (IFM) using the TOPEX total electron content measurements, *Radio Sci.* 41, RS5S11, doi:10.1029/2005RS003336.

13.6 Dates of Development and Authors

13.6.1 Dates

2004 Initial version of GAIM-GM completed.

2006 GAIM-GM delivered to the Community Coordinated Modeling Center for runs on request.

2006 GAIM-GM became operational at the Air Force Weather Agency.

2010 Further modifications are in progress.

13.6.2 Developers/authors: R. W. Schunk, L. Scherliess, J. J. Sojka, D. C. Thompson and L. Zhu.

13.7 Model Codes and Sources

The code is not available, but the authors frequently run the model in collaborative studies with other scientists.

14 JPL/USC GAIM: The Jet Propulsion Laboratory/University of Southern California Global Assimilative Ionospheric Model

14.1 Model Content

The University of Southern California (USC) and the Jet Propulsion Laboratory (JPL) have jointly developed GAIM to monitor space weather, study storm effects, and provide ionospheric calibration for space weather applications. JPL/USC GAIM is a physics-based, three-dimensional data assimilation model that uses both 4DVAR and Kalman filter techniques to solve for the ion and electron density state and key drivers such as equatorial electrodynamics, neutral winds, and ion production terms (Wang et al., 2004; Pi et al., 2003, 2004, 2009). The various Kalman filter versions include separate band-limited, nested grid versions with high-resolution inner and medium-resolution outer regions, and real-time GAIM capabilities. JPL/USC GAIM is capable of ingesting multiple data sources, updates the three-dimensional electron density grid every 5–12 minutes, and solves for improved drivers every 1–2 hours. Since the forward physics model and the adjoint model were explicitly designed for data assimilation and computational efficiency, all of this can be accomplished on a single dual-processor UNIX workstation.

14.2 Model Resolution and Limitations

The GAIM grid resolution varies from 2.5° to 5.0° in latitude, 10.0° to 15.0° in longitude, and 40 to 80 km in height. The nested-grid GAIM resolution is typically 1° by 1° lat/long, and 20 or 40 km in height. As an example, 40 km as an approximate height resolution results in about 100,000 voxels globally. (Actual height resolution varies with latitude based on the pql grid, i.e., intersections of constant magnetic field lines, constant magnetic geopotential lines, and constant magnetic latitudes.)

14.3 Basis of the Model

The GAIM Forward Ionospheric Model (first-principles physics) is a global three-dimensional, time-dependent model for ion densities. The conservation of mass and momentum equations are solved on an Earth-fixed Eulerian grid (Pi et al., 2003, 2004). The volume elements have surfaces parallel to either the magnetic field and potential lines or geomagnetic meridional planes. Using the most recent ionospheric “state” (ion densities in each volume element or voxel) and ionospheric driving forces, the forward model propagates the state to a future time. The observation operator then maps the future state to the incoming measurements. These predicted measurement values are differenced from the actual measurements creating an “innovation vector.” In the assimilation step, the Kalman filter adjusts the electron densities based on the innovation vector and the prior covariance matrix to compute a statistically minimum variance estimate of the electron density. The Kalman filter works to reduce the residuals in a least squares sense over the entire grid at once, weighted by the uncertainty in each voxel and the uncertainty in the incoming data sources. In case of the 4DVAR approach, only the driving force parameters are adjusted to produce a least squares estimate of the driving forces as well as electron density (Pi et al., 2003).

14.4 Model Input Parameters and Validation

GAIM physics uses various ionospheric model inputs including solar EUV radiation flux, thermospheric densities and temperature, and winds computed from various empirical models. The Kalman filter then assimilates a variety of data sources, including slant ground and space-based GPS TEC measurements, *in situ* measurements of electron density, and UV airglow radiances. After the GAIM runs are complete, validation is routinely performed using independent electron densities and density profiles, GIM-derived vertical TEC (VTEC), Jason-2 VTEC, Incoherent Scatter Radar (ISR) electron densities, and ionosonde-derived h_mF_2 , and n_mF_2 measurements (Mandrake et al., 2005; Komjathy et al., 2010).

14.5 Publication References

14.5.1 Komjathy, A., B. Wilson, X. Pi, V. Akopian, M. Dumett, B. Iijima, O. Verkhoglyadova, and A.J. Mannucci (2010), JPL/USC GAIM: On the impact of using COSMIC and ground-based GPS measurements to estimate ionospheric parameters, *J Geophys. Res.*, doi:10.1029/2009JA014420.

14.5.2 Mandrake, L., B. Wilson, C. Wang, G. Hajj, A. Mannucci, and X. Pi (2005), A performance evaluation of the operational Jet Propulsion Laboratory/University of Southern California Global Assimilation Ionospheric Model (JPL/USC GAIM), *J. Geophys. Res.* 110, A12306, doi:10.1029/2005JA011170.

14.5.3 Pi, X., C. Wang, G.A. Hajj, G. Rosen, B.D. Wilson, and G.J. Bailey (2003), Estimation of $\mathbf{E} \times \mathbf{B}$ drift using a global assimilative ionospheric model: an observation system simulation experiment, *J. Geophys. Res.* 108(A2), 1075, doi:10.1029/2001JA009235.

14.5.4 Pi, X., G.A. Had, B.D. Wilson, A.J. Mannucci, A. Komjathy, L. Mandrake, C. Wang, and I.G. Rosen (2004), 3-dimensional assimilative ionospheric modeling for regions of large TEC gradient, *Pmc ION NTM*, San Diego, January 2004.

14.5.5 Pi, X, A.J. Mannucci, B.A. Iijima, B.D. Wilson, A. Komjathy, T.F. Runge, and V. Akopian (2009), Assimilative modeling of ionospheric disturbances with FORMOSAT-3/COSMIC and ground-based GPS measurements, *Terr. Atmos. Ocean Sci.* 20(1), 273–285.

14.5.6 Wang, C., G. Hajj, X. Pi, I.G. Rosen, and B. Wilson (2004), Development of the global assimilative ionospheric model, *Radio Sci.* 39, RS1S06, doi:10.1029/2002RS002854.

14.6 Dates of Development

In 1999, the Department of Defense identified global ionospheric data assimilation as one of the 12 topics for the Multidisciplinary University Initiative (MURI) program. Since then, multiple versions of GAIM have been developed including the Kalman filter, 4DVAR, nested-grid GAIM, and real-time GAIM capabilities.

14.7 Model Codes and Sources

The original version of GAIM was developed in Fortran. Since then it has been rewritten in modern C++ with python supporting the front-end processing of GPS ground and space-borne GPS measurements. The intellectual property is owned by the California Institute of Technology. Government and commercial licensing are available for the source code and/or executables.

15 Ionosphere Forecast Model (IFM)

15.1 Model Content

The Ionosphere Forecast Model is a numerical model of the global ionosphere that calculates the three-dimensional, time-dependent density distributions for four major ions (NO^+ , O_2^+ , N_2^+ , O^+) at E-region altitudes and two major (O^+ , NO^+) and two minor (N_2^+ , O_2^+) ions at F-region altitudes. The model also calculates the isotropic ion and electron temperature distributions and the plasma drift velocities at both E- and F-region altitudes. The IFM contains a simple prescription for calculating H^+ densities in the F-region and topside ionosphere. The model covers the altitude range from 90 to 1500 km and outputs density values at a spatial resolution of 4 km in the E-region and 20 km in the F-region. The model outputs the density and temperature distributions in either a geographic or geomagnetic coordinate system with a 3° latitude resolution and a 7.5° longitude resolution.

The IFM takes account of field-aligned diffusion, cross-field electrodynamic drifts, thermospheric winds, neutral composition changes, energy-dependent chemical reactions, ion production (due to solar UV/EUV radiation, star light, and auroral precipitation), thermal conduction, diffusion-thermal heat flow, and a myriad of local heating and cooling processes. The IFM also accounts for the displacement between the geomagnetic and geographic poles.

The IFM is a modified version of the USU Time-Dependent Ionosphere Model (TDIM) that has been simplified, and is faster and easier to run.

15.2 Model Uncertainties and Limitations

15.2.1 To a large extent, the accuracy of the calculated ionospheric parameters depends on the accuracy of the inputs.

15.2.2 The topside plasma scale heights depend on the topside boundary conditions.

15.2.3 Plasma instabilities and bubbles are not taken into account.

15.3 Basis of the Model

The IFM is based on a numerical solution of the ion and electron continuity, momentum, and energy equations. Like the TDIM, the equations are solved versus altitude or along \mathbf{B} for individual convecting flux tubes of plasma, and the three-dimensional nature of the model is obtained by following a large number of plasma flux tubes (typically thousands of flux tubes). The numerical technique used in the solution and the upper and lower boundary conditions are the same as those used in the TDIM. The spatial and temporal resolutions used in the numerical solution are finer than the output resolution.

15.4 Model Input Parameters

The main global inputs for the IFM are the neutral densities, temperatures, and winds; the high-latitude and equatorial electric field distributions; the auroral electron precipitation pattern; and the protonosphere exchange flux and downward electron heat flux at the upper boundary. These global inputs are needed as a function of time. They can be obtained from measurements, empirical models, or physics-based models. In the default setting, the drivers of the IFM (neutral densities, winds, electric fields, and precipitation) are given by empirical models. In this case, the IFM is self-contained and easy to use, being driven by a few simple geophysical indices. The model drivers include $F_{10.7}$, year, day, start time, duration of the model run, and the temporal variation of K_p from 3 hours prior to the start time to the end of the simulation.

15.5 Publication References

15.5.1 Schunk, R.W. (1988), A mathematical model of the middle and high latitude ionosphere, *Pure Appl. Geophys.* 127, 255–303.

15.5.2 Schunk, R.W., J.J. Sojka, and J.V. Eccles (1997), Expanded capabilities for the ionosphere forecast model, *Final Report*, AFRL-VS-HA-TR-98-0001, 1-142.

15.5.3 Sojka, J.J. (1989), Global scale, physical models of the F region ionosphere, *Rev. Geophys.* 27, 371–403.

15.5.4 Sojka, J.J., R.W. Schunk, M.D. Bowline, J. Chen, S. Slinker, J. Fedder, and P. Sultan (1998), Ionospheric storm simulations driven by magnetospheric MHD and empirical models; with data comparisons, *J. Geophys. Res.* 103, 20669–20684.

15.6. Dates of Development and Authors

15.6.1 Dates

1997 Main IFM modifications completed.

1998 Capability for different external drivers added.

2010 Further modifications are in progress.

15.6.2 Authors

Primary authors: R. W. Schunk, J. J. Sojka, and J. V. Eccles.

15.7 Model Codes and Sources

The code is generally not available, but the authors frequently run the model in collaborative studies with other scientists.

16 Ionosphere-Plasmasphere Model (IPM)

16.1 Model Content

The Ionosphere-Plasmasphere Model is a model of the global ionosphere-plasmasphere system (Schunk et al., 2004; Scherliess et al., 2004). The model calculates three-dimensional, time-dependent density distributions for four major ions (NO^+ , O_2^+ , N_2^+ , O^+) at E-region altitudes and three major ions (O^+ , He^+ , H^+) in the F-region and plasmasphere. The IPM, which uses the International Geomagnetic Reference Field (IGRF), covers geomagnetic latitudes from about 60°N to 60°S and equatorial crossing altitudes from 90 to 30,000 km. The IGRF properly accounts for the offset of the geographic and geomagnetic equators and the bending of the B-field lines with latitude. These features are important at low and mid latitudes. The inclusion of He^+ as a major ion is also important because, at Arecibo, it is frequently observed to be a dominant ion in a distinct altitude range and the IPM calculations are consistent with the observations. The spatial resolution of the IPM along \mathbf{B} is about 1 km at E and F region altitudes, 4 km in the topside ionosphere, and 240 km at an altitude of 17,000 km.

16.2 Model Uncertainties and Limitations

16.2.1 To a large extent, the accuracy of the calculated ionosphere and plasmasphere parameters depends on the accuracy of the inputs and model parameters.

16.2.2 Empirical models are typically used to describe the global inputs to the IPM.

16.2.3 Plasma instabilities and bubbles are not taken into account.

16.3 Basis of the Model

The IPM is based on a numerical solution of the ion and electron continuity and momentum equations. The model includes chemical, radiation, and transport processes that are similar to those in the Ionosphere Forecast Model (IFM), but H^+ , He^+ , and interhemispheric transport are taken into account. At E-region altitudes, chemical equilibrium is assumed and the continuity equations for NO^+ , O_2^+ , N_2^+ , and O^+ are solved simultaneously at each grid point for the ion densities. At F-region altitudes and above, a Euler-Lagrange hybrid numerical scheme is used. The continuity and momentum equations for H^+ , O^+ , and He^+ are solved along dipole magnetic field lines for individual plasma flux tubes taking into account corotation, low-latitude electric fields, and interactions with the neutral atmosphere. The field-aligned transport equations are first transformed to spherical coordinates, then dipolar coordinates, and finally to a “sinh” variable (Schunk and Nagy, 2000). Next, the dipolar field lines are adjusted to agree with the IGRF magnetic field. Finally, the plasma flux tubes are followed as they convect through a moving neutral atmosphere perpendicular to \mathbf{B} due to corotational and dynamo electric fields. The three-dimensional nature of the model is obtained by following many plasma flux tubes, while keeping track of their positions at all times.

16.4 Model Input Parameters

The main global inputs for the IPM are the neutral densities, temperatures, and winds; the low-latitude electric field distribution; and the ion and electron temperature distributions. These global inputs are needed as a function of time. Currently the IPM uses the MSIS thermosphere model (Hedin, 1991), the Horizontal Wind Model (Hedin et al., 1991), the Scherliess and Fejer low-latitude drift model (1999), and the Titheridge plasma temperature model (1998).

16.5 Publication References

16.5.1 Hedin, A.E. (1991), Extension of the MSIS thermospheric model into the middle and lower atmosphere, *J. Geophys. Res.* 96, 1159.

16.5.2 Hedin, A.E., et al. (1991), Revised global model of thermospheric winds using satellite and ground-based observations, *J. Geophys. Res.* 96, 7657.

16.5.3 Scherliess, L., and B.G. Fejer (1999), Radar and satellite global equatorial F region vertical drift model, *J. Geophys. Res.* 104, 6829.

16.5.4 Scherliess, L., et al. (2004), Development of a physics-based reduced state Kalman filter for the ionosphere, *Radio Sci.* 39, RS1S04, doi:10.1029/2002RS002797.

16.5.5 Schunk, R.W., et al. (2004). Global assimilation of ionospheric measurements (GAIM), *Radio Sci.* 39, RS1S02, doi:10.1029/2002RS002794.

16.5.6 Schunk, R.W., and A.F. Nagy (2009), *Ionospheres*, second edition, Cambridge University Press, United Kingdom.

16.5.7 Titheridge, J.E. (1998), Temperatures in the upper ionosphere and plasmasphere, *J. Geophys. Res.* 103, 2261.

16.6 Dates of Development and Authors

16.6.1 Dates

2004 The core IPM model completed.

2010 Further modifications are in progress.

16.6.2 Authors

Primary authors: R. W. Schunk, L. Scherliess, D. C. Thompson, and L. Zhu.

16.7 Model Codes and Sources

The code is not available, but the authors are willing to run the model in collaborative studies with other scientists.

17 Ionosphere–Polar Wind Model (IPWM)

17.1 Model Content

The Ionosphere–Polar Wind Model is a time-dependent, three-dimensional, multi-ion model of the global ionosphere–polar wind system that covers the altitude range from 90 to 9000 km at latitudes greater than 50° magnetic (Schunk and Sojka, 1989, 1997). The numerical model yields density distributions for electrons and several ions (NO^+ , O_2^+ , N_2^+ , O^+ , H^+) as a function of latitude, longitude, and altitude. The model also calculates the isotropic electron temperature, the ion temperatures parallel and perpendicular to the magnetic field, and the plasma drift velocities on the same grid. The spatial resolution is 4 km in the E-region and 10 km in and above the F-region.

17.2 Model Uncertainties and Limitations

17.2.1 The accuracy of the calculated ionosphere and polar wind parameters depends on the accuracy of the inputs, including the magnetospheric electric field, the auroral precipitation patterns, and the neutral densities, temperatures, and winds.

17.2.2 Kinetic processes and high-altitude acceleration processes are not included.

17.2.3 Plasma instabilities and wave-particle interactions are not taken into account.

17.3 Basis of the Model

At low altitudes (90–800 km), three-dimensional distributions for the electron and ion (NO^+ , N_2^+ , O_2^+ , O^+ , He^+) densities, temperatures (T_e , T_i), and drifts are obtained from a numerical solution of the time-dependent continuity, momentum, and energy equations (e.g., the Ionosphere Forecast Model, IFM). The equations are solved in the collision-dominated limit, where ordinary diffusion and thermal conduction prevail. Therefore, the differential equations solved are coupled, second-order, parabolic, partial differential equations. At high altitudes (800–9000 km), the time-dependent, nonlinear, continuity, and momentum equations for O^+ , H^+ , and electrons are solved self-consistently with the ionosphere equations, taking into account collisions, charge exchange chemical reactions, gravity, electrostatic forces, and magnetic field divergence. The equations are non-linear, first-order, hyperbolic, partial differential equations. Chemical equilibrium and local heating and cooling processes are assumed to dominate at the lower boundary (90 km). Plasma outflow is assumed at the upper boundary (9000 km).

The model can describe supersonic flow, shock formation, low-frequency wave phenomena, and ion energization associated with expanding plasmas. The equations describing the coupled ionosphere–polar wind system are solved along \mathbf{B} for individual convecting flux tubes of plasma, and hence, the three-dimensional nature of the ionosphere–polar wind model is obtained by following many plasma flux tubes. In simulations of the storm-time dynamics of the ionosphere–polar wind system, more than 1000 flux tubes are followed, which yields a spatial resolution of less than 200 km in the polar cap (Demars and Schunk, 2002); for studies involving plasma structures such as propagating polar wind jets, 1500 flux tubes are followed (Schunk et al., 2005).

17.4 Model Input Parameters

The main global inputs for the IPWM are the neutral densities, temperatures, and winds; the high-latitude electric field distribution; the auroral electron precipitation pattern; and the downward electron heat flux at the upper boundary. These global inputs are needed as a function of time. They can be obtained from measurements, empirical models, or physics-based models.

17.5 Publication References

17.5.1 Demars, H.G., and R.W. Schunk (2002), Three-dimensional velocity structure of the polar wind, *J. Geophys. Res.* 107, 1250, doi:10.1029/2001JA000252.

17.5.2 Schunk, R.W., H.G. Demars, and J.J. Sojka (2005), Propagating polar wind jets, *J. Atmos. Solar-Terr. Phys.* 67, 357.

17.5.3 Schunk, R.W., and J.J. Sojka (1989), A three-dimensional time-dependent model of the polar wind, *J. Geophys. Res.* 94, 8973.

17.5.4 Schunk, R.W., and J.J. Sojka (1997), Global ionosphere-polar wind system during changing magnetic activity, *J. Geophys. Res.* 102, 11625.

17.6 Dates of Development and Authors

17.6.1 Dates

1989 Main IPWM code constructed.

2000 1000–1500 plasma flux tubes followed for high-resolution simulations.

17.6.2 Authors

Primary authors: R. W. Schunk and J. J. Sojka

17.7 Model Codes and Sources

The code is not user-friendly and is not available, but the authors will run the model in collaborative studies with other scientists.

DRAFT--For Public Review Only--Dec 2013

18 Ionosphere–Polar Wind–PIC (IPW-PIC) Model

18.1 Model Content

The Ionosphere–Polar Wind–Particle-In-Cell (PIC) Model is a time-dependent, three-dimensional, multi-ion model of the global ionosphere–polar wind system that covers the altitude range from 90 to several Earth radii at latitudes greater than 50° magnetic (Barakat and Schunk, 2006). The numerical model yields electron and ion (NO^+ , O_2^+ , N_2^+ , O^+ , H^+) density, drift velocity, and temperature distributions as a function of altitude, latitude, and longitude from a fluid formulation for altitudes from 90 to 1200 km. Above 1200 km, the ions are described by a macroscopic PIC method, which can describe both fluid and kinetic plasma processes. The model not only yields the standard transport parameters (densities, drift velocities, parallel and perpendicular temperatures, etc.), but also the ion velocity distributions. The three-dimensional nature of the model is obtained by following a large number of convecting plasma flux tubes.

18.2 Model Uncertainties and Limitations

18.2.1 The accuracy of the calculated ionosphere and polar wind parameters depends on the accuracy of the inputs, including the magnetosphere electric field configuration, the auroral precipitation pattern, and the neutral densities, temperatures, and winds.

18.2.2 Millions of ions are needed for each plasma flux tube in order to calculate accurate velocity distribution functions at high altitudes.

18.2.3 More than 1000 plasma flux tubes are needed to get a horizontal spatial resolution less than 200 km in the polar cap at F-region altitudes. At altitudes above the F-region, the horizontal resolution is more than 200 km because the geomagnetic field diverges with altitude.

18.3 Basis of the Model

The IPW-PIC model is composed of two components: a fluid ionosphere–polar wind model from 90–1200 km (Schunk and Sojka, 1989, 1997) and a macroscopic PIC model from 1200 km to several Earth radii (Barakat and Schunk, 2001, Barakat et al., 2003). With the coupled model, the relevant equations are solved along magnetic flux tubes that convect across the high-latitude region. Typically, 1000 plasma flux tubes are followed and more than one million particles per flux tube are needed, which means that each simulation includes more than one billion particles. In general, the simulated plasma consists of H^+ and O^+ ions as well as cold (ionosphere) and hot (magnetosphere) electron populations. The ions are treated kinetically, while the electrons are assumed to obey the Boltzmann relation. The effects of gravity, polarization, electrostatic field, magnetic mirror force, centripetal acceleration, ion self-collisions, low-altitude auroral ion energization, and wave-particle interactions are considered. Also, the IPW-PIC model properly accounts for the $\mathbf{E} \times \mathbf{B}$ drift of the plasma flux tubes. The computing-intensive nature of the model requires utilization of supercomputers with thousands of processors. A three-dimensional picture is assembled from the temporal evolution of the individual flux tubes by keeping track of their locations.

18.4 Model Input Parameters

The main global inputs for the IPW-PIC model are the neutral densities, temperatures, and winds; the high-latitude electric field distribution; the auroral electron precipitation pattern; and the hot magnetosphere electron population. These global inputs are needed as a function of time. They can be obtained from measurements, empirical models, or physics-based models.

18.5 Publication References

18.5.1 Barakat, A.R., and R.W. Schunk (2001), Effects of wave-particle interactions on the dynamic behavior of the generalized polar wind, *J. Atmos. Solar-Terr. Phys.* 63, 75-83.

18.5.2 Barakat, A.R., R.W. Schunk, and H.G. Demars (2003), Seasonal and solar activity dependence of the generalized polar wind with low-altitude auroral ion energization, *J. Geophys. Res.* 108(A11), 1405, doi:10.1029/2002JA009360.

18.5.3 Barakat, A.R., and R.W. Schunk (2006), A three-dimensional model of the generalized polar wind, *J. Geophys. Res.* 111(A12314), doi:10.1029/2006JA011662.

18.5.4 Schunk, R.W., and J.J. Sojka (1989), A three-dimensional time-dependent model of the polar wind, *J. Geophys. Res.* 94, 8973.

18.5.5 Schunk, R.W., and J.J. Sojka (1997), Global ionosphere-polar wind system during changing magnetic activity, *J. Geophys. Res.* 102, 11625.

18.6 Dates of Development and Suthors

18.6.1 Dates

2003 Main Polar Wind-PIC code constructed.

2006 1000 plasma flux tubes followed for high-resolution storm simulation.

18.6.2 Authors

Primary authors: A. R. Barakat and R. W. Schunk.

18.7 Model Codes and Sources

The code is not user-friendly and is not available, but the authors will run the model in collaborative studies with other scientists.

19 Thermosphere-Ionosphere Forecast Model (TIFM)

19.1 Model Content

The Thermosphere-Ionosphere Forecast Model (TIFM) is a global model of the upper atmosphere that is composed of a global thermosphere model coupled to a global ionosphere model (Ma and Schunk, 1995; Schunk and Demars, 2003, 2005; Schunk et al., 2008). The thermosphere model calculates three-dimensional, time-dependent, high-resolution distributions of the neutral mass density, individual densities (N_2 , O_2 , O), temperature, and three components of the neutral wind at altitudes from 90 to 500 km. The spatial resolution in the model is adjustable. Frequently, global simulations are conducted with a horizontal resolution of 0.5° in latitude and 3° in longitude (50 km resolution in the polar caps), but runs have been conducted with $3^\circ \times 5^\circ$ and test simulations with $0.1^\circ \times 5^\circ$ (12 km resolution in latitude, pole-to-pole). In the vertical direction (90–500 km), the layers are distributed non-uniformly according to the neutral gas scale height, and typically 49 or 60 layers are used. The thermosphere model can describe subsonic, transonic, and supersonic flows, and wave phenomena, including shock waves. The model can also take account of planetary, tidal, and other waves that propagate up from the lower atmosphere. The thermosphere model can be driven by, or coupled to, different global ionosphere models, including time-dependent, empirical ionosphere models and time-dependent, self-consistent, numerical ionosphere models.

The TIFM can account for small-scale (50–100 km) features. The model has been used to calculate the thermosphere's response to sub-auroral ion drift events, single and multiple propagating plasma patches, circular and cigar-shaped plasma patches, single and multiple sun-aligned polar cap arcs, theta aurora, equatorial plasma bubbles, and the cusp neutral fountain. The model has also successfully described the supersonic neutral winds that are observed in the polar caps during strong plasma convection. In addition, the TIFM was able to properly describe the upward propagation of migrating tides and large-scale gravity waves from the lower atmosphere, as well as traveling atmospheric disturbances (TADs) excited during pulsating magnetic storms (see Schunk et al., 2008; Gardner and Schunk, 2010; and references therein).

19.2 Model Uncertainties and Limitations

2.1 To a large extent, the accuracy of the parameters calculated by the TIFM depends on the accuracy of the inputs.

2.2 Minor species are not calculated.

2.3 Instabilities and wave turbulence are not taken into account.

19.3 Basis of the Model

The thermosphere model calculates a simultaneous solution of the neutral gas continuity, momentum, energy, and mean mass equations, which produces global distributions of the mass density, individual densities for the major species, temperature, and all three components of the neutral wind at altitudes from 90 to 500 km. The equations are solved in a spherical coordinate system fixed to the Earth using a multidimensional flux-corrected transport (FCT) technique. The equations take account of the non-linear inertia term, pressure gradients, the Coriolis force, centripetal acceleration, ion-neutral collisions, advection, thermal conduction, exothermal chemical reactions, auroral heating, solar heating, several local cooling processes, and the displacement between the geographic and geomagnetic poles. The model uses altitude, not a pressure coordinate, in the vertical direction and non-hydrostatic equilibrium flows are allowed. The FCT method is a well-known numerical technique that was designed to handle subsonic, transonic, and supersonic flows, as well as wave phenomena and shocks. Planetary, tidal, and other waves that propagate up from the lower atmosphere can be taken into account at the lower boundary (90 km).

19.4 Model Input Parameters

The main global inputs for the TIFM model are the high-latitude and equatorial electric field distributions and the auroral electron precipitation distribution. These global inputs are needed as a function of time. They can be obtained from measurements, empirical models, or physics-based models. The TIFM has frequently been run with a time-dependent empirical ionosphere model. Specifically, runs have been conducted using the International Reference Ionosphere (IRI; Bilitza, 1990) to obtain the global ion density distributions. In addition to the IRI background ionosphere, ionization due to auroral particle precipitation was accounted for by using the method of Roble and Ridley (1987). In these simulations, there was no feedback from the thermosphere model to the ionosphere.

19.5 Publication References

19.5.1 Bilitza, D., (Ed.) (1990), International reference ionosphere 1990, *Rep. NSSDC 90-22*, National Space Science Data Center, Greenbelt, MD.

19.5.2 Gardner, L.C., and R.W. Schunk (2010), Generation of traveling atmospheric disturbances during pulsating geomagnetic storms, *J. Geophys. Res.* (115).

19.5.3 Ma, T.-Z., and R.W. Schunk (1995), Effect of polar cap patches on the polar thermosphere, *J. Geophys. Res.* 100, 19,701.

19.5.4 Roble, R.G., and E.C. Ridley (1987), An auroral model for the NCAR thermospheric general circulation model (TGCM), *Ann. Geophys.* 5A, 369-382.

19.5.5 Schunk, R.W., and H.G. Demars (2003), Effect of equatorial plasma bubbles on the thermosphere, *J. Geophys. Res.* 108(A6), 1245.

19.5.6 Schunk, R.W., and H.G. Demars (2005), Thermospheric weather due to mesoscale ionospheric structures, *Proceedings of the 2005 Ionospheric Effects Symposium*, JMG Associates, National Technical Information Services, Springfield, VA.

19.5.7 Schunk, R. W., et al. (2008), Effect of lower atmospheric waves on the ionosphere and thermosphere, *Proceedings of the 2008 Ionospheric Effects Symposium*, JMG Associates, National Technical Information Services, Springfield, VA.

19.6 Dates of Development and Authors

19.6.1 Dates

1995 Main TIFM model completed.

2008 Coupling of the global thermosphere model to the Ionosphere Forecast Model.

2013 Further modifications are in progress.

19.6.2 Authors

Primary authors: T.-Z. Ma, R. W. Schunk, and L. Gardner.

19.7 Model Codes and Sources

The code is generally not available, but the authors will run the model in collaborative studies with other scientists.

20 NRL SAMI2/SAMI3 Models

20.1 Model Content

SAMI2 (a Two-Dimensional Model of the Ionosphere) and SAMI3 (a Three-Dimensional Model of the Ionosphere) are first-principle physics models of the earth's ionosphere. SAMI2 models the mid-latitude ionosphere in a plane of magnetic longitude from 90–20,000 km. SAMI3 models the global three-dimensional ionosphere over a magnetic latitude range $\pm 89^\circ$.

20.2 Basis of the Model

SAMI2 and SAMI3 describe the dynamic plasma and chemical evolution of seven ion species (H^+ , He^+ , N^+ , O^+ , N_2^+ , NO^+ , and O_2^+). The ion continuity and momentum equations are solved for all seven ion species. Thermal balance equations are solved for three ion species (H^+ , He^+ , and O^+) and for the electrons. SAMI2 and SAMI3 use a non-orthogonal, non-uniform, fixed grid. The grid is designed to optimize the numerical mesh so that the spatial resolution decreases with increasing altitude. The plasma is transported transverse to the geomagnetic field using a finite volume method in conjunction with the donor cell method. The models include the $\mathbf{E} \times \mathbf{B}$ drift of the plasma and ion inertia in the ion momentum equations for plasma motion along the dipole field line.

20.3 Model Inputs

The neutral atmosphere is specified using empirical codes (e.g., NRLMSISE00 and HWM93/HWM07) or a global circulation model (e.g., TIMEGCM). The $\mathbf{E} \times \mathbf{B}$ drift can be specified analytically or from the Fejer-Scherliess model in both SAMI2 and SAMI3. Additionally, there is a version of SAMI3 that calculates the $\mathbf{E} \times \mathbf{B}$ drift self-consistently from a potential equation. SAMI2 and SAMI3 can use several models to specify the ionizing radiation from the sun: EUVAC, NRLEUV, and FISM.

20.4 Publication References

20.4.1 Huba, J.D., K.F. Dymond, G. Joyce, S.A. Budzien, S.E. Thonnard, J.A. Fedder, and R.P. McCoy (2002), Comparison of O^+ density from ARGOS data analysis and SAMI2 model results, *Geophys. Res. Lett.* 29, doi:10.1029/2001GL013089.

20.4.2 Huba, J.D., G. Joyce, and J.A. Fedder (2000), Sami2 is another model of the ionosphere (SAMI2): A new low-latitude ionosphere model, *J. Geophys. Res.* 105, 23,035-23,053.

20.4.3 Huba, J.D., H.P. Warren, G. Joyce, X. Pi, and B. Iijima (2005), Global response of the low- to mid-latitude ionosphere due to the Bastille Day Flare, *Geophys. Res. Lett.* 32, L15103, doi:10.1029/2005GL02329.

20.5 Authors

Primary author: J.D. Huba (huba@ppd.nrl.navy.mil).

20.6 Model Codes and Sources

SAMI2/3 are written in Fortran-77 and have been developed on a Linux system. They have been tested using the Absoft, Lahey, and Portland Group Fortran compilers. The codes are fully parallelized using the Message Passing Interface (MPI) method, which is critical to computational efficiency for large-scale simulations.

A single processor version of SAMI2 is available online. The URL for the SAMI2 Open Source Project is <http://wwwppd.nrl.navy.mil/sami2-OSP/>. The web site is divided into a number of sections: Home, Introduction, Ionospheric Physics, Registration/Download, Source Code Description, Tutorial, Graphics, Feedback, Publications, License, and Notice. There is sufficient information to get the code running and to view the output using IDL.

21 Texas Reconfigurable Ionosphere-Plasmasphere Logarithmic Data Assimilator (TRIPL-DA)

21.1 Model Content

The Texas Reconfigurable Ionosphere Plasmasphere Logarithmic Data Assimilator (TRIPL-DA) is an objective analysis algorithm based upon three-dimensional variational data assimilation. TRIPL-DA is a successor algorithm to the Ionospheric Data Assimilation Three-Dimensional (IDA3D) algorithm (Bust et al., 2004), which evolved from the ionospheric tomography techniques developed at the Applied Research Laboratories, the University of Texas at Austin (ARL: UT).

TRIPL-DA generates three-dimensional coherent maps (or specifications) of the Earth's ionospheric electron density on a user-provided grid. Like all objective analysis algorithms, TRIPL-DA generates these maps from a synthesis of a background density specific (from either a theoretical or empirical model) and all available electron density and electron content measurements.

21.2 Model Uncertainties and Limitations

The main uncertainty in TRIPL-DA is the error and correlation estimates. Most background models produce reasonable density distribution, but do not produce quantitative error estimates at all grid points (though some empirical models do). Similarly, the errors, and the correlations among these errors, represent the physics and chemistry not included within the background model, usually because the physics is not understood well enough to model.

The other major uncertainty is the observation error, of which the dominant term is representativeness error. This is the error created by the observation of density structures on scale sizes smaller than the TRIPL-DA grid.

21.3 Basis of the Model

TRIPL-DA is based upon three-dimensional variational data assimilation. This mathematical technique is similar to a least squares fit between the full set of observations and a background specification. As with all analysis algorithms, the observations are interpolated onto a predetermined grid, which allows the measurements to be shown collectively, and larger scale (larger than a single observation) phenomena to be observed. 3DVAR not only uses the specification and observation errors, but also includes the correlation between grid points. Ideally, the observations completely span the system, and 3DVAR (and hence IDA3D) is only an interpolation algorithm. However, such data sets do not exist, so a background specification is needed to complete the system.

21.4 Model Inputs

TRIPL-DA is designed for flexibility. As a consequence, it requires numerous inputs. These include a background electron density specification with error estimates, an estimate of the inherent correlations within the ionosphere, a set of ionospheric density and electron content measurements (with error estimates) that is large enough to span the physics of interest, and a user-provided grid on the scale of interest. The grid can be either regional or global so long as it is large enough to include a sufficient number of observations to drive the specification. Similarly, the grid resolution is user dependent, but TRIPL-DA cannot resolve phenomena on scales smaller than the intrinsic scale of the observations.

21.5 Publication References

21.5.1 Bust, G.S., T.W. Garner, and T.L. Gaussiran II (2004), Ionospheric Data Assimilation Three-Dimensional (IDA3D): a global, multisensor, electron density specification algorithm, *J. Geophys. Res.* 109, doi:10.1029/2003JA010234.

21.5.2 Garner, T.W., G.S. Bust, T.L. Gaussiran II, and P.R. Strauss (2006), Variations in the mid-latitude and equatorial ionosphere during the October 2003 magnetic storm, *Radio Sci.* 41, doi:10.1029/2005RS003399.

21.5.3 Bust, G.S., G. Crowley, T.W. Garner, T.L. Gaussiran II, R.W. Meggs, C.N. Mitchell, P.S.J. Spencer, P. Yin, and B. Zapfe, Four-dimensional GPS imaging of space weather storms, *Space Weath.* 5, doi:10.1029/2006SW000237.

21.6 Dates of Development, Authors, and Sponsors

21.6.1 Dates

1993–1998 Development of ionospheric tomography techniques.
1999 IDA3D developed in IDL to solve for the electron density.
2001 IDA3D version 1 released in Fortran-90.
2003 The algorithm is formulated to work with the log of the electron density.
2003 MPI implementation released.
2010 TRIPL-DA version 1 released.

21.6.2 Authors

T. L. Gaussiran, T. W. Garner, R. Calfais, D. Munton, and D. Rainwater.

21.7 Model Codes and Sources

The code has been developed in Fortran-90 using numerous separate modules, and is intended to run over several processors at one time. Collaborations are welcome; interested parties should contact Thomas Gaussiran (gauss@arlut.utexas.edu) or Trevor Garner (garner@arlut.utexas.edu).

22 Ionospheric Data Assimilation Four-Dimensional (IDA4D)

22.1 Model Content

Ionospheric Data Assimilation Four-Dimensional (IDA4D) (Bust et al., 2000, 2004) provides the global three-dimensional, time-evolving distribution of the ionospheric electron density. IDA4D is an ionospheric data assimilation algorithm that has been in development for over 15 years. It takes in a wide variety of data sources, and produces an estimate of the log of the electron density, along with a formal estimate of the 1-sigma error levels. IDA4D predicts forward in time with either a Gauss-Markov Kalman Filter or a continuity equation forward model. The forward model allows for ingestion of data-driven estimates (AMIE, SuperDARN, equatorial radars, and magnetometers) of electric fields to drive the transport. The user can select which type of forward prediction is desired.

IDA4D currently obtains the global electron density distribution with a spatial resolution of ~100–500 kilometers horizontally and 10–50 kilometers vertically. The temporal cadence is user selectable and only limited by the cadence of the data collected. Typical cadences are 5 min, but this could be made as short as a few seconds if necessary to support the science or application. These three-dimensional images are typically updated every 5 min, providing continuous global four-dimensional estimates of electron density over hours or days. The code is suitable for applications requiring accurate specification of the ionospheric bottomside for HF propagation, among other applications, and can be run in real-time.

22.2 Model Uncertainties and Limitations

The main uncertainties in IDA4D are the background model prediction of electron density and mis-specification of the model error-covariances. A secondary source of uncertainty are data errors (primarily mis-specification of the representation errors) and bad data getting through the quality control algorithms. Since the user has complete control of model and error-covariance inputs, several runs can be computed with different model and covariance inputs to determine the robustness of the solution.

The IDA4D algorithm has been well documented in the literature (Bust et al., 2004, 2007; Bust and Mitchell, 2008). It has been used in several scientific studies (Nicolls et al., 2009; Datta-Barua et al., 2009; Bust and Crowley, 2007, 2008; Bust et al., 2007), and has been well validated (e.g., Coker et al., 2001; Watermann et al., 2002). Recently a study was undertaken where IDA4D results were compared to *in situ* measurements of plasma density in the F-region from the CHAMP satellite (Bust et al., 2011). Four separate months in 2007 and 2008 were analyzed, with the overall RMS error of the IDA4D specification ~20–25% for F-region densities.

22.3 Basis of the Model

IDA4D is based on a 3DVAR maximum likelihood estimate (Daley and Barker, 2001) method. IDA4D solves for the log of electron density to guarantee a positive definite electron density field, and because electron densities have been shown to be more likely to obey log-normal statistical distributions. The IDA4D solution can be derived by minimizing the following cost function J:

$$J = 0.5[\bar{y} - \tilde{H}\bar{x}_a]^T \tilde{R}^{-1}[\bar{y} - \tilde{H}\bar{x}_a] + 0.5[\bar{x}_f - \bar{x}_a]^T \tilde{P}_f^{-1}[\bar{x}_f - \bar{x}_a]$$

where the data is given by the vector \bar{y} , \tilde{H} is the geometry matrix connecting the unknown electron density field (\bar{x}_a) to the data, \tilde{R} is the data error-covariance (including representation errors), \bar{x}_f is the model forecast of electron density, and \tilde{P}_f is the forecast model error-covariance. The solution is obtained via non-linear iterations. The m^{th} iterative solution for the analyzed electron density is given as

$$\mathbf{x}_a^m = \mathbf{x}_a^{m-1} + \tilde{\mathbf{P}}_f (\tilde{\mathbf{H}}^{m-1})^T [\tilde{\mathbf{R}} + \tilde{\mathbf{H}}^{m-1} \tilde{\mathbf{P}}_f (\tilde{\mathbf{H}}^{m-1})^T]^{-1} [\mathbf{y} - \mathbf{H}(\mathbf{x}_a^{m-1}) + \tilde{\mathbf{H}}^{m-1}(\mathbf{x}_a^{m-1} - \mathbf{x}_f)]$$

When the final solution has been obtained, the solution is output along with a formal estimate of the error.

22.4 Model Inputs

22.4.1 Data sources

IDA4D can ingest a wide variety of observations from various data sources and types. The observations can be linearly or non-linearly related to electron density. Some observations (6300 Angstrom all-sky images, for example) include parameters that need to be modeled (neutral densities). These parameters are typically modeled by TIMEGCM or a combination of empirical models (IRI, MSIS). The current version of IDA4D accepts the following data sources:

- Ground-based GPS TEC
- Ground-based DORIS TEC
- Ground-based Ionosonde non-linear virtual height versus frequency observations
- Ground-based ISR electron densities
- Ground-based bi-static HF non-linear time-delay versus frequency observations
- Ground-based 6300/7774 Angstrom all-sky imager observations
- Satellite-based GPS TEC occultation observations
- Satellite-based Topside, over-satellite electron content GPS TEC
- Satellite-based *in-situ* electron densities
- Satellite-based 1356 Angstrom radiances

22.4.2 Grid, model, and error covariances

One of the powerful features of IDA4D is that the inversion grid is user-selectable and need not be regular. The IDA4D horizontal grid (latitude and longitude) is a completely arbitrary (irregular) grid. Latitudes and longitudes are simply considered an array of ordered pairs of positions, while the vertical grid is given by a regular array of altitude points. The user has the ability to completely specify the IDA4D grid via an input netcdf file.

IDA4D allows for any type of initial background model specification since the model is ingested simply as a netcdf file. Typical models used by IDA4D include TIMEGCM, IRI (including a plasmaspheric version), and SAMI2. In addition to the background model specification of electron density, the background model and data error covariances are required. IDA4D has a sophisticated internal model for the background model variances and spatial correlations, and it allows the user to input all the correlation and variance parameters via a netcdf file.

22.5 Publication References

22.5.1 Bust, G.S., D. Coco, and J. Makela (2000), Combined ionospheric campaign 1: ionospheric tomography and GPS total electron count (TEC) depletions, *Geophys. Res. Lett.* 27(18), 2849-2852.

22.5.2 Bust, G.S., T.W. Garner, and T.L. Gaussiran II (2004), Ionospheric Data Assimilation Three-Dimensional (IDA3D): a global, multisensor, electron density specification algorithm, *J. Geophys. Res.* 109, doi:10.1029/2003JA010234.

22.5.3 Bust, G.S., G. Crowley, T.W. Garner, T.L. Gaussiran II, R.W. Meggs, C.N. Mitchell, P.S.J. Spencer, P. Yin, and B. Zapfe, Four-dimensional GPS imaging of space weather storms, *Space Weath.* 5, doi:10.1029/2006SW000237.

22.5.4 Bust, G.S. and G. Crowley (2007), Tracking of polar cap patches using data assimilation, *J. Geophys. Res.* 112, A05307, doi:10.1029/2005JA011597.

22.5.5 Bust, G.S., and G. Crowley (2008), Mapping the time-varying distribution of high-altitude plasma during storms, in *Midlatitude Ionospheric Dynamics and Disturbances*, *Geophys. Monogr. Ser.*, vol. 181, edited by P.M. Kintner, A.J. Coster, T. Fuller Rowell, A.J. Mannucci, M. Mendillo, and R. Heelis, pp. 91-98, AGU, Washington, DC.

22.5.6 Bust, G.S., and C.N. Mitchell (2008), The history, current state, and future directions of ionospheric imaging, *Rev. Geophys.* 46, RG1003, doi:10.1029/2006RG000212.

22.5.7 Bust, G.S., R. Bishop, and G. Crowley, Comparison of CHAMP in-situ electron densities with

IDA4D estimates of electron density, *Radio Sci.*, in preparation.

22.5.8 Coker, C., G. Kronschnabl, D.S. Coco, G.S. Bust, and T.L. Gaussiran II (2001), Verification of ionospheric sensors, *Radio Sci.* 36(6), 1523–1529.

22.5.9 Daley R., and E. Barker (2001), NAVDAS: formulation and diagnostics, *Month. Weath. Rev.* 129, 869-883.

22.5.10 Datta-Barua, S., G.S. Bust, G. Crowley, and N. Curtis (2009), Neutral wind estimation from 4-D ionospheric electron density images, *J. Geophys. Res.* 114, A06317, doi:10.1029/2008JA014004.

22.5.11 Nicolls, M.J., F.S. Rodrigues, G.S. Bust, and J.L. Chau (2009), Estimating E region density profiles from radio occultation measurements assisted by IDA4D, *J. Geophys. Res.*, doi:10.1029/2009JA014399

22.6 Dates of Development and Authors

22.6.1 Dates

1993–1998 Development of ionospheric tomography techniques.

1999 IDA3D developed in IDL to solve for the electron density.

2001 IDA3D version 1 released in Fortran-90.

2003 The algorithm is formulated to work with the log of the electron density.

2003 MPI implementation released.

2007 Continuity equation forward modeling added (name changed to IDA4D).

2007 Non-linear ionosonde and HF data added to IDA4D.

2008 6300/7774 and 1356 data added to IDA4D.

22.6.2 Authors: G. S. Bust, G. Crowley, F. Rodrigues, A. Reynolds, and N. Curtis.

22.7 Model Codes and Sources

The code has been developed in Fortran-90 using numerous separate modules, and is intended to run over several processors at one time. The code is not user-friendly, but runs can be made at ASTRA for collaborations. Interested parties should contact Gary Bust (gbust@astraspace.net) or Geoff Crowley (gcrowley@astraspace.net).

23 Incoherent Scatter Radar Ionospheric Models (ISRIMs)

23.1 Model Content

As one of the most powerful ground-based instruments for probing the Earth's upper atmosphere, incoherent scatter radar (ISR) directly measures ionospheric electron density N_e , electron and ion temperatures T_e and T_i , and line-of-sight ion velocity over a broad height range. Empirical ionospheric models have been developed from long-term datasets of seven ISRs in American, European, and Asian longitudes. These models output N_e , T_e , T_i , and ion drifts in the E- and F-regions, providing a quantitative description of ionospheric properties. The models are fully described by Zhang et al. (2007, 2008) and are briefly described here.

23.1.1 ISRIM local climatology models

Ionospheric local climatology for the ISR sites is listed below (see Table 3). Variations as a function of the time of day, season, solar activity, and geomagnetic activity are included. Model parameters are N_e , T_e , and T_i . Parallel ion drift models have also been developed for Sondrestrom, Millstone, and Arecibo.

Table 3 — Local climatology for ISR sites

Station	Latitude	Longitude	Invariant Latitude	Heights/km
Svalbard	78.1	16.0	74.9	100–500
Sondrestrom	67.0	309.0	73.2	100–500
Tromso	69.6	19.2	66.4	100–500
Millstone	42.6	288.5	53.4	100–1000
St. Santin	44.6	2.2	46.3	100–500
Arecibo	18.3	293.2	32.2	100–500
Shigaraki	34.8	136.1	24.5	200–500

23.1.2 ISRIM regional climatology models

The ISR at Millstone Hill operates with a fully steerable antenna that provides a geographical latitudinal coverage of 35–55° in the subauroral region. Corresponding models (Millstone Hill Regional Models) are available for N_e , T_e , and T_i for 200–600 km heights.

The American Regional Model (ARM) is a result of combining ISR data from the above sites in Eastern America to represent latitudinal changes within 18–78°N geodetic for 100–500 km height range. The models of N_e , T_e , and T_i vary also with local time, season, solar, and magnetic activity.

23.1.3 ISRIM local variability models

ISRIM local variability models are similar to their corresponding local climatology models. The ISRIM local variability models are based on the difference between the ISRIM local climatology and the individual measurements that were used for constructing the ISRIM climatology. For any given time, season, and height, the squared difference is expressed as a function of a constant background term and linear terms of solar flux and magnetic activity.

23.1.4 ISRIM high-latitude convection model

The model provides high-latitude (between invariant latitudes 55° and 78°) convection speed and potential patterns, regional to America Sector. The convection speed and potential patterns represent average and steady patterns of the convection as driven by the IMF B_Y and B_Z or by the K_p and the B_Y

direction. The model varies with season. Long-term observations from Millstone Hill and Sondrestrom ISRs were used for creating the model.

23.2 Model Uncertainties and Limitations

Compared to other ground-based instruments, ISRs operate less frequently. Particularly, the ISR database has limited data for E- and lower F-regions at night. Due to sparse data, the model dependency on magnetic activity may not be accurate enough. Comparisons between ISRIMs and IRI were made (Zhang et al., 2007), and indicated a reasonable agreement in N_e and T_i , but not quite in T_e . Dependency of T_e on solar activity, which is not included in IRI, is complicated and hard to model well.

23.3 Basis of the Model

ISRIMs were obtained from a bin-fit technique. For local climatology (variability) models, the ISR data are binned by month and local time with 3 month and 1 hr bin sizes. In this initial step of data binning, we assume a linear variation between any two consecutive altitude nodes. The constant and linear coefficient in the linear equation for each height segment is then calculated. Each constant and linear coefficient is further assumed to be linear in the solar activity index $F_{10.7}$ and magnetic activity index 3-hourly A_p . A sequential least squares fit to the solar and magnetic activity dependence and to the piecewise-linear function for altitude dependence is then performed, generating coefficients for the constant, $F_{10.7}$, and A_p terms. The initial binning results are then represented by a three-dimensional basis with a cubic B-spline function to give twice-differentiable height variations, and harmonics with 12-, 6-, and 4-month periodicities for seasonal changes, and with 24-, 12-, 8-, and 6-hr periodicities for local time changes. This process is applied to N_e , T_e , and T_i for each ISR site.

Local models from similar longitudes in America are combined to form an American Regional Model (ARM) using appropriate mathematical approximations. Harmonics with 24-, 12-, 8-, and 6-hr components, and with annual and semiannual components, cubic B-splines with nine breaks for height variations between 100 and 500 km, and cubic B-splines with seven breaks between geodetic latitudes 18° and 78° for latitudinal variations are used to give analytical representations of seasonal, local time, height, and latitudinal variations. $F_{10.7}$ and A_p are used to control solar activity and magnetic activity effects.

High-latitude convection models and patterns have been obtained based on a composite analysis of ISR observations at Millstone Hill and Sondrestrom. These observations span a combined latitude range between 55° and 78° . The vector velocity, derived from the radar line-of-sight measurements and giving the electric field, is fitted to generate patterns of electrostatic potentials, which are expressed as a periodic bicubic spline function in apex magnetic altitude and apex magnetic local time. The spline has knots distributed at 3-hr and 3° intervals. The fit is extended over the polar cap by solving Laplace's equation.

23.4 Database

All ISR data were obtained from the Madrigal database. Data up to December 2004 have been used. The number of experiments for Svalbard (operational since 1996) was over 600, for Sondrestrom (operational since 1983) over 1000, for the EISCAT Tromso (operational since 1981) over 1200 (over 900 for the UHF radar), for Millstone Hill (operational since 1960) over 1000 experiments, for St. Santin (operational during 1963–1987) about 100 experiments, for Shigaraki (operational since 1986) about 200 experiments, and for Arecibo (operational since 1963) over 100 experiments. At high latitudes, data were sparse in the summer, as compared to other seasons. St. Santin had the least amount of data, but they were nearly equally distributed by month. Outside the polar and auroral areas, there was considerably more F-region data than E-region data.

23.5 Publication References

23.5.1 Zhang S.-R., and J.M. Holt (2008a), Climatology and variability of the ionosphere: incoherent scatter radar observations, CP974, *Radio sounding and plasma physics*, edited by P. Song, J. Foster, M. Mendillo, and D. Bilitza, American Institute of Physics, pp. 71–80. doi:10.1063/1.2885035.

23.5.2 Zhang, S.-R., and J.M. Holt (2008b), Ionospheric climatology and variability from long-term and multiple incoherent scatter radar observations: variability, *Ann. Geophys.* 26, 1525–1537.

23.5.3 Zhang, S.-R., J.M. Holt, D. Bilitza, et al. (2007), Multiple-site comparisons between models of incoherent scatter radar and IRI, *Adv. Space Res.* 39, 910–917, doi:10.1016/j.asr.2006.05.027.

23.5.4 Zhang, S.-R., and J.M. Holt (2007), Ionospheric climatology and variability from long-term and multiple incoherent scatter radar observations: climatology in eastern American sector, *J. Geophys. Res.* 12, A06328, doi:10.1029/2006JA012206.

23.5.5 Zhang, S.-R., J.M. Holt, and M. McRae (2007), High latitude convection model based on long-term incoherent scatter radar observations in North America, *J. Atmos. Sol.-Terr. Phys.* 69, 1273–1291, doi:10.1016/j.jastp.2006.08.017.

23.5.6 Zhang, S.-R., J.M. Holt, A.P. van Eyken, et al. (2005), Ionospheric local model and climatology from long-term databases of multiple incoherent scatter radars, *Geophys. Res. Lett.* 32, L20102, doi:10.1029/2005GL023603.

23.5.7 Holt, J.M., S.-R. Zhang, and M.J. Buonsanto (2002), Regional and local ionospheric models based on Millstone Hill incoherent scatter radar data, *Geophys. Res. Lett.* 29(8), doi:10.1029/2002GL014678.

23.6 Dates of Development, Authors, and Sponsors

23.6.1 Dates: 2001–2008

23.6.2 Authors: Shunrong Zhang, John Holt

23.6.3 Sponsors: NSF Space Weather

23.7 Model Codes and Sources

The model was developed in Fortran code that can work on PC or workstation. A MATLAB interface and web interface to the Fortran are available. Model website: <http://madrigal.haystack.mit.edu/models>

Contact Shunrong Zhang, MIT Haystack Observatory, Off Route 40, Westford, MA 01886 (email: shunrong@haystack.mit.edu)

24 Probabilistic Topside Ionosphere Model

24.1 Model Content

The Probabilistic Topside Ionosphere Model is an empirical model of the topside total ion/electron density based upon over 10 years of plasma observations from the Special Sensors-Ions, Electrons and Scintillation (SSIES) instruments on board Defense Meteorological Satellite Program (DMSP) spacecraft. The model provides estimates for the parameters of a three-parameter lognormal distribution, which best characterizes the distribution of DMSP density observations when binned by solar activity, magnetic latitude, day of year, and solar local time or solar zenith angle. These parameters (representing the topside density floor, the median density above this floor, and the variability of the distribution) can be combined with the lognormal cumulative distribution function to determine the occurrence frequency of a given density in the topside ionosphere.

24.2 Model Limitations

This model is limited to the topside ionosphere. Since it is based exclusively upon DMSP observations from 830 to 860 km, it should not be used outside of this region. The input DMSP data set occurred over a wide range of solar conditions, but did not cover a full solar cycle. Additionally, the DMSP spacecraft fly in sun-synchronous orbit, and the DMSP database only covered four local times.

24.3 Basis of the Model

The probabilistic topside ionosphere model is based upon the estimated parameters of the distribution of DMSP density measurements. It was found that the topside density measurements tend to obey a three-parameter lognormal distribution given by

$$f(n) = \int \frac{m}{(n - \theta)\sigma\sqrt{2\pi}} \exp\left[\frac{-\ln\left(\frac{n - \theta}{m}\right)^2}{2\sigma^2}\right]$$

where n is the topside density, θ is the density floor, m = median, $(n) - \theta$ is the median density above the floor, and σ is variability of the distribution. Using the cumulative distribution function, the percentile occurrence for any given density will be

$$\frac{1}{2} \left[1 + \operatorname{erf}\left(\frac{\ln\frac{n - \theta}{m}}{\sqrt{2}\sigma}\right) \right]$$

24.4 Model Inputs and Database

The model can be run using either lookup tables of the distribution parameters or by using the fits for these parameters. Either way, these parameters are functions of the $F_{10.7}$ cm solar radio flux, magnetic latitude, day of year, and local time or solar zenith angle.

24.5 Publication References

24.5.1 Garner, T.W., B.T. Taylor, T.L. Gaussiran II, W.R. Coley, M.R. Hairston, and F.J. Rich (2010), The statistical behavior of the topside electron density as determined from DMSP observations: a probabilistic climatology, *J. Geophys. Rev.* 115, doi: 10.1029/2009JA014695.

24.6 Dates of Development and Authors

24.6.1 Dates:

2008–2009 Development of model lookup tables and the characterization of the binned density distributions.

2010 Version 1.

24.6.2 Authors: T. W. Garner, B. T. Taylor, T. L. Gaussiran II, W. R. Coley, M. R. Hairston, and F. J. Rich.

24.7 Model Codes and Sources

The model lookup tables of the density floor, median densities, and the variability of the density distribution can be obtained as flat ASCII files by contacting Trevor Garner at the ARL: UT (email: garner@arlut.utexas.edu).

DRAFT--For Public Review Only--DEC 2013

25 Algebraic Model

25.1 Model Content

The D-region has the most complex chemistry of any ionospheric region by far, and, to this day, its chemistry has not been elucidated fully. Nevertheless, there has been success in modeling the D-region, especially the electron concentrations of the disturbed D-region. This achievement has been made possible largely because ion-ion recombination (neutralization) coefficients all appear to be near $10^{-7} \text{ cm}^{-3} \text{ s}^{-1}$ (Smith et al., 1976), regardless of the type of ions involved. Hence, even though the negative ion chemistry is still unsatisfactory as to the concentrations of the various individual ions, the electron concentration can be determined with some confidence, as seen in Fig. 1 of Smith (1976), where the model to be discussed is shown to match well the upleg data for a Solar Proton Event (SPE) or Polar Cap Absorption (PCA) event.

The formation of the model is purely a sequence of algebraic expressions that yield solutions, after sufficient iterations, for the electron concentration [e] and all the individual ions currently in the model: 21 positive ions and 8 negative ions. Especially for disturbed events, but even for quiet conditions, D-region processes are sufficiently rapid, compared with the complexity of the chemistry that steady-state conditions are appropriate, except during twilight.

Transport is ignored. Collision frequencies may be included for calculating the absorption of electromagnetic waves (Swider and Chidsey, 1977).

25.2 Model Uncertainties and Limitations

The model has been fitted well to the November 1969 PCA event (Swider and Foley, 1978; Swider, 1988). Indeed, for electron concentrations under disturbed conditions, the day and night empirical expressions given above for initial [e] may be sufficiently accurate (Swider, 1988). For quiet conditions, the accuracy of the outputs is less certain, in part because D-region data for quiet conditions are also of low accuracy.

25.3 Basis of Model

An iterative scheme was developed to solve for all species concentrations. Using initial concentrations for electrons [e] and the positive ion sum SP, the individual negative ion concentrations are first determined and summed, NSUM. Then the positive ions are individually calculated and summed, PSUM. A new

$$[e] = \{ \text{previous } [e] + \text{PSUM} / (1 + \lambda) \} / 2$$

where $\lambda = \text{NSUM} / \text{previous } [e]$, and a new

$$\text{SP} = \{ \text{previous } [e] + \text{NSUM} + \text{PSUM} \} / 2$$

are then determined. This sequence is repeated until $\text{PSUM} = \text{NSUM} + [e]$ within a specified precision. For the November 1969 SPE, not more than nine iterations were required to reach $\pm 1\%$ for altitudes 40–90 km.

Initial daytime concentrations were derived from $[e] - (q/\Psi)^{-}$, where the effective recombination coefficient Ψ is that derived from the Nov. 2–5, 1969, SPE (Swider and Dean, 1975). The values determined (in $\text{cm}^{-3} \text{ s}^{-1}$) were 3.4×10^{-7} (85 km), 4.8×10^{-7} (80 km), 1.1×10^{-6} (75 km), 1.8×10^{-6} (70 km), 4×10^{-6} (65 km), 8.8×10^{-6} (60 km), 5.5×10^{-5} (55 km), 5.1×10^{-4} (50 km), and 3.5×10^{-2} (45 km).

Initial nighttime electron concentrations were derived from (Swider et al., 1975)

$$[e] = \{ (L(A) / 2\alpha_D)^2 + q / \alpha_D \}^{-} - L(A) / 2\alpha_D$$

where the mean (ion-electron) recombination coefficient α_D is $4 \times 10^{-7} \text{ cm}^{-3} \text{ s}^{-1}$, and where

$$L(A) = k_{61}[\text{O}_2]^2 + k_{62}[\text{O}_2][\text{N}_2]$$

is the loss rate (s^{-1}) for electrons through attachment to O_2 , with k_{xx} a specific reaction rate.

Initial total positive ion concentrations were determined from

$$SP = \{q(5[O]/\alpha_D + [O_3]/\alpha_i) / (5[O] + [O_3])\}^{-1}$$

with α_i the mean ion-ion recombination coefficient, $6 \times 10^{-8} \text{ cm}^3 \text{ s}^{-1}$.

Concentrations of electrons, 21 positive ions and 8 negative ions, are determined to two significant figures. Also printed are q , λ , Ψ , $L(A)$, $PSUM$, $NSUM + [e]$, initial $[e]$, and initial SP .

25.4 Model Input Parameters

The following neutral concentrations are required: O , O_2 , O_3 , $O_2(1\Delta)$, N_2 , CO_2 , H_2O , NO , NO_2 , temperature T , and total neutral concentration M . The relationships $[N_2] = 0.7808[M]$, $[O_2] = 0.2095[M]$, $CO_2 = 3 \times 10^{-4}[M]$ may be used. Values for total ionization production q must be provided. For quiet conditions in the daytime, q may be derived from the photoionization of NO by $H \text{ Ly}\alpha$, nominally (Swider, 1978)

$$q(NO^+) = 6 \times 10^{-7}[NO] \exp\{-10^{-20}[O^2]H\}$$

where H is the scale height of the atmosphere.

Processes and rate coefficients are listed in Tables 1 and 2 of Swider (1978). Photodissociation rates were multiplied by unity for daytime and zero for nighttime. Choices for α_i and α_D were given above.

25.5 Publication References

25.5.1 Smith, D., N.G. Adams, and M.J. Church (1976), Mutual neutralization rates of ionospheric important ions, *Planetary Space Sci.* 24, 697–703.

25.5.2 Swider, W. (1978), Daytime nitric oxide at the base of the thermosphere, *J. Geophys. Res.* 83, 4407–4410.

25.5.3 Swider, W. (1988), Electron loss and the determination of electron concentrations in the D -region, *PAGEOPH.* 127, 403–414.

25.5.4 Swider, W., and I.L. Chidsey Jr. (1977), HF/VHF absorption in the disturbed D region, *J. Geophys. Res.* 82, 1617–1619.

25.5.5 Swider, W., and W.A. Dean (1975), Effective electron loss coefficient of the disturbed daytime D region, *J. Geophys. Res.* 80, 1815–1819.

25.5.6 Swider, W., and C.I. Foley (1978), AFGL-TR-78-0155.

25.5.7 Swider, W., R.S. Narcisi, T.J. Keneshea, and J.C. Ulwick (1971), Electron loss during a nighttime PCA event, *J. Geophys. Res.* 76, 4691–4694.

25.6 Model Codes and Sources

The model (Swider and Foley, 1978) may be ordered from National Technical Information Service.

26 Numerical Model of D-Region Ion Chemistry, 1995

26.1 Model Content

The Numerical Model Sodankyla Ion Chemistry (SIC) was developed as an alternative approach to those D-region ion-chemistry models that combine the more doubtful chemical reactions to effective parameters, the values of which are set against experimental data. A detailed chemical scheme, in a conceptually simple model, was built to be a tool for interpretation of D-region incoherent scatter experiments and cosmic radio-noise absorption measurements, both of which form the basis of D-region research done at Sodankyla Geophysical Observatory. The number of different ions in the current version is 55, of which 36 are positive and 19 are negative. Burns et al. (1991) first applied the model in a study of incoherent scatter measurements. A detailed description of the first version of the model is given by Turunen et al. (1992, 1996). The SIC model can be run either as a steady-state model or a time-dependent model. The model solves for ion and electron concentrations in ionospheric D- and lower E-regions. Local chemical equilibrium can be calculated in the altitude range from 50 to 100 km at 1 km steps. The solution for the steady state can be advanced in time to solve for response of the ion concentrations to a sudden disturbance, e.g., in ion production rates or in neutral-gas properties. Originally the model was developed for applications during geophysically quiet conditions. Consequently, as ionization sources acting on five primary neutral components N_2 , O_2 , O , NO , and $O_2(^1\Delta_g)$, the solar radiation at wavelength range 5–134 nm and galactic cosmic rays were considered. At present, however, the model is extended to include electron precipitation as an ionization source. A similar extension was made to use the model during solar-proton events, as in the application of the SIC model by Turunen (1993).

26.2 Model Uncertainties and Limitations

A detailed ion-chemical scheme with many reactions is subject to the uncertainties and inaccuracies in the reaction rate constants. Neutral chemistry and ion chemistry are not coupled in this model. The neutral atmosphere is taken only as a static background. If the effect of particle fluxes is considered in detail, one should care about the dissociation of neutral minor constituents. For investigations around sunset and sunrise, the effects of neutral photochemistry should be included in detail. Hard x-rays and scattered radiation at night are not included as ionization sources. In addition to the presently included components, heavier cluster ions, heavier clusters of negative ions, and more metallic ions are known to exist in the D-region. The assumptions on which the model is based are as follows:

1. The neutral atmosphere is described by the semi-empirical model MSIS-90 (Hedin, 1991).
2. The ionospheric D-region is sunlit. This restricts the range of the solar zenith angle to be below 95° .
3. Ionization during quiet time is primarily caused by photoionization and galactic cosmic rays. Ionization by solar protons and precipitating electrons is calculated using measured particle-energy deposition rates in air.
4. We neglect any transport effects. Chemical lifetimes of the ions are assumed to be short with respect to transport processes.
5. The concentrations of neutral species are much higher than those of ions and thus assumed to be unaffected by ion chemistry.
6. An overall charge neutrality prevails.

26.3 Basis of the Model

In addition to the above-mentioned neutrals, Ar, He, and CO_2 also are included in photoionization calculations, because they absorb the solar radiation at the relevant wavelength range. To account for important ion-chemical reactions we need to include also H_2O , N, H, O_3 , OH, NO_2 , HO_2 , NO_3 , HNO_2 , CO_3 , H_2 , HCl, HNO_3 , Cl, ClO, CH_4 , and CH_3 in the list of the neutral components of the model.

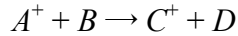
Continuity equation for ion i (transport effects neglected):

$$\frac{\partial n_i}{\partial t} = P_i - n_i \cdot L_i$$

where

$$P_i = \sum_{\text{production processes } m} P_{im}, \quad L_i = \sum_{\text{loss processes } m} l_{im}$$

Consider reaction



for

$$C^+:$$

and for

$$A^+ : l_{A^+ m} = k[A^+][B]$$

Assume constant neutral concentrations:

$$p_{C^+ m} = \Pi_{C^+ m} [A^+], \quad l_{A^+ m} = \Lambda_{A^+ m} [A^+]$$

Continuity equation in matrix form:

$$\frac{\delta \vec{N}}{\delta t} = \vec{F}(\vec{N}) = \Gamma(\vec{N})\vec{N} + \vec{Q}(\vec{N})$$

Γ is a 55×55 matrix. Elements Π and Λ describe the production and loss rates of each ion. N is a vector containing the 55 unknown ion concentrations. Q is a vector that contains the constant primary ionization rates. Chemical equilibrium may be solved by setting

$$\frac{\partial n_i}{\partial t} = 0$$

Starting from the equilibrium solution of the ion concentrations, we advance the concentrations in time by taking small time steps according to the expression

$$\vec{N}_{n+1} = \vec{N}_n + \Delta t \left[\vec{F}(\vec{N}_n) + \frac{\delta \vec{F}}{\delta \vec{N}} \Big|_{\vec{N}=\vec{N}_n} \cdot (\vec{N}_{n+1} - \vec{N}_n) \right]$$

where the elements ϕ_{ij} of the matrix

$$\frac{\delta \vec{F}}{\delta \vec{N}} \Big|_{\vec{N}=\vec{N}_n}$$

are the partial derivatives

$$\Phi_{ij} = \frac{\delta F_i}{\delta N_j} \Big|_{\vec{N}=\vec{N}_n}$$

The expression above is a set of linear equations, which has to be solved for each time step.

26.4 Database and Input to the Model

As input to the neutral atmosphere model, MSIS-90, one gives time, location, and information about solar and geomagnetic activity. The resulting neutral constituent concentrations are then used to calculate ion production rates and chemical reaction rates. For those neutral constituents that are not covered by the MSIS-90 model, fixed reference profiles may be selected. Also fixed mixing ratios of 3×10^4 and 1×10^6 for CO_2 and H_2O , respectively, can be used. Some applications may require that a set of the neutral minor constituent profiles is kept fixed while selected concentrations are varied.

Absorption cross-sections for N_2 , O_2 , O , and He are from Torr et al. (1979); for NO and Ar , the constants from the tables of Ohshio et al. (1966) are used; and for CO_2 , the data are from McEwan and Phillips (1975). Photoionization efficiencies come from the same references as the absorption cross-sections.

A reference solar spectrum was collected from the spectrum by Torr et al. (1979) and from spectrum R74113 by Heroux and Hinteregger (1978). The intensities for wavelengths 103.76 nm and 110.8 nm were taken from the paper of Huffman et al. (1971). For our reference spectrum, Ly- α line was chosen from Lean and Skumanich (1983). The intensities can be varied according to the chosen level of solar activity. Heaps (1978) has derived a convenient parameterization of the empirical rate of ion-pair production by cosmic rays, Q_{cr} , as a function of latitude, altitude, and solar activity.

The spectrum of precipitating electrons can be given in a parameterized form of the differential energy spectrum. Alternatively, a precise form of the spectrum can be given, e.g., in the form of fluxes at selected energy channels. Input of the proton flux is formulated to correspond to measurements at predefined energy channels, e.g., those used by the satellite GOES-7.

For the chemical schemes, the main contributions were taken from the works by Chakrabarty et al. (1978), Dymek (1980), Wisenberg and Kockarts (1980), Torkar and Friedrich (1983), and Thomas and Bowman (1985). The reaction rate constants were updated from several sources.

26.5 Publication References

26.5.1 Burns, C.J., E. Turunen, H. Matveinen, H Ranta, and J.K Hargreaves (1991), Chemical modelling of the quiet summer *D*- and *E*-regions using EISCAT electron density profiles, *J. Atmos. Terr. Phys.* 53, 115.

26.5.2 Chakrabarty, D.K., P. Chakrabarty, and G. Witt (1978), An attempt to identify the obscured paths of water cluster ions build-up in the *D*-region, *J. Atmos. Terr. Phys.* 40, 437.

26.5.3 Dymek, M.K. (1980), *Low latitude aeronomical processes*, edited by A.P. Mitra, COSPAR Symposium Series, Pergamon Press, Oxford and New York, Vol. 8, p. 118.

26.5.4 Heaps, M.G. (1978), Parametrization of the cosmic ray ion-pair production rate above 18 km, *Planetary Space Sci.* 26, 513.

26.5.5 Hedin, A.E. (1991), Extension of the MSIS Thermosphere Model into the middle and lower atmosphere, *J. Geophys. Res.* 96, 1159.

26.5.6 Heroux, L., and H.E. Hinteregger (1978), Aeronomical reference spectrum for solar UV below 2000 Å, *J. Geophys. Res.* 83, 5305.

26.5.7 Huffman, R.E., D.E. Paulsen, J.C. Larrabee, and R. B. Cairns (1971), Decrease in *D*-region O_2 ($^1\Delta_g$) Photoionization rates resulting from CO_2 absorption, *J. Geophys. Res.* 76, 1028.

26.5.8 Lean, J.L., and A. Skumanich (1983), Variability of the Lyman alpha flux with solar activity, *J. Geophys. Res.* 88, 5751.

26.5.9 McEwan, M.J., and L.F. Phillips (1975), *Chemistry of the atmosphere*, Edward Arnold Ltd.,

London.

26.5.10 Thomas, L., and M.R. Bowman (1985), Model studies of the *D*-region negative-ion composition during day-time and night-time, *J. Atmos. Terr. Phys.* 47, 547.

26.5.11 Torkar, K.M., and M. Friedrich (1983), Tests of an ion-chemical model of the *D*- and lower *E*-region, *J. Atmos. Terr. Phys.* 45, 369.

26.5.12 Torr, M.R., D.G. Torr, R.A. Ong, and H.E. Hinteregger (1979), Ionization frequencies for major thermospheric constituents as a function of solar cycle 21, *Geophys. Res. Lett.* 6, 771.

26.5.13 Turunen E. (1993), EISCAT incoherent scatter radar observations and model studies of day to twilight variations in the *D*-region during the PCA event of August 1989, *J. Atmos. Terr. Phys.* 55, 767–781.

26.5.14 Turunen, E., H. Matveinen, and H. Ranta (1992), *Sodankyla Ion Chemistry (SIC) Model*, Sodankyla Geophysical Observatory, Rept. 49, Sodankyla, Finland.

26.5.15 Turunen, E., J. Tolvanen, H. Matveinen, and H. Ranta (1996), *D Region Ion Chemistry Model*, *STEP Handbook of Ionospheric Models*, edited by R.W. Schunk. SCOSTEP and Utah State University, 1.

26.5.16 Wisenberg, J., and G. Kockarts (1980), Negative ion chemistry in the terrestrial *D* region and signal flow graph theory, *J. Geophys. Res.* 85, 4642.

26.6 Dates of Development, Authors, and Sponsors

26.6.1 Dates:

1989 Version 1.0, 35 ions.

1991 Version 1.1, reaction rates updated.

1994 Version 2.0, adding and removing reactions.

1995 Version 2.1, 55 ions.

1995 Version 3.0, time-dependent code.

26.6.2 Authors (principal): Esa Turunen, Head of the Ionospheric Station, SGO; Helena Matveinen, Scientist, SGO.

26.6.3 Sponsor: Finnish Academy of Science and Letters, Geophysical Observatory, Sodankyla, Finland.

26.7 Model Codes and Sources

The early versions of the model were based on Fortran code, which we no longer support. The present version of the model is coded in MATLAB language, which makes the model user-friendly, easy to adapt, and easy to tailor to specific needs. The current version is written using MATLAB 4.2c. The code runs on computers that can run MATLAB. The code is not optimized for speed, but any user could do this. The latest version will be made available to anyone interested. Contact person: Esa Turunen, Sodankyla Geophysical Observatory, FIN-99600 Sodankyla, Finland (email: Esa.Turunen@sgo.fi).

27 Solar EUV and Chemistry Model

27.1 Model Content

A modeling technique of Keneshea (1967) was applied by Keneshea et al. (1970) to the E-region for detailed comparisons with ionic compositions measured at twilight (two at sunset and two at sunrise). The experiments were conducted under normal (quiet) conditions, at mid-latitudes, near Eglin Air Force Base, Florida, during April 1967. This month was one of moderate solar activity, with a mean sunspot number of 69.5.

27.2 Model Uncertainties and Limitations

It is our experience that [NO] appears generally to be greater in the E-region than many models assume. Thus some models yield $O_2^+ \gg NO^+$ near 95–100 km, whereas the observational data, with perhaps one exception, do not support this result (Swider, 1994). The values of [NO] used here are in the higher range of those determined from gamma-band data. However, these values have worked well. Again, our use of a somewhat higher x-ray flux appears justified by the model's favorable comparison with the observational ionic data. There have been suggestions that there is insufficient ionization produced near 95–100 km, implying a missing source of ionization. However, none have offered any specific details, and our model agrees quite well with incoherent scatter data in the lower E-region (Trost, 1979).

27.3 Basis of Model

The model was set up to simultaneously solve a set of coupled partial differential equations

$$\frac{\delta n_i}{\delta t} = Q_i - L_i$$

where n_i is the number density of the i species, with Q_i and L_i as the respective production and loss terms for that species, which terms commonly include other species concentrations.

Concentrations were calculated for negative ions O^- , O_2^- , O_3^- , NO_2^- , NO_3^- , and CO_3^- ; positive ions O^+ , O_2^+ , N_2^+ , and NO^+ ; and electrons [e]. In addition, different equations were solved for the following neutral species: NO, N, NO_2 , O, N_2O , O_3 , CO_2 , H_2 , H, OH, HO_2 , H_2O , H_2O_2 , O_2 , and N_2 . However, in applying the code to the E-region, NO and N were held fixed. The major gases changed very little over the course of the run: about one day commencing at noon, when the solar zenith angle was 21.6° . The major species (O_2 , N_2) changed imperceptibly over this period, and negative ions were negligible. As we were not focusing on the chemistry of the minor neutrals, but rather on the major positive ions and electrons, we list only their relevant chemistry (Summary of Reference and Standard Ionospheres), which has changed little over the intervening years.

Transport was ignored in this model. However, because one sunset observation was quite distorted, a special calculation was performed (Keneshea and MacLeod, 1970), which compared well with the data. This model variation included transport terms using the full continuity equations. The velocities required for the divergence term were derived from the measured neutral wind profiles for an earlier flight and used in a collision-geomagnetic equilibrium expression

$$v_i = \frac{1}{1 + p_i^2} [p_i^2 u + p_i u \times \Gamma + (u \cdot \Gamma) \Gamma]$$

where p_i is the ratio of neutral-ion collision frequency to gyrofrequency, Γ a unit vector in the geomagnetic field direction, and u the neutral wind (MacLeod, 1966).

The method of solution for the partial differential equations uses a fourth-order Runge Kutta integration with a variable mesh. When a species enters its quasi-equilibrium state, its differential equation is removed from the set, and its equilibrium equation is inserted into the simultaneous algebraic set, which

is solved by the methods of successive substitutions. The overall solution is obtained by iteration between the differential and algebraic sets.

A numerical solution to this problem that requires the use of a high-speed digital computer has been discussed (Keneshea, 1962). The computer program resulting from that study, although it developed satisfactory solutions within a minimum of computer time, can be used only at E-region altitudes. One reason for this restriction is that the number density of NO^+ ions is always computed from the requirement of balance of charge. (The sum of the positive ions equals the sum of the electrons and the negative ions.) This method is applicable, however, only if NO^+ is the most abundant ion. Although this appears to be true in the E-region, it will not be the case at lower altitudes in the D-region. Because the system is solved on a digital computer, it is not possible to accurately determine the concentration of a minor species through conservation of charge. The required number density is located in the least significant bits of the computer word, and, depending upon the amount of accumulated round-off error, the result could be erroneous.

27.4 Model Input Parameters

Solar fluxes and absorption cross-sections were taken from Watanabe and Hinteregger (1962) above about 100Å. Below this wavelength, the values listed by Nicolet and Aiken (1960) for quiet solar conditions were adopted. The solar flux in the range 10–170Å was increased by a factor of 4 over the values cited above in order to best match the data. The proper x-ray flux for the E-region is still of concern in more recent codes, which aim to determine minor odd nitrogen species, particularly N and NO. An H Ly α flux of 4 egs cm⁻² sec⁻¹ was adopted, and the ionization effects of the scattered H Ly α and H Ly β radiations were approximated by setting their fluxes at 1% and 0.4%, respectively, of their noontime height-dependent direct flux profiles. The paper by Strobel et al. (1980) should be consulted for a detailed analysis of nighttime ionization sources and their intensities. The declination of the sun was fixed at 8.62° for comparison with the specific experimental data, with the noontime solar zenith angle χ being 21.63°. Atmospheric concentrations and temperatures were taken from the mean 1965 COSPAR International Reference Atmosphere (CIRA). All particles were assumed to have the same temperature distribution. In calculating the optical depth, appropriate CIRA concentrations were integrated along the various solar zenith angles. The nitric oxide concentrations essentially were a smooth version of Barth's (1966) results, but lower at 85 km, the lowest altitude of the calculation. Atomic nitrogen concentrations were effectively negligible, $[\text{N}] = 10^{-2}[\text{NO}]$. Both species were held constant throughout the time-dependent solutions of the charged constituents.

The specific nitric oxide concentrations used were (in 10^6 cm^{-3}) 3 (140 km), 5.4 (130 km), 11 (120 km), 25 (110 km), 34 (105 km), 40 (100 km), 38 (95 km), 25 (90 km), and 10 (85 km). Calculations were performed only at these altitudes. Nitric oxide plays two major roles. First, it converts O_2^+ ions into NO^+ ions via the charge transfer reaction (#9 in Summary of Reference and Standard Ionospheres). However, it is the product $k_9 [\text{NO}]$ that is important. Thus, as k_9 is now about 25% lower than the value in Summary of Reference and Standard Ionospheres, the $[\text{NO}]$ used is effectively 4/3 the values cited. More significant is that, near a solar zenith angle of 90°, the attenuation of H Ly α near 100–110 km is negligible, and the main ionization source is therefore $\text{H Ly}\alpha + \text{NO} \rightarrow \text{NO}^+ + \text{e}$. If $[\text{NO}]$ is enhanced, as is often the case for the auroral region, E-region concentrations $[\text{e}]$ at sunrise increase, too, as $[\text{e}]^2$ is proportional (numerically) to $[\text{NO}]$ (Swider and Keneshea, 1993).

27.5 Publication References

- 27.5.1** Barth, C.A. (1966), Nitric oxide in the upper atmosphere, *Ann. Geophys.* 22, 198–207.
- 27.5.2** Keneshea, T.J. (1967), A technique for solving the general reaction-rate equations in the atmosphere, AFCRL-67-0221.
- 27.5.3** Keneshea, T.J., and M.A. MacLeod (1970), Wind-Induced Modification of E Region Ionization Profiles, *J. Atmos. Sci.* 27, 981–984.

27.5.4 Keneshea, T.J., R.S. Narcisi, and W. Swider, Jr. (1970), Diurnal model of the *E* region, *J. Geophys. Res.* 75, 845–854.

27.5.5 Nicolet, M., and A.C. Aikin (1960), The formation of the *D* region of the ionosphere, *J. Geophys. Res.* 65, 1469–1483.

27.5.6 Strobel, D.F., C.B. Opal, and R.R. Meier (1980), Photoionization rates in the night-time *E*- and *F*-region ionosphere, *Planetary Space Sci.* 28, 1027–1033.

27.5.7 Swider, W., and T.J. Keneshea (1993), The quiet sunrise *E* region: Enhancements at high latitudes in winter due to increased nitric oxide, *J. Geophys. Res.* 98, 1725–1728.

27.5.8 Trost, T.F. (1979), Electron concentrations in the *E* and upper *D* region at Arecibo, *J. Geophys. Res.* 84, 2736–2742.

27.5.9 Watanabe, K., and H.E. Hinteregger (1962), Photoionization rates in the *E* and *F* regions, *J. Geophys. Res.* 67, 999–1006.

27.6 Model Codes and Sources

A version of the model may be available (contact W. Swider), but it may not be worth running in view of the published outputs, especially because others undoubtedly have codes much faster than the one discussed here. The original printout is available (W. Swider). The originator/writer of the code (T. J. Keneshea) has expanded it to include transport and IR emissions, but its availability through Visidyne Research, Inc., may be limited.

28 AFRL Boltzmann-Fokker-Planck Model for the Daytime Lower Ionosphere

28.1 Model Content

The Boltzmann-Fokker-Planck (BFP) model calculates the energy-dependent electron distribution function, the electron density, the electron temperature, and the densities of four ion species (O^+ , N_2^+ , O_2^+ , N_2^+) in the earth's daytime lower ionosphere. Electron and ion production rates per unit volume are also calculated. The model assumes a steady state and uses a local approximation. Thus the above quantities are calculated for a given time, location, and altitude. To develop any spatial or temporal information requires that a series of calculations be made for the different altitudes, locations, and times of interest. Past use has usually focused on several altitudes at a specific time and place.

28.2 Model Uncertainties and Limitations

One source of model inaccuracy lies in the uncertainties in our knowledge of various cross-sections and reaction rates needed for the calculation. Fortunately, most of the cross-sections and reaction rates have been measured so that there is an empirical basis for the values that are used. Another limitation to the model accuracy occurs because of the need to know the geophysical conditions of the time and place being modeled.

As described earlier, the model is restricted to the lower ionosphere, which typically means the E- and F1-regions. In previous work, the model has been used down to around 100 km. There is potential for going down to around 90 km. However, in any particular case, the appropriate lower boundary is defined wherever processes normally associated with the D-region can no longer be neglected. The upper boundary is typically slightly below the F2 peak and, for any particular case, should be determined by where electron and ion transport become important. At mid latitudes this altitude is typically 220–250 km.

The model is strictly a daytime model, with the solar flux acting as the primary source of ionization. As such, it is generally inappropriate for use in the auroral regions or any daytime location that is undergoing significant particle precipitation.

The model calculates the zero-order state of the photoelectron distribution function and does not include any wave–particle or wave–wave plasma interactions.

28.3 Basis of the Model

The BFP model produces a numerical solution of a kinetic equation for the isotropic portion of the steady-state electron distribution function (EDF) and of four ion continuity equations for the ion densities. The equations solved can be derived by beginning with a system of one-particle plasma kinetic equations, where one equation appears for each state of each kind of particle. By assuming that the ion distribution functions are local Maxwellian functions and that transport effects can be neglected (local approximation), a steady-state equation for each ion density can be derived. For the lower ionosphere, this results in four coupled equations for the ion densities. In these four equations, there are terms that depend on the energy-dependent EDF, which is considered unknown. An equation for this distribution function is derived by assuming a steady state, by neglecting the anisotropic portion of the distribution function, and by integrating the kinetic equation for the EDF over angles in velocity space. The resulting equation contains a series of terms that describe the rates of change of the EDF due to photoionization and collision processes. The name of the model comes from the fact that the explicit expressions for each of these terms come from using either Boltzmann or Fokker-Planck methods. Finally, both the electron density and temperature can be found from their definitions once the EDF is known. The primary sources and sinks of ionization are photoionization and recombination, respectively. The electron-neutral processes included are elastic collisions, excitation collisions, de-excitation collisions, and ionizing collisions. Also included are elastic electron–ion and electron–electron collisions. These terms are nonlinear in the EDF and are formulated in terms of the Rosenbluth potentials. Included are a variety of chemical reactions that involve the above ions and the three major neutral species (O , N_2 , O_2) of the earth's atmosphere.

In solving the kinetic equation for the EDF, a non-uniform grid of several hundred energy points is used that typically spans from 1×10^{-9} to 225 eV. As mentioned, a single computer run of the model performs the calculation for a specific altitude, time, and location.

28.4 Model Input Parameters

The model requires geophysical inputs as well as a variety of cross-sections and reaction rates. The cross-sections and rates are provided by a series of data files that can be updated whenever new values are available. The geophysical inputs are the solar flux, neutral densities, neutral temperatures, and ion temperatures. These are generally supplied by empirical or statistical models for these quantities.

28.5 Publication References

28.5.1 Jasperse, J.R. (1976), Boltzmann-Fokker-Planck model for the electron distribution function in the Earth's ionosphere, *Planetary Space Sci.* 24, 33–40.

28.5.2 Jasperse, J.R. (1977), Electron distribution function and ion concentrations in the Earth's lower ionosphere from Boltzmann-Fokker-Planck theory, *Planetary Space Sci.* 25, 743–756.

28.5.3 Jasperse, J.R. (1981), The photoelectron distribution function in the terrestrial ionosphere, *Physics of Space Plasmas*, edited by T. Chang, B. Coppi, and J.R. Jasperse, SPI Conference Proceedings and Reprint Series, Scientific Publishers, Cambridge, MA, Vol. 4, p. 53.

28.5.4 Winningham, J.D., D.T. Decker, J.U. Kozyra, J.R. Jasperse, and A.F. Nagy (1989), Energetic (> 60 eV) atmospheric photoelectrons, *J. Geophys. Res.* 94, 15,335–15,348.

28.6 Dates of Development, Authors, and Sponsors

28.6.1 Dates

1973 Coupled nonlinear equations for electron distribution function in the earth's ionosphere are derived.

1976 Numerical solution of electron kinetic equation and local ion continuity equations is completed.

1982 Low-energy electron and photon cross-sections are updated.

1989 BFP model compared with other photo-electron models.

28.6.2 Authors: John R. Jasperse, Phillips Laboratory/GPIM; Neil J. Grossbard, Boston College; and Dwight T. Decker, Boston College.

28.6.3 Sponsors: Air Force Office of Scientific Research and Phillips Laboratory of the U.S. Air Force Material Command.

28.7 Model Codes and Sources

The model is in the form of a large Fortran code, but it is not user-friendly. Anyone interested in results from this code should contact John R. Jasperse.

29 AFRL Transport Model for the Electron-Proton-Hydrogen Atom Aurora

29.1 Model Content

The PL transport model for the combined electron-proton-hydrogen atom aurora describes the energy deposition, ionization, and excitation of optical emissions by the precipitating electrons, protons, and hydrogen atoms associated with the auroral zone for steady-state conditions. The numerical code solves a coupled set of three linear transport equations for the three particle species to obtain the particle fluxes as functions of altitude, energy, and pitch angle. The altitude profiles of the rates of energy deposition, ionization, and excitation of optical emissions are then calculated from the fluxes. The code also calculates the electron-density profile associated with the combined aurora. Densities of the important ion species are calculated by using a detailed chemistry model that solves a set of coupled rate equations. The electron density is then specified by requiring charge neutrality. The model can also be used to study a pure electron aurora or a pure proton-hydrogen atom aurora by choosing the appropriate boundary conditions. At present the model calculates volume emission rates for the following optical features: N_2 first negative group (3914 Å), N_2 second positive group (3371 Å), selected N_2 Lyman-Birge-Hopfield bands (1325 Å, 1354 Å, 1383 Å, 1493 Å, and all bands between 1700 and 1800 Å), OI (1356 Å), NI (1493 Å), $L\alpha$ (1216 Å), $H\beta$ (4861 Å), and $H\alpha$ (6563 Å). More optical features will be added to the model as their cross-sections become available.

The transport model assumes steady-state conditions with no electric fields present, plane-parallel geometry, and a uniform geomagnetic field (magnetic mirroring effects are neglected). The effect of the atmospheric lateral spreading of the incident proton stream due to charge-changing processes (charge exchange and stripping), which is neglected in the plane-parallel geometry, can be included, to a good approximation, by multiplying the incident flux with an appropriate correction factor (Jasperse and Basu, 1982).

The inputs for the model are: (1) the cross-sections for the various collision processes involving electrons, protons, and hydrogen atoms; (2) effective cross-sections for selected emission features; (3) the neutral atmosphere; and (4) the incident particle (electron and proton) fluxes at the upper boundary of the atmosphere.

29.2 Model Uncertainties and Limitations

29.2.1 The reliability of the calculated aurora-related quantities largely depends on the accuracy with which the input quantities can be specified.

29.2.2 The steep bottomside profile, which is the general characteristic of the precipitating particle fluxes, requires fine altitude grid points to obtain a desired accuracy.

29.2.3 The model does not take into account the effect of magnetic mirroring on the pitch-angle distribution of the particle fluxes.

29.3 Basis of the Model

The model is based on a coupled set of three transport equations for the electrons, protons, and hydrogen (H) atoms that includes all the elastic and inelastic collision processes involving these particles and the neutral particles. The proton and H atom fluxes are coupled only to each other because of the charge-changing collisions, whereas the electron flux is coupled to both the proton and the H atom fluxes through the secondary electrons that they generate. The equations for protons and H atom fluxes are first converted into integral equations and then solved on a two-dimensional grid of energy (E) points, from E_{\min} to E_{\max} , and altitude (z) points, from z_{\min} to z_{\max} (for details, see Basu et al., 1990). These fluxes are used to calculate the secondary-electron source terms in the electron transport equation. The electron transport equation is then solved to obtain the degraded primary and secondary electron fluxes by using a discrete ordinate and eigenvalue technique (for details, see Strickland et al., 1976; Basu et al., 1993). From the particle fluxes as a function of altitude, energy, and pitch angle, various quantities of interest are calculated by using rigorous theoretical formulae (Basu et al., 1993).

29.4 Model Input Parameters

29.4.1 The set of particle impact and effective emission cross-sections used in the model and the sources of these cross-sections are given by Basu et al. (1990) and Strickland et al. (1993).

29.4.2 The model can use any neutral atmosphere specified by the user. Presently, it uses the MSIS-86 thermospheric model.

29.4.3 The incident electron and proton fluxes are specified by analytic functions. Two commonly used energy distributions for the incident electron flux are: (1) a Maxwellian distribution with the options of adding low- and high-energy tails, and (2) a Gaussian distribution with the same options. For the protons, a Maxwellian or a Kappa distribution, or some combination of them, is used.

29.5 Publication References

29.5.1 Basu, B., J.R. Jasperse, and N.J. Grossbard (1990), A numerical solution of the coupled proton-H atom transport equations for the proton aurora, *J. Geophys. Res.* 95, 19,069.

29.5.2 Basu, B., J.R. Jasperse, R.M. Robinson, R.R. Vondrak, and D.S. Evans (1987), Linear transport theory of auroral proton precipitation: a comparison with observations, *J. Geophys. Res.* 92, 5920.

29.5.3 Basu, B., J.R. Jasperse, D.J. Strickland, and R.E. Daniell (1993), Transport-theoretic model for the electron-proton-hydrogen atom aurora, 1. Theory, *J. Geophys. Res.* 98, 21,517.

29.5.4 Daniell, R.E., and D.J. Strickland (1986), Dependence of auroral middle UV emissions on the incident electron spectrum and neutral atmosphere, *J. Geophys. Res.* 91, 321.

29.5.5 Decker, D.T., B. Basu, J.R. Jasperse, D.J. Strickland, J.R. Sharber, and J.D. Winningham (1995), Upgoing electrons in an electron-proton-hydrogen atom aurora, *J. Geophys. Res.* 100, 21,409.

29.5.6 Jasperse, J.R., and B. Basu (1982), Transport theoretic solutions for auroral proton and H atom fluxes and related quantities, *J. Geophys. Res.* 87, 811.

29.5.7 Strickland, D.J., D.L. Book, T.P. Coffey, and J.A. Fedder (1976), Transport equation techniques for the deposition of auroral electrons, *J. Geophys. Res.* 81, 2755.

29.5.8 Strickland, D.J., J.R. Jasperse, and J.A. Whalen (1983), Dependence of auroral FUV emissions on the incident electron spectrum and neutral atmosphere, *J. Geophys. Res.* 88, 8051.

29.5.9 Strickland, D.J., R.R. Meier, J.H. Hecht, and A.B. Christenson (1989), Deducing composition and incident electron spectra from ground based auroral optical measurements: theory and model results, *J. Geophys. Res.* 94, 13,527.

29.5.10 Strickland, D.J., R.E. Daniell, J.R. Jasperse, and B. Basu (1993), Transport-theoretic model for the electron-proton-hydrogen atom aurora, 2. Model results, *J. Geophys. Res.* 98, 21,533.

29.6 Dates of Development, Authors, and Sponsors

29.6.1 Dates

1976 Original electron transport code for a one-constituent medium.

1982 Original proton-H-atom transport model and its analytic solutions for a one-constituent medium.

1983 Generalization of electron transport code to a multi-constituent medium and application to an auroral study.

1987 Study of a pure proton aurora with the proton-H-atom transport model.

1989 Application of electron transport code to an auroral study.

1990 Numerical proton-H-atom transport code for a multi-constituent medium.

1993 Electron-proton-H-atom transport code for a multi-constituent medium.

1995 Study of up-going electrons in an electron-proton-hydrogen-atom aurora with transport code.

29.6.2 Authors: B. Basu and J. R. Jasperse, Phillips Laboratory/GPIM, Hanscom AFB, MA 01731; D. J. Strickland and R. E. Daniell, Computational Physics, Inc., 2750 Prosperity Avenue, Suite 600, Fairfax, VA 22031; D. T. Decker, Institute for Scientific Research, Boston College, Newton, MA 02159.

29.6.3 Sponsors: Air Force Office of Scientific Research (AFOSR), Defense Nuclear Agency (DNA), Defense Meteorological Satellite Program (DMSP), National Science Foundation (NSF), and Air Force Phillips Laboratory (PL).

29.7 Model Codes and Sources

The model is in the form of a research-type Fortran code and is not very user-friendly. However, the authors frequently run the model in collaborative studies with experimentalists and other modelers. Anyone interested in such a study should contact J. R. Jasperse, Phillips Laboratory/GPIM, 29 Randolph Road, Hanscom AFB, MA 01731 (email: basub@plh.af.mil).

DRAFT--For Public Review Only--DEC 2013

30 Two-Cell Ionospheric Convections Model

30.1 Model Content

In the F-region ionosphere, the plasma drifts perpendicular to the magnetic field under the influence of the electric field such that $\mathbf{V} = \mathbf{E} \times \mathbf{B}/B^2$. The electric field may be expressed in terms of a scalar electrostatic potential, and then electric equipotential lines indicate the instantaneous flow paths of the plasma. The F-region plasma motion is highly dependent on conditions in the interplanetary medium, particularly the interplanetary magnetic field (IMF) and the solar wind velocity. When the IMF is directed southward, most *in situ* and remote sensing of the plasma motion at high latitudes in the F-region ionosphere confirms the existence of a two-cell circulation of the plasma, with antisunward flow at highest latitudes and sunward flow at lower latitudes largely confined to the regions of the auroral zone. This model provides an analytical expression for the electrostatic potential that describes a two-cell convection pattern and its first-order dependencies on the IMF. Specification of the potential distribution is achieved by defining a circular region (the polar cap) at high latitudes, within which the plasma flow is antisunward. The radius of the polar cap and the potential distribution across it determine the magnitude of the antisunward plasma flow. These variables may be specified by the user, or simple functional dependencies derived from observations from the Dynamics Explorer spacecraft and residing within the model algorithm may be invoked. Outside the polar cap, the sunward flow in the auroral region is determined by the distribution of the potential around the polar cap boundary and by a specification of the effective width of the auroral zone. These dependencies may also be fully specified by the user, or simple functional dependencies derived from DE-2 data may be invoked.

30.2 Model Uncertainties

This model does not represent a synthesis of data in any way. It simply provides a tool by which major observed characteristics of the high-latitude convection pattern can be mimicked or by which specific observations of the electrostatic potential can be fit. The simple analytical functions that are employed do not allow convection features with scale sizes less than 10° in latitude or 6 hr in local time to be reproduced. The simple functional dependencies on the IMF presently provided by the algorithms are based on a rather limited database from DE-2 and may differ significantly from those derived from other sources. Care should therefore be exercised when comparing derived results utilizing different specifications of the convection pattern. The model may presently be applied to conditions of southward IMF when confidence is high that a two-cell convection pattern exists. It is not applicable to times of weakly southward IMF or northward IMF when significant variations from the two-cell configuration are likely.

30.3 Basis of the Model

Many studies of the high-latitude ionospheric convection describe a two-cell circulation (e.g., Foster, 1983; Heppner and Maynard, 1987). An original description of this convection configuration was given by Volland (1975). This model represents extensions to the functional forms given by Heelis et al. (1982) and dependencies of the driving parameters on the IMF given by Hairston and Heelis (1990). The model determines a distribution of electrostatic potential around a circular boundary defining the polar cap. This distribution is specified by a maximum and minimum potential, each of which occupies a local time extent dependent on the y component of the IMF. These local time regions are connected around the boundary using cubic s -lines through zero points that are also dependent on the y component of the IMF. The potential distribution inside this boundary is completed using a cubic spline that connects the specified boundary potentials with the location of a zero potential dependent on the y component of the IMF. Equatorward of the polar cap boundary, the electrostatic potential is specified by the segment of a Gaussian with a half-width dependent on local time only.

30.4 Database

The functional forms utilized in the model are those that adapt most readily to the variety of two-cell convection patterns described by a number of workers. The dependence of the major driving parameters on the IMF was derived from fits to the derived potential distributions available from the DE-2 database.

30.5 Publication References

30.5.1 Volland, H. (1975), Models of the global electric fields within the magnetosphere, *Ann. Geophys.* 31, 159.

30.5.2 Heelis, R.A., J.K. Lowell, and R.W. Spiro (1982), A model of the high-latitude ionospheric convection pattern, *J. Geophys. Res.* 87, 6339.

30.5.3 Foster, J.C. (1983), An empirical electric field model derived from Chatanika radar data, *J. Geophys. Res.* 88, 981–987.

30.5.4 Heppner, J.P., and N.C. Maynard (1987), Empirical high latitude electric field models, *J. Geophys. Res.* 92, 4467–4489.

30.5.5 Hairston, M.R., and R.A. Heelis (1990), A model of the ionospheric convection pattern for southward IMF based on DE-2 observations, *J. Geophys. Res.* 95, 2333–2343.

30.6 Authors

Primary author: R. A. Heelis (heelis@utdallas.edu).

30.7 Model Codes and Sources

Functional forms that constitute the model are available in the published literature. Source codes that provide callable subroutines to provide the potential at any given location are available from R. A. Heelis, W. B. Hanson Center for Space Sciences, University of Texas at Dallas, Box 830688, Richardson, TX 75083-0688, USA (email: heelis@utdallas.edu).

31 Heppner-Maynard Electric Field Models

31.1 Model Content

The Heppner-Maynard Electric Field Models of high-latitude convection electric fields were derived from the DE-2 satellite electric field measurements using a pattern recognition technique (Heppner and Maynard, 1987). The models are empirically derived potential patterns for various interplanetary magnetic field (IMF) orientations and for varying levels of K_p . The original patterns were presented for a nominal K_p level of 3+ with rules for changing size and potential strength as K_p varied. These patterns were parameterized using fits to spherical harmonic functions by Rich and Maynard (1989). The parameterized version covers K_p levels up through 7.

Convection patterns in the high-latitude ionosphere vary; however, basic signatures in the data tend to repeat for similar IMF conditions (Heppner, 1973). The goal was to develop a minimum set of patterns that would be representative of most conditions. Three patterns for IMF B_z south were derived. The BC pattern is representative of convection in the northern (southern) hemisphere for B_y negative (positive) conditions. In the BC and DE patterns, the polar cap convection is tilted to one side or the other. The A pattern is symmetric across the polar cap and is more often found in the sunlit hemisphere for appropriate IMF conditions.

For northward IMF, two levels of distortion of the southward IMF patterns were proposed. These patterns are qualitative but are conceptually useful. For pure B_z north, the pattern is more likely to be a four-cell pattern rather than the distorted two-cell. Both the distorted two-cell and the four-cell patterns are seen in the empirical models of Rich and Hairston (1994), which are derived from averaging DMSP ion drift data.

The advantage of a pattern recognition technique is that features near noon and midnight, which tend to shift back and forth in magnetic local time, retain their crispness of definition. A straight averaging technique tends to wash out detail in these regions because of the dynamics of these regions.

The Rich-Maynard parameterization of the Heppner-Maynard patterns requires the IMF B_z and B_y polarities to specify the pattern's type and the K_p level. The output is a map of the potential. All patterns are given in magnetic-latitude/magnetic-local-time coordinates in a coordinate system corotating with the Earth. This is the natural system of the ionosphere. Conversion of these patterns into the inertial system, which is the natural system of the magnetospheric source, can be found in Maynard et al. (1995).

31.2 Model Uncertainties and Limitations

The model is valid at all altitudes in the ionosphere, assuming equipotential magnetic field lines. The projection of the electric fields along the magnetic field assumes that $\mathbf{E} \times \mathbf{B} = 0$. Above the ionosphere, field-aligned electric fields at auroral latitudes may distort the projection back to the magnetospheric source.

The model is meant to represent the potential pattern for typical conditions for given model inputs. The model may or may not replicate the real convection pattern in any individual circumstance. This is especially true in the noon and midnight portions of the pattern, where considerable shifts in the pattern with magnetic local time are possible. Local mesoscale processes that may exist within the global system may distort areas of these global scale patterns.

The northward IMF patterns are conceptual only. The complexity of the patterns and the limited database do not provide the statistical significance that exists with the southward IMF patterns. For weak northward IMF, the appropriate southward patterns for the given K_p conditions will approximate actual conditions. As the IMF turns more northward, the patterns evolve to the mildly distorted patterns and eventually toward the strongly distorted patterns or into a four-cell pattern.

31.3 Basis of Model

The Heppner-Maynard patterns have been fitted to a spherical harmonic function based on Legendre polynomials. The resulting equipotential contours describe the plasma flow directions based on $\mathbf{E} \times \mathbf{B} = 0$ and the convective flow $\mathbf{E} \times \mathbf{B}/B^2$ in an incompressible fluid.

The global scale validity of the southward IMF models is attested to by the field-aligned current patterns derived by Rich and Maynard (1989) using the Heppner-Maynard patterns and the Hardy et al. (1987) conductivity patterns (averaging patterns based on DMSP energetic electron precipitation statistical patterns). The divergence of the perpendicular currents calculated from these two empirical average patterns combines to produce reasonable facsimiles of the Iijima and Potemra (1976) average field-aligned current patterns based on Triad data.

31.4 Database

The Heppner-Maynard patterns were derived from the double-probe electric field data from the DE-2 satellite covering the period from August 1981 to February 1983. This is a solarmax database.

31.5 Publication References

31.5.1 Hardy, D.A., M.S. Gussenhoven, R. Raistrick, and W.J. McNeil (1987), Statistical and functional representations of the patterns of auroral energy flux. Number flux and conductivity, *J. Geophys. Res.* 92, 12,275.

31.5.2 Heppner, J.P. (1972), Polar cap electric field distributions related to the interplanetary magnetic field, *J. Geophys. Res.* 77, 4877.

31.5.3 Heppner, J.P., and N.C. Maynard (1987), Empirical high-latitude electric field models, *J. Geophys. Res.* 92, 4467.

31.5.4 Iijima, T., and T.A. Potemra (1976), The amplitude distribution of field-aligned currents at northern high latitudes observed by triad, *J. Geophys. Res.* 81, 2165.

31.5.5 Maynard, N.C., W.F. Denig, and W.J. Burke (1995), Mapping ionospheric convection patterns to the magnetosphere, *J. Geophys. Res.* 100, 1713.

31.5.6 Rich, F.J., and M. Hairston (1994), Large-scale convection patterns observed by DMSP, *J. Geophys. Res.* 99, 3827.

31.5.7 Rich, F.J., and N.C. Maynard (1989), Consequences of using simple analytical functions for the high-latitude convection electric field, *J. Geophys. Res.* 94, 3697.

31.6 Dates of Development, Authors, and Sponsors

31.6.1 Dates

1976 Beginning of NASA Dynamics Explorer program.

1981 Satellites launched.

1987 Model completed and published.

1989 Parameterization of the models completed and published.

31.6.2 Authors (principal): J. P. Heppner, NASA Goddard Space Flight Center (now at Hughes STX, Lanham, MD); N. C. Maynard, NASA Goddard Space Flight Center and Phillips Laboratory (now at Mission Research Corporation, Nashua, NH); and F. J. Rich, Phillips Laboratory.

31.6.3 Sponsors: NASA, Phillips Laboratory, and Air Force Office of Scientific Research.

31.7 Model Codes and Sources

The model is written in Fortran and is easily run on a workstation. It is available from F. J. Rich, Space Physics Division (Mail Code GPSG), Phillips Laboratory, 29 Randolph Road, Hanscom AFB, MA 01731 (email: rich@plh.af.mil).

DRAFT--For Public Review Only--Dec 2013

32 Millstone Hill Empirical Electric Field Model, 1986

32.1 Model Content

The Millstone Hill Empirical Electric Field Models are average patterns of ionospheric electric field derived from Millstone Hill incoherent scatter radar observations covering all local times at sub-auroral and auroral latitudes. Over 2.5 million radar measurements of plasma convection velocity, taken over the six-year interval from 1978–1984 were used in a variety of models. Bin-averaged convection models were generated from the radar data for each of the nine levels of an empirical high-latitude particle precipitation model derived from NOAA/TIROS satellite observations (Foster et al., 1986). Data were binned and averaged vectors calculated each 0.5 hr of local time in 2° steps between 55° and 75° apex magnetic latitude. (Apex latitude is nearly identical to invariant latitude at Millstone Hill's longitude.) Averaged velocity vectors were determined completely independently in each cell. Assuming that the observed plasma velocities are the result of $\mathbf{E} \times \mathbf{B}$ drifts in a time-stationary electric field, an analytical potential model with 12 (14)° of freedom in local time (latitude) was fit to each bin-averaged velocity pattern; these are available as coefficients of the B-spline expansion of the ionospheric electric field in magnetic latitude-local time coordinates. The methodology followed in constructing these empirical models accentuates the close relationship between electric field and conductances at ionospheric heights. The relationship, as presented in these models, was discussed by Kamide and Richmond (1987) and by Foster (1987). Averaged patterns of ionospheric conductances, derived in a similar fashion from the NOAA/TIROS database, were presented by Fuller-Rowell and Evans (1987); these were combined with the Millstone Hill electric field models to provide quantitative patterns of field-aligned currents by Foster et al. (1989). IMF sector dependence of auroral-latitude convection is represented by a set of models that binned the radar velocity observations by the 1-hr averaged values of IMF B_y and B_z components (Foster et al., 1986b). These IMF-dependent models were extended to polar latitudes through the inclusion of five years of data from the Sondrestrom incoherent scatter radar. The Millstone Hill empirical electric field models are used as electric field basis functions in studies of high-latitude electrodynamics using the KRM (Richmond et al., 1988) and AMIE (Knipp et al., 1989) techniques.

32.2 Model Uncertainties and Limitations

The electric fields presented in these models describe average conditions on Millstone Hill's longitude (285°E), and electric field patterns determined here may reflect the unique Northern Hemisphere relationship between solar-produced and auroral conductivities found in this sector. These are numerically averaged models and, as such, do not contain external biases due to data selection or interpretation. However, averaging smoothes boundaries (spatially) and reduces the extreme values in the patterns. The effects of individual substorms are not represented in these models, which average over such temporal/spatial effects.

32.3 Basis of Model

Assume that the observed plasma velocities are the result of $\mathbf{E} \times \mathbf{B}$ drifts in a time-stationary electric field.

32.4 Input to the Model

Either the precipitation activity index or its associated value of K_p (Foster et al., 1986a) determines which averaged pattern is accessed. Alternately, models dependent on IMF B_y/B_z are available. The analytic subroutine provided with the model coefficients outputs field components or potential value at a user-specified latitude and local time.

32.5 Publication References

32.5.1 Evans, D.S., T.J. Fuller-Rowell, S. Maeda, and J. Foster (1987), Specification of the heat input to the thermosphere from magnetospheric processes using TIROS/NOAA auroral particle observations, *Adv. Astronaut. Sci.* 65, 1649–1668.

32.5.2 Foster, J.C., J.M. Holt, R.E. Musgrove, and D.S. Evans (1986a), Ionospheric convection associated with discrete levels of particle precipitation, *Geophys. Res. Letters* 13, 656–659.

32.5.3 Foster, J.C. (1987a), Radar-deduced models of the convection electric field, *Quantitative Modeling of Magnetosphere-Ionosphere Coupling Processes*, pp. 71–76, edited by Y. Kamide, Kyoto Sangyo Univ. Publishers, Kyoto.

32.5.4 Foster, J.C. (1987b), Reply to Kamide and Richmond, *Geophys. Res. Lett.* 14, 160–161.

32.5.5 Foster, J.C., J.M. Holt, R.G. Musgrove, and D.S. Evans (1986b), Solar wind dependencies of high-latitude convection and precipitation, *Proceedings of the Chapman Conference on Solar Wind-Magnetosphere Coupling*, edited by Y. Kamide and J. Slavin, Boston: D. Reidel, pp. 477–494.

32.5.6 Foster, J.C., T. Fuller-Rowell, and D.S. Evans (1989), Quantitative patterns of large-scale field-aligned currents in the auroral ionosphere, *J. Geophys. Res.* 94, 2555–2564.

32.5.7 Fuller-Rowell, T., and D.S. Evans (1987), Height-integrated Hall and Pedersen conductivity patterns inferred from the NOAA-TIROS satellite data, *J. Geophys. Res.* 92, 7606–7618.

32.5.8 Maeda, S., T.J. Fuller-Rowell, D.S. Evans, and J.C. Foster (1987), Numerical simulations of thermospheric disturbances excited by magnetospheric energy input, *Quantitative Modeling of Magnetosphere-Ionosphere Coupling Processes*, pp. 22–27, edited by Y. Kamide, Kyoto Sangyo Univ. Publishers, Kyoto.

32.5.9 Kamide, Y., and A.D. Richmond (1987), Comment on “Ionospheric convection associated with discrete levels of particle precipitation,” *Geophys. Res. Lett.* 14, 158–159.

32.5.10 Knipp, D.J., A.D. Richmond, J.C. Foster, et al. (1989), Electrodynamical patterns for September 19, 1984, *J. Geophys. Res.* 94, 16913–16923.

32.5.11 Richmond, A.D., Y. Kamide, B.H. Ahn, et al. (1988), Mapping electrodynamic features of the high-latitude ionosphere from localized observations: combined incoherent-scatter radar and magnetometer measurements for 1984 January 18–19, *J. Geophys. Res.* 93, 5760–5776.

32.6 Dates of Development, Authors, and Sponsors

32.6.1 Dates:

- 1986 Precipitation index/ K_p models.
- 1986 IMF B_y/B_z models.
- 1988 Millstone/Sondrestrom merged models.

32.6.2 Author (principal): John Foster, Associate Director, MIT Haystack Observatory, Westford, MA.

32.6.3 Sponsor: U.S. National Science Foundation.

32.7 Model Code

Fortran codes to generate full LT/latitude patterns of electrostatic potential or electric field components or magnitude have been distributed to the community or are available from the authors. The model has been deposited in the NCAR/CEDAR database for research community use.

33 APL High-Latitude Convection Model

33.1 Model Content

The Atmospheric and Ionospheric Remote Sensing group of the Johns Hopkins University Applied Physics Laboratory (APL) has developed an empirical model of high-latitude magnetospheric plasma convection. The principal product is the distribution of electrostatic potential in invariant latitude and MLT coordinates above $\sim 50^\circ\Lambda$. The contours of constant electrostatic potential delineate the plasma drift trajectories. The values of the electric field and drift velocity at any position can be directly inferred. The model is keyed to such indices of geomagnetic conditions as the IMF and K_p .

The model can be reduced to a set of coefficients that describe a series expansion of the potential in spherical harmonics. Equipped with these coefficients and the transformation formulas given below, the user can generate all convection parameters.

At the current stage of development, the most complete modeling has been done for the primary IMF dependencies, namely, IMF magnitude in the y-z plane (three levels) and orientation (45° step in IMF y-z clock angle). There is also a detailed solution for the IMF y-z clock angle dependencies under moderately disturbed conditions, $2 < K_p < 3+$.

33.2 Model Uncertainties and Limitations

33.2.1 The model is statistical in nature and hence can only approximate real-time convection, which is known to be highly variable. For example, the transient effects associated with substorm phases cannot be reliably imaged.

33.2.2 Beyond the effective latitudinal limits of radar coverage ($65\text{--}85^\circ\Lambda$), the convection is partly solved by applying Laplace's condition,

$$\nabla^2 \Phi = 0$$

subject to boundary conditions that include the assumption that the region below a reference latitude Λ_0 is shielded from the convection electric field. The model can be expected to be less reliable outside the region of direct radar observations.

33.2.3 The radar velocity coverage becomes sparse for more restricted conditions, e.g., small steps in IMF clock angle or K_p disturbance level. The indicial sorting intervals are selected for reliable mapping of the large-scale convection over as large a range of indicial variation as possible. Where the statistics are insufficient, a reduction in the quality of the results may be apparent.

33.2.4 The geomagnetic field model of Baker and Wing (1989) was applied in the analysis. The field models in common usage can differ in latitude by several degrees.

33.3 Basis of the Model

33.3.1 The model is based on observations carried out with the coherent-scatter HF radar located at Goose Bay, Labrador, over the period September 1987–July 1993. This instrument measures the $\mathbf{E} \times \mathbf{B}$ drift of F-region plasma at invariant latitudes greater than $65^\circ\Lambda$.

33.3.2 To generate the model for a set of specified conditions, the line-of-sight velocity data are first sorted and averaged in 12 min UT bins. Two-dimensional vectors are generated by examining the variation of the line-of-sight velocity within MLT/latitude cells with UT. The vectors are then fitted to a polynomial expansion of the electrostatic potential distribution. The mapping of the potential is extrapolated to the high polar cap and lower latitude regions. Finally, the potential distribution is expressed as a series expansion in spherical harmonics.

33.3.3 The product of the analysis is the set of coefficients required to solve for the electrostatic potential via the expression

$$\Phi(\theta, \varphi) = \sum_{l=0}^{\infty} \sum_{-l}^l A_{lm} Y_{lm}(\theta, \varphi)$$

where the spherical harmonics are defined by

$$Y_{lm}(\theta, \varphi) = \sqrt{\frac{2l+1}{4\pi} \frac{(l-m)!}{(l+m)!}} P_l^m(\cos\theta) e^{im\varphi}$$

and the effective colatitude is given by

$$\theta = \frac{\pi}{\left(\frac{\pi}{2} - \Lambda_0\right)} \left(\frac{\pi}{2} - \Lambda\right)$$

where φ is the MLT clock angle in radians measured from 0 MLT, Λ is the invariant latitude in radians, and Λ_0 is a reference latitude in radians that is output by the model. The electric field and convection velocity can be solved from the relations

$$\mathbf{E} = -\nabla\Phi \text{ and } \mathbf{v} = (\mathbf{E} \times \mathbf{B}) / B^2$$

33.3.4 The derivation of the model and the related analysis were described by Ruohoniemi and Greenwald (1995, 1996).

33.4 Database

The primary measurements of convection velocity were made with the Goose Bay HF radar. This instrument is located at 299.5°E longitude and 53.3°N latitude. It operates around the clock and completes an azimuthal scan of the F-region ionosphere north of the site every 2 min. The Goose Bay radar is part of a network of HF radars that have recently been installed at high latitudes as part of the SuperDARN initiative (Greenwald et al., 1995). The IMF data were culled from the records of the IMP8 spacecraft provided by several sources of geophysical data.

33.5 Publication References

33.5.1 Baker, K.B., and S. Wing (1989), A new magnetic coordinate system for conjugate studies of high latitudes, *J. Geophys. Res.* 94, 9139–9143.

33.5.2 Greenwald, R.A., et al. (1995), DARN/SuperDARN: a global view of high-latitude convection, *Space Sci. Rev.* 71, 763–796.

33.5.3 Ruohoniemi, J.M., and R.A. Greenwald (1995), Observations of IMF and seasonal effects in high-latitude convection, *Geophys. Res. Lett.* 9, 1121–1124.

33.5.4 Ruohoniemi, J.M., and R.A. Greenwald (1996), Statistical patterns of high latitude convection obtained from Goose Bay HF radar observations, *J. Geophys. Res.* 101, 21,743–21,763.

33.6 Dates of Development, Authors, and Sponsors

33.6.1 Date

1995 Development of code to reduce archival Goose Bay HF radar velocity data to maps of high-latitude convection.

33.6.2 Authors: J. Michael Ruohoniemi and Raymond A. Greenwald.

33.6.3 Sponsor: The National Science Foundation.

33.7 Model Codes and Sources

The model, or portions thereof, can be readily acquired either in the form of global maps of the electrostatic potential or as sets of coefficients that describe expansions of the potential patterns in terms of spherical harmonics. A small package of IDL routines allows easy access to the outputs of the model in graphical or digital form. The inventory of currently available solutions was described in Sec. 1. Interested persons should contact the authors at mike_ruohoniemi@jhuapl.edu or ray_greenwald@jhuapl.edu.

DRAFT--For Public Review Only--Dec 2013

34 Weimer Electric Potential, Current, and Joule Heating Models

34.1 Model Content

The Weimer ionosphere model is a combination of two models, one for high-latitude electric potentials and the other representing field-aligned currents (FAC). Combined, the models also provide the Poynting flux into the ionosphere, which is dissipated in the ionosphere as Joule heating. The models require solar wind and interplanetary magnetic field (IMF) values for input, and output the potential in kilovolts (kV), current in microamperes per square meter ($\mu\text{A}/\text{m}^2$), and energy flux in milliwatts per square meter (mW/m^2). The current and energy flux/heating are mapped to an altitude of 110 km. Input locations are specified as latitude and magnetic local time (MLT) in modified apex coordinates, similar to altitude-adjusted corrected geomagnetic coordinates.

34.2 Model Uncertainties and Limitations

Comparing the most recent (2005) model predictions of electric potential with the DE-2 measurements of electric potential, the following results were obtained: taking the average of the difference between the potentials at all points along the track, the median error is 6.0 kV, and in 90% of the passes the errors were less than 12.3 kV. Taking the differences between the polar cap potential drop (maximum potential minus minimum potential), the median error is 8.7 kV, and 90% of the passes were within 26.6 kV. The passes where the errors are the largest use IMF measurements from the ISEE-3 spacecraft rather than IMP-8. As ISEE-3 was often located over 100 R_E away from the Earth–Sun line, the IMF measured there is sometimes not the same as what impacts the magnetopause.

The model is limited by insufficient measurements with the DE-2 satellite during times having IMF magnitudes over 15 nT. The 2005 version has a saturation curve that seems to produce reasonable values at higher IMF magnitudes, where accuracy is uncertain.

The model does not mimic the ionosphere's tendency to change faster on the dayside than on the nightside when there is an IMF transition. Also, in sudden solar wind pressure pulses, it is known that the polar cap potential increases momentarily then decays; the model does not have this feature. The model does not have the ability to predict substorm variations, nor small, km-scale fluctuations. The electric potentials and currents in the model are always zero at the lower-latitude boundary. This model does not include the subauroral polarization streams (SAPS/SAID), strong, subauroral ion flow following geomagnetic storms and substorms.

Currently in progress is a project to compare the integrated Poynting energy flux with changes in total thermospheric energy, as derived from density measurements with the GRACE and CHAMP satellites. Preliminary results indicate that the model can very accurately predict changes in the global nighttime minimum exospheric temperature. At heating levels over 500 GW a reduction in the model output is required to match the measurements, indicating that the model results are too high in saturation.

34.3 Basis of Model

The models are based on measurements from the Dynamics Explorer-2 satellite, which orbited at altitudes of 300 to 1000 km from August 1981 to March 1983. The electric potential model is derived from measurements from the Vector Electric Field Instrument (VEFI), using the double floating probe technique. Electric potentials were obtained by integrating the electric field in the direction of motion along the orbit track. The field-aligned current model is based on measurements from a triaxial fluxgate magnetometer on DE-2. An integral of the vector component perpendicular to the orbit plane was used to obtain a scalar, magnetic Euler potential along orbit paths. Simultaneous IMF measurements are from the IMP-8 and ISEE-3 satellites. IMP-8 measurements could be used only while the spacecraft was on the sunward side of the magnetosphere and bow shock. The total number of passes available was limited by instrument duty cycles, as well as availability of IMF measurements. The processed database contains 2608 polar cap passes with electric potential, and 2403 passes with magnetic potential.

The most recent version of the model (2005) is based on spherical cap harmonic analysis (SCHA) functions to the order of 2 and degree of 12. Each coefficient in the harmonic expansion varies according

to the IMF and the tilt angle. Potentials are zero at the lower-latitude boundary, the spherical cap half-angle. The size of this cap expands and contracts according to the IMF. Field-aligned currents are derived from the magnetic potential by two-dimensional Laplacian on the spherical surface. Poynting fluxes are derived from the cross-product of electric fields and magnetic field perturbations. The electric field comes from the gradient of the electric potential function, and the magnetic perturbation comes from the gradient of the magnetic potential function, rotated by 90° .

34.4 Model Input Parameters

The model requires specification of location as geomagnetic latitude (degrees) and MLT (hours). IMF is specified in GSM coordinates as magnitude in the y-z plane in nT, and “clock angle” in degrees (clock angle is zero in the GSM +z direction, 90° in the GSM +y direction). Solar wind velocity is in km/s, and proton number density is in number/cm³. Optional AL index input is in units of nT. The IMF parameters should be averages over the prior 15 to 20 min, following propagation to the location of Earth if measured at L1 orbit. The dipole tilt angle in degrees is required, which controls the seasonal variation. The dipole tilt is the angle of rotation that converts between GSM and SM coordinates (positive when the northern magnetic pole is tilted toward the Sun).

34.5 Publication References

- 34.5.1** Weimer, D. (1995), Models of high-latitude electric potentials derived with a least error fit of spherical harmonic coefficients, *J. Geophys. Res.* 100, 19,595.
- 34.5.2** Weimer, D. (1996), A flexible, IMF dependent model of high-latitude electric potential having “space weather” applications, *Geophys. Res. Lett.* 23, 2,549.
- 34.5.3** Weimer, D. R. (2000), A new technique for the mapping of ionospheric field-aligned currents from satellite magnetometer data, in *Magnetospheric Current Systems*, *Geophys. Monogr. Ser.*, vol. 118, edited by S. Ohtani et al., pp. 381–388, AGU, Washington, D. C., doi:10.1029/GM118p0381.
- 34.5.4** Weimer, D. (2001a), An improved model of ionospheric electric potentials including substorm perturbations and application to the geospace environment modeling November 24, 1996, event, *J. Geophys. Res.* 106, 407.
- 34.5.5** Weimer, D. (2001b), Maps of ionospheric field-aligned currents as a function of the interplanetary magnetic field derived from Dynamic Explorer 2 data, *J. Geophys. Res.* 106, 12,889.
- 34.5.6** Weimer, D.R. (2005a), Improved ionospheric electrodynamic models and application to calculating Joule heating rates, *J. Geophys. Res.* 110, A05306, doi: 10.1029/2004JA010884.
- 34.5.7** Weimer, D.R. (2005b), Predicting surface geomagnetic variations using ionospheric electrodynamic models, *J. Geophys. Res.* 110, A12307, doi: 10.1029/2005JA011270.

34.6 Dates of Development, Authors, and Sponsors

34.6.1 Dates

- 1995 First publication of ionospheric potential patterns, using least squares fitting with spherical harmonics.
- 1996 First version of electric potential model, for arbitrary IMF inputs. Low-latitude boundary fixed at 45° magnetic latitude.
- 2000 Description of method for mapping field-aligned currents from magnetometer measurements.
- 2001 Revised electric potential model and new field-aligned current model. Latitude of low-latitude boundary varies as function of IMF.
- 2005 Both models revised and combined in the same program, including calculation of Poynting flux/Joule heating. Most recent revision followed in the same year, using SCHA functions, with description

of method for calculating geomagnetic perturbations on the ground. Polar cap half-angle varies as function of IMF.

34.6.2 Author: Daniel R. Weimer, now at Virginia Tech, Center for Space Science and Engineering Research. (Mail address: National Institute of Aerospace, 100 Exploration Way, Hampton, VA 23666)

34.6.3 Sponsors: NSF, NASA, and Air Force Research Laboratory.

34.7 Model Codes and Sources

The models are all written in IDL. The latest version is distributed as precompiled IDL modules, which can run on various platforms using the IDL Virtual Machine (available at <http://www.itvis.com>). This distribution package includes versions for interactive graphics display, as well as batch-style, gridded output to text files. Output to geographic coordinates is an option. A Fortran version of only the electric potential model is also available. Requests should be sent to D. Weimer (email: dweimer@vt.edu). Real-time maps and updates will be posted at <http://mist.nianet.org>.

DRAFT--For Public Review Only--Dec 2013

35 The Assimilative Mapping of Ionospheric Electrodynamics (AMIE)

35.1 Model Content

The Assimilative Mapping of Ionospheric Electrodynamics (AMIE) procedure is one in which ground and space-based observations create a coherent and objective picture of the high-latitude ($>50^\circ$ magnetic) ionospheric electrodynamic system. The analytic algorithm combines information from physical models and data. It satisfies Maxwell's equations and Ohm's law and fits data by a weighted least squares method, consistent with the data uncertainty. The result is a snapshot of the system in terms of electric field, electric potential, and horizontal currents as well as height-integrated conductance, Joule heating, and field-aligned currents mapped to 110 km. The snapshots are often used, in sequence, as the basis for other dynamical models such as the NCAR TIME-GCM.

35.2 Model Uncertainties and Limitations

The procedure incorporates a number of features, including checking for data outliers to identify extreme or bad data. It also estimates uncertainties in the mapped output. It uses available statistical information concerning average patterns, standard deviations, and correlation distances of the various parameters.

The method assumes a simplified ionospheric current geometry: radial field-aligned currents and thin current layers for the ionospheric and induced terrestrial current systems, and negligible wind-dynamo effects. The algorithm is analytic rather than time evolutionary, thus there is no explicit time dependence.

35.3 Basis of the Model

The Assimilative Mapping of Ionospheric Electrodynamics (AMIE) procedure combines space-based and ground-based electrodynamic observations with an empirical model of the high-latitude global convection to infer distributions of high-latitude ionospheric electric fields and currents, geomagnetic-field-aligned currents, and the associated geomagnetic perturbation fields at both ground and low-Earth-orbit altitudes. Ohm's law relates the height-integrated electric current to the electric field with the assumption of *a priori* ionospheric Pedersen and Hall conductance distributions, while the Biot-Savart relation is used to relate the magnetic perturbation fields to the ionospheric and field-aligned currents. The procedure carries out an objective multivariate functional analysis of high-latitude ionospheric electrodynamic variables, with all the variables presumed linearly related under the assumption that the ionospheric conductance is known. The result is a least squares fit to the difference between the data and a background model. This fit is then added to the background model. This allows for a stable result with even minimal amounts of data and prevents non-physical solutions. The background models are typically statistical models driven by the solar wind and interplanetary magnetic field or the hemispheric power index. The algorithm functions when data are sparse by reverting to the background model.

The AMIE procedure is often run in two steps. The first assimilation step derives global estimates of Pedersen and Hall conductances at 110 km. The derivations proceed by choosing an appropriate climatological background conductance model (which includes solar zenith and hemispheric power information). Subsequently, satellite low-energy particle and ground magnetometer data, previously processed through empirical models to give local estimates of conductance, are assimilated. *A priori* information helps to determine the physical nature of the fit. For example, the auroral zone is known to be stretched in longitude and rather narrow in the dayside and thicker on the nightside. These characteristics can be described mathematically in the covariance matrix of the procedure, dependent on the chosen basis functions. The output of the first step is the conductance distribution maps, which provide information about the state of the ionosphere in their own right, but are also used as a key input into the second assimilation step that estimates the electric potential pattern for the high latitude ionosphere.

In the second step of the AMIE procedure, interplanetary magnetic field and solar wind data are used to select an appropriate climatological electric potential pattern. Ion drift and radar data are then assimilated along with ground magnetometer and/or satellite magnetometer data that have been previously related to the electric field via appropriate physics and conductance models. Once the electric potential pattern is

determined, Maxwell's equations and other laws of physics guide the assimilation procedure in creating the maps of ionospheric fields, currents, and other parameters.

35.4 Database and Input to the Model

35.4.1 Data ingest: Ground magnetometer data (background removed), incoherent and coherent scatter radar measurements, Low Earth orbiting satellite ion drift, magnetic perturbations, precipitating particles measurements, and estimates of conductance based on satellite imagery. The background conductance model may use Fuller-Rowell and Evans (1987). Climatological electric field models may include the Foster Convection Model (1986), Heppner and Maynard Electric Field Model (1987), Weimer Electric Potential Model (1996, 2001), and Ruohoniemi and Greenwald Convection Model (1996).

35.4.2 Background models:

Foster, J.C., J.M. Holt, R.G. Musgrove, and D.S. Evans (1986), Ionospheric convection associated with discrete levels of particle precipitation, *Geophys. Res. Lett.* 13, 656–659.

Fuller-Rowell, T.J., and D.S. Evans (1987), Height-integrated Pedersen and Hall conductivity patterns inferred from the TIROS-NOAA satellite data, *J. Geophys. Res.* 92, 7606–7618.

Heppner, J.P., and N.C. Maynard (1987), Empirical high-latitude electric field models, *J. Geophys. Res.* 92, 4467–4489.

Ruohoniemi, J.M., and R.A. Greenwald (1996), Statistical patterns of high-latitude convection obtained from Goose Bay HF radar observations, *J. Geophys. Res.* 101, 21,743–21,763.

Weimer, D. (1996), A flexible, IMF dependent model of high-latitude electric potential having “space weather” applications, *Geophys. Res. Lett.* 23, 2,549.

Weimer, D.R. (2001), An improved model of ionospheric electric potentials including substorm perturbations and application to the GEM November 24, 1996 event, *J. Geophys. Res.* 106, 407.

34.5 Publication References

34.5.1 Crowley, G., and C.L. Hackert (2001), Quantification of high latitude electric field variability, *Geophys. Res. Lett.* 28(14), 2783–2786.

34.5.2 Emery, B.A., et al. (1996), Assimilative mapping of ionospheric electrodynamic in the thermosphere-ionosphere general circulation model comparisons with global ionospheric and thermospheric observations during the GEM/SUNDIAL period of March 28–29, 1992, *J. Geophys. Res.* 101.

34.5.3 Kihn, E.A., and A.J. Ridley (2005), A statistical analysis of the assimilative mapping of ionospheric electrodynamic auroral specification, *J. Geophys. Res.* 110, 1–11.

34.5.4 Knipp, D.J. (1989), Quantifying and reducing uncertainty in the assimilative mapping of ionospheric electrodynamic procedure, Ph D Dissertation, University of California, Los Angeles.

34.5.5 Lu, G., et al. (1998), Global energy deposition during the January 1997 magnetic cloud event, *J. Geophys. Res.* 103, 11,695–11,684.

34.5.6 Richmond, A.D., and Y. Kamide (1988), Mapping electrodynamic features of the high-latitude ionosphere from localized observations: technique, *J. Geophys. Res.* 93, 5741–5759.

34.6 Dates of Development, Authors, and Sponsors

34.6.1 Dates: 1986–1989; see also <http://www.hao.ucar.edu/modeling/amie/DOCS/references.html>

34.6.2 Authors: A. Richmond and Y. Kamide

34.6.3 Sponsors: National Center for Atmospheric Research

34.7 Model Codes and Sources

The model was developed in Fortran. It is scheduled for a major upgrade sponsored by the NSF National Space Weather Program during 2011–2013. Iridium satellite magnetometer data will be included. AMIE is used extensively by Atmospheric and Space Technology Research Associates, LLC.

DRAFT--For Public Review Only--Dec 2013

36 HWM Empirical Wind Model

36.1 Model Content

The HWM (Horizontal Wind Model) provides an estimate of the climatological average meridional and zonal components of the atmospheric wind vector as a function of altitude, latitude, longitude, day of year, time of day, and solar and magnetic activity. Solar and magnetic activity variations are only included for the thermosphere. Solar diurnal and semidiurnal tides are included in the stratosphere and above, with annual and semiannual variations at all altitudes. Longitude and UT variations related to magnetic field control of energy input and drag forces are included in the thermosphere and stationary wave longitude variations in the lower atmosphere (7–90 km).

36.2 Model Uncertainties and Limitations

Solar activity variations are weak and not very clearly delineated by the data. Because of the sparsity of data between 130 and 220 km and concern with providing reasonable continuity through this region, a simplifying assumption of proportionality to exospheric winds was introduced in this region. Rapid changes in winds at high latitudes resulting from magnetic control are likely underestimated by the small number of harmonics used. Quasi-biennial variations in the lower atmosphere are not included. Longitude variations in the lower atmosphere were only represented by the non-divergent vector field and had to be dependent on gradient wind derivations. Meridional winds are assumed to be zero below 45 km. There appear to be unresolved discrepancies between measurement techniques in the mesopause region, which are a difficulty for model generation at these altitudes.

Overall root mean square differences between data and model values are on the order of 100–150 m/sec in the high-latitude thermosphere and 50 m/sec or less at mid to low latitudes. Root mean square differences are 15 m/sec in the mesosphere and 10 m/sec in the stratosphere for zonal winds, and 10 and 5 m/sec, respectively, for meridional winds.

36.3 Basis of the Model

The model represents spatial variations in the wind vector by an expansion in vector spherical harmonics, with each expansion coefficient represented by a Fourier series in universal time and/or day of year as appropriate, and with simplified supplemental equations for solar activity and magnetic activity variations. The expansion involves two orthogonal vector fields, the divergence B field and the rotational C field. Above 200 km, the altitude variations of the wind components are each represented by an analog of the Bates formula as used for thermospheric temperature profiles. Below 200 km, the wind profiles are represented by a cubic spline between specified nodes, with first and second derivatives continuous across interior nodes. The variation of the wind at each node is represented by an independent spherical harmonic/Fourier expansion.

36.4 Database and Input to the Model

The primary data incorporated in the model depends upon altitude. For the thermosphere (Hedin et al., 1991a), these are satellite mass spectrometer (WATS on DE-2 and NATE on AE-E) and Fabry-Perot (FPI on DE-2) instruments, ground-based incoherent scatter radar, and ground-based Fabry-Perot optical instrumentation. In the esosphere/lower thermosphere (Hedin et al., 1996), data are included from a wide range of MF radar and meteor radar stations, rocketsondes, rocket grenade soundings, gradient winds from MSISE-90 (Hedin et al., 1991b), CIRA-86, and earlier data tabulations. In the stratosphere, the data include rocketsondes and rocket grenade soundings, CIRA-86, and some earlier data tabulations. In the troposphere, the model is essentially a recasting of CIRA-86. The influence of gradient wind estimates was minimized in favor of direct wind measurements whenever possible. In addition to position and time coordinates, the model (in the thermosphere) requires a 3-month average and previous day value of the 10.7 cm solar flux index (at the earth), and either the daily A_p magnetic index or a prescribed history of 3 hr A_p indices.

36.5 Publication References

36.5.1 Hedin, A.E., N.W. Spencer, and T.L. Killeen (1988), Empirical global model of upper thermosphere winds based on atmosphere and dynamics explorer satellite data, *J. Geophys. Res.* 93, 9959–9989.

36.5.2 Hedin, A.E., et al. (1991a), Revised global model of thermosphere winds using satellite and ground-based observations, *J. Geophys. Res.* 96, 7657–7688.

36.5.3 Hedin, A.E., et al. (1991b), Extension of the MSIS thermosphere model into the middle and lower atmosphere, *J. Geophys. Res.* 96, 1159–1172.

36.5.4 Hedin A.E., et al. (1996), Empirical wind model for the upper, middle and lower atmosphere, *J. Atmos. Terr. Phys.* 58, 1421–1447.

36.6 Dates of Development, Authors, and Sponsors

36.6.1 Dates

1988 HWM-87 satellite-based thermosphere only model.

1991 HWM-90 satellite-based and ground-based thermosphere model.

1996 HWM-93 extension to lower atmosphere (no change in thermosphere).

36.6.2 Author (principal): Alan E. Hedin.

36.6.3 Sponsor: NASA.

36.7 Model Codes and Sources

Fortran subroutines are available from the National Space Science Data Center Request Coordinator Office, NSSDC, Code 633, NASA Goddard Space Flight Center, Greenbelt, MD 20771, tel. 301-286-6695 (email: request@nssdca.gsfc.nasa.gov; <http://nssdc.gsfc.nasa.gov>).

37 Global Empirical Models of T_e

37.1 Model Content

Satellite Langmuir probe measurements have been used extensively to devise global empirical models of F-region T_e and sometimes N_e . The use of *in situ* measurements for this purpose offers many challenges, since orbital limitations and the limited duration of the databases make it difficult to separate spatial and temporal variations (altitude, latitude, local time, season, solar cycle, geomagnetic activity). Therefore, it is usually necessary to devise models that describe limited aspects of ionosphere structure at specific times, such as the latitudinal and local time structure at a fixed altitude or the latitudinal structure at fixed local times and at specific seasons. It is particularly difficult to resolve the solar cycle variations, because satellite lifetimes are usually much shorter than a solar cycle or half of a cycle. One can sometimes combine two or three satellite databases to identify the solar cycle effects, but differences in the inclinations and altitudes of the orbits can make the task more difficult. The following describes several attempts to devise such models using Langmuir probe measurements from the Atmosphere Explorer (AE-C), ISIS-1, ISIS-2, and Dynamic Explorer (DE-2) satellites.

37.2 Global Models for Fixed Altitudes

Brace and Theis (1981) employed measurements from Atmosphere Explorer-C, ISIS-1, and ISIS-2 to define the coefficients of global models that described the variations of T_e at several fixed altitudes (300, 400, 1400, and 2000 km) as a function of dip latitude and local time. Corresponding N_e models were not attempted because the much larger altitude and solar cycle variations of N_e tended to hide or distort the geographical variations. The circular orbit phase of AE-C provided data at altitudes of 300 and 400 km at solar minimum (1975–77), which became the basis for global T_e models for these altitudes. ISIS-2 provided measurements from a circular, near-polar orbit at 1400 km at low to moderate levels of solar activity in 1971–72. The T_e data were used to define the coefficients of a spherical harmonic model of T_e that described the latitude and local time variations at that altitude. The Langmuir probes on ISIS-1 provided data over a range of altitudes between 600 and 3600 km during the relatively weak solar maximum of 1969–70. The T_e data obtained between 2000 and 3600 km were averaged to define the latitude and local time variations at 3000 km.

37.3 Inverse Relationship Between N_e and T_e in the F-Region

During the elliptical orbit phase of the AE-C mission (1973–74), when the perigee was being maintained deep in the lower thermosphere, N_e and T_e were measured frequently down to about 130 km. Brace and Theis (1978) employed these data to investigate the relationship between N_e and T_e in the daytime ionosphere. (In that mission, the total ion density N_i was measured rather than N_e .) As expected, N_e and T_e were found to be inversely related, probably because the electron-ion cooling rate varies as the product of N_i and N_e or N_e^2 . This is the dominant process that determines T_e at altitudes near the F2 peak, whereas electron-neutral cooling becomes more important in the lower F-region and E-region. Since the elliptical phase of the mission lasted only through 1974 (low solar activity), the effect of the solar cycle on the inverse relationship between N_e and T_e could only be determined from later measurements in the circular orbit phase (1975–78) when the orbit was maintained between 250 and 400 km.

The above study of the inverse behavior of N_e and T_e applied only to the daytime ionosphere at latitudes below 50° . Higher latitudes were avoided to eliminate high-latitude electron heat sources. In general, N_e and T_e do not exhibit this inverse behavior in regions where there is no electron heat source (such as in the mid- and low-latitude nighttime ionosphere), since T_e and T_i cool to the gas temperature when the heat source is removed. For example, the nightside does exhibit inverse variations in N_e and T_e at geomagnetic latitudes between 40° and 60° . The electron heating is understood to be caused by heat conduction from the overlying plasmasphere, the time constant for cooling of which is longer than one night. The plasmasphere is also heated by collisions with magnetospheric ring current ions, and this heat causes an elevation of T_e at these latitudes, whereas the behavior of N_e is controlled by plasma and neutral gas transport processes.

37.4 Solar Cycle Effects on the Relationship Between N_e and T_e

The AE-C mission (altitudes between 300 and 400 km) extended well into the period of rising solar activity in 1977 and 1978, thus permitting the solar cycle variations of the F-region to be investigated. Brace and Theis (1984) found little response of T_e to the rising solar activity, although N_e increased significantly. The increased effect of electron heating with increasing solar activity was canceled by increased electron-ion and electron-neutral cooling that goes along with increased ion and neutral gas densities.

The DE-2 Langmuir probe measurements allowed the above AE-C study to be extended through the following solar maximum (1981–83). Brace and Theis (1984) combined the AE-C and DE-2 data to study the effect of solar activity on the relationship between N_e and T_e . Their equation gives the ratio T_e/T_e model as a function of $F_{10.7}$, where T_e represents individual measured values, and T_e model refers to the Brace and Theis (1978) solar minimum model discussed above. At solar maximum, T_e/T_e model is enhanced by nearly a factor of two relative to solar minimum values, although T_e itself did not change much during the solar cycle while N_e increased.

37.5 T_e and N_e Models at Solar Maximum

The DE-2 satellite also provided global Langmuir probe measurements at solar maximum (1981–83). Brace and Theis (1990) used these data to devise an empirical model of the global variation (geomagnetic latitude and local time) of N_e and T_e at 400 km. Legendre polynomials through the fifth order were retained. Their comparisons of the DE-2 and AE-C models with the IRI model showed that the two exhibited similar solar cycle variations. They confirm the fact that T_e does not vary greatly with solar activity, but N_e varies by nearly an order of magnitude from solar minimum to solar maximum.

37.6 Models of the Latitude Variation of N_e and T_e at Fixed Altitudes

An important limitation of the global models (Brace and Theis, 1990) is that the nature of the selected orbit provided insufficient coverage of all the important spatial and temporal variations of the ionosphere. This means that many aspects of the latitudinal and local time structure could not be captured with high resolution; thus, the 1990 global model was limited to fifth-order polynomial. Brace and Theis (1991) attempted to improve the latitudinal resolution by employing subsets of the DE-2 measurements that suppressed the local time, latitude, and seasonal variations. This allowed them to define a seventeenth-order polynomial model of the latitudinal variation of N_e and T_e at fixed altitudes and fixed local times that were allowed by the orbit. This was achieved by limiting the database to narrow altitude slices and single sweeps of perigee from pole to pole. Comparisons of the resulting high-resolution models with the corresponding T_e and N_e measurements themselves showed that most of the latitudinal structure that had previously been washed out in the fifth-order global models (Brace and Theis, 1990) was captured by the higher-order models.

37.7 Publication References

37.7.1 Brace, L.H., and R.F. Theis (1981), Global empirical models of ionospheric electron temperature in the upper F-region and plasmasphere based on in situ measurements from the Atmosphere Explorer-C, ISIS-2 satellites, *J. Atmos. Terr. Phys.* 43, 1317–1343.

37.7.2 Brace, L.H., and R.F. Theis (1978), An empirical model of the interrelationship of electron temperature and density in the daytime thermosphere at solar minimum, *Geophys. Res. Lett.* 5, 275–278.

37.7.3 Brace, L.H., and R.F. Theis (1984), Solar cycle effects upon the relationship of N_e and T_e in the F-region, *Adv. Space Res.* 4(1), 89–91.

37.7.4 Brace, L.H., and R.F. Theis (1990), Global models of N_e and T_e at solar maximum based on DE-2 measurements, *Adv. Space Res.* 10(11), 39–45.

37.7.5 Brace, L.H., and R.F. Theis (1991), Empirical models of the latitudinal variations of T_e and N_e in the ionosphere at solar maximum, *Adv. Space Res.* 11(10), 159–166.

37.8 Authors

Primary authors: L.H. Brace and R.F. Theis.

37.9 Model Codes and Sources

Not available.

DRAFT--For Public Review Only--Dec 2013

38 Empirical Model of the Ionospheric Electron and Ion Temperatures

38.1 Model content

The empirical model provides electron temperatures T_e [K] and ion temperatures T_i [K] as a function of

- Altitude: 50–4000 km
- Attitude: Dipole latitude, N_2 , O_2 , O, NO
- Time: Day count d (annual variation), magnetic local time τ
- Solar activity: Solar flux $F_{10.7}$ for quiet geophysical conditions ($K_p \leq 3$)

The electron and ion temperatures are obtained from the appropriate figures of Köhnlein (1986) at $F_{10.7} = 84 \times 10^{-22} \text{ Wm}^{-2} \text{ Hz}^{-1}$ and $K_p \leq 3$:

Average temperature (time-independent): see Köhnlein (1986, Figs. 4 and 5),

$T_{e,i}$ vs. altitude

Time-independent temperature (latitudinal): see Köhnlein (1986, Figs. 6–11),

$T_{e,i}$ vs. altitude at $\phi = 90^\circ, 45^\circ, 0^\circ, -90^\circ$

$T_{e,i}$ vs. dipole latitude at discrete heights

Annual variation: see Köhnlein (1986, Figs. 12–17),

$T_{e,i}$ vs. altitude at equinox and solstice conditions ($d = 80, 173, 266, 356$)

Comparison with data: $T_{e,i}$ vs. day count at discrete heights

$\Delta T_{e,i}$ (relative): Dipole latitude vs. day count at discrete heights

Diurnal variation: see Köhnlein (1986, Figs. 18–25),

$T_{e,i}$ vs. altitude at $\phi = 0^\circ, 45^\circ$ and $\tau = 0 \text{ hr}, 6 \text{ hr}, 12 \text{ hr}, 18 \text{ hr}$

Comparison with data: $T_{e,i}$ vs. magnetic local time at discrete heights and $\phi = 0^\circ, 45^\circ$

$\Delta T_{e,i}$ (relative): Dipole latitude vs. magnetic local time at discrete heights

and superpositions thereof, i.e., diurnal variation + relative annual variation

- ⇒ diurnal variation at a selected day of the year
- ⇒ annual variation + relative diurnal variation
- ⇒ annual diurnal variation at a selected magnetic local time

38.2 Model Uncertainties and Limitations

The discrepancies between the model and the observations (used) are shown for the annual and diurnal variations in Köhnlein (1986, Figs. 13, 16, 20, 21, 23, 24). In general, the model agrees well with the observations.

The uncertainties of the model are mainly due to the uneven data coverage and the simplicity of the analytical approach (e.g., linearity, no longitudinal terms, no disturbed conditions).

Data from epochs not used in the database may show stronger deviations toward the model. This is especially true for disturbed geophysical conditions that are not considered in the model.

38.3 Basis of the Model

The vertical and horizontal structures of the model are treated on an equal footing.

The electron and ion temperatures are expanded into spherical harmonics (Köhnlein, 1986, Eqs. 1–12) wherein the model coefficients depend on altitude, solar flux $F_{10.7}$, and geomagnetic index K_p .

Restricting the model to quiet geophysical conditions ($K_p \leq 3$), the above coefficients depend linearly on $F_{10.7}$, whereas their height variations are expressed by cubic spline functions.

38.4 Database

The database of the model consists of observations by satellites, incoherent scatter stations, and rocket profiles covering the time interval 1964–1979 (Köhnlein, 1986, Table 1; Brace and Theis, 1981).

38.5 Publication References

38.5.1 Brace, L.H., and Theis, R.F. (1981), Global empirical model of ionospheric electron temperature in the upper F-region and plasmasphere based on in situ measurements from the Atmospheric Explorer-C, ISIS-1, and ISIS-2 satellites, *J. Atmos. Terr. Phys.* 43, 1317.

38.5.2 Köhnlein, W. (1986), A model of the electron and ion temperatures in the ionosphere, *Planetary Space Sci.* 34(7), 609–630.

38.6 Dates of Development, Authors, and Sponsors

38.6.1 Date: 1983.

38.6.2 Author: W. Köhnlein.

38.6.3 Sponsors: Deutsche Forschungsgemeinschaft and University of Bonn.

38.7 Model Codes and Sources

The model was developed in Fortran code, specifically adapted to a CDC-computer. Because of the detailed graphical representation, Köhnlein (1986) can be used as a quick reference for ionospheric temperatures (T_e , T_i) at low solar fluxes ($F_{10.7} \approx 84$) and quiet geophysical conditions ($K_p \leq 3$) in the altitude interval 50–4000 km.

39 Photochemical Equilibrium Model for Ionospheric Conductivity

39.1 Model Content

The Photochemical Equilibrium Model of the high-latitude ionosphere calculates density profiles for four ions (N_2^+ , O_2^+ , NO^+ , and O^+) and electrons over the altitude range from 85 to ~220 km. The densities are then used to calculate Pedersen and Hall conductivities. The model takes account of photoionization, impact ionization due to energetic electron precipitation, and ionization due to resonantly scattered solar radiation, starlight, and recombination radiation. The model outputs the ion and electron density profiles, altitude profiles for the Hall and Pedersen conductivities, and height-integrated conductivities.

39.2 Model Uncertainties and Limitations

The model is based on the assumption of chemical equilibrium and, therefore, is valid only at the altitudes where transport processes are negligible. The model results are also sensitive to certain inputs, including the auroral electron energy flux and characteristic energy, and the adopted ion and electron temperatures.

39.3 Basis of the Model

39.3.1 The model is based on a numerical solution of the coupled continuity equations for the ions NO^+ , O_2^+ , N_2^+ , and O^+ , assuming chemical equilibrium conditions prevail. The coupled nonlinear equations are solved with an iterative procedure at the specified altitudes and times.

39.3.2 The momentum equations are solved to obtain expressions for the Hall and Pedersen conductivities assuming steady-state conditions and neglecting spatial gradients. In calculating the appropriate collision frequencies, account is taken of ion collisions with the neutrals N_2 , O_2 , O , N , and NO .

39.3.3 The height-integrated conductivities are obtained by using a trapezoidal rule to integrate in height.

39.4 Model Input Parameters

The model requires the electron energy flux and characteristic energy of the auroral precipitation, the neutral densities and temperature, and the ion and electron temperatures. These inputs are described by empirical models if they are not specified.

39.5 Publication References

39.5.1 Rasmussen, C.E., R.W. Schunk, and V.B. Wickwar (1988), A photochemical equilibrium model for ionospheric conductivity, *J. Geophys. Res.* 93, 9831–9840.

39.6 Dates of Development

39.6.1 Date

1988 Developed this year, but no improvements since then.

39.7 Model Codes and Sources

The model is in the form of a Fortran code, and it can be obtained from the lead author of the referenced publication.

40 Empirical Model of Conductivities

40.1 Model Content

The global patterns of the integral energy flux and average energy of precipitating auroral electrons are used to determine height-integrated Hall and Pedersen conductivities as a function of corrected geomagnetic latitude (CGL) and magnetic local time (MLT) for a range of magnetospheric conditions parameterized by either K_p or by IMF B_z and V_{sw} (see “Auroral Electron and Ion Fluxes” section 41 of this report).

40.2 Model Uncertainties and Limitations

40.2.1 The individual statistical maps were constructed from anywhere between 0.2 and 3.8 million spectra (depending on the magnetospheric activity sort parameter), which were binned and averaged into a spatial grid (CGL \times MLT). By their very nature, statistical maps obscure the short-lived, small-scale-length precipitation features (Redus et al., 1988). Thus, these models are not expected to track the ionospheric conductivities (as determined by electron precipitation) throughout individual (sub)storms with high precision, but they do provide a reasonable measure of the gross variations in an average sense. Whether the B_z - V_{sw} maps resolve the short-lived, small-scale-length features more successfully than do the K_p maps has never been investigated, although they are expected to because the sort parameters are more directly tied to solar wind–magnetospheric coupling (hence electron precipitation), and the parameter space has a finer grid (30 B_z - V_{sw} maps vs. 7 K_p maps).

40.2.2 The steep gradient (with respect to CGL) in conductivity at the time-dependent equatorward and poleward auroral boundary introduces an intrinsic difficulty in predicting conductivities along a specified orbit trajectory in proximity to such boundaries (as is the case for auroral precipitation flux). An uncertainty of 2° – 4° in magnetic latitude in the boundary location can mean up to a factor of two differences in conductivity, depending on whether the trajectory is cutting through the oval or just skimming it.

40.3 Basis of the Model

40.3.1 This model is based on a compilation of statistical hemispherical maps of auroral electron precipitation derived from measurements made by Air Force particle detectors flown primarily on the DMSP (and, to a lesser extent, P78-1) satellites under a wide range of magnetospheric conditions.

40.3.2 These statistical maps were created from electron flux databases, which were separated according to the magnetic activity index K_p (Hardy et al., 1985) and according to the z component of the interplanetary magnetic field (B_z) and the solar wind speed (V_{sw}) (Brautigam et al., 1991). For the K_p models, the separation resulted in seven intervals of K_p : $K_p = 0, 0^+, K_p = 1^-, 1, 1^+$, etc., up to $K_p = 5^-, 5, 5^+$, and for $K_p \geq 6^-$. For the B_z - V_{sw} models, each map was defined by a discrete point in the parameter space defined by ordered pairs of $B_z = (-4.5, -2.2, -0.7, 0.7, 2.2, 4.5 \text{ nT})$ and $V_{sw} = (346, 408, 485, 572, \text{ and } 677 \text{ km/sec})$.

40.3.3 The various maps were all created using the same spatial grid defined by CGL and MLT. The high-latitude region was separated into 30 zones in CGL between 50° and 90° and 48 0.5-hr zones in MLT. The zones in latitude are 2° wide between 50° and 60° and between 80° and 90° ; they are 1° wide between 60° and 80° latitude. Although the nominal altitude of the DMSP satellites is 840 km, particle fluxes are mapped down the magnetic field lines to 110 km (base of the ionospheric E-layer) before constructing the statistical maps.

40.3.4 In each spatial element, and at each level of activity, the average flux value in each of the energy channels was determined. The resulting average spectra were extrapolated to 100 keV. The final spectra were integrated over energy (from 0.5 to 100 keV) to determine the average integral number flux and the average integral energy flux of the precipitating electrons in each spatial element. The average energy was calculated by dividing the integral energy flux by the integral number flux. The Hall and Pedersen conductivities were then determined from the average energy and energy flux.

40.3.5 Finally, the conductivities were fit to Epstein functions, with the function coefficients published as a representation of the statistical maps: (1) K_p models (Hardy et al., 1987); and (2) B_z - V_{sw} models (McNeil and Brautigam, 1998).

40.4 Model Input Parameters

There is a version of the conductivity models that is driven by the magnetic activity index K_p , and one that is driven by a pair of parameters: the z component of the interplanetary magnetic field (B_z) and solar wind speed (V_{sw}). One source for these parameters is the web site <http://nssdc.gsfc.nasa.gov/omniweb>.

40.5 Publication References

40.5.1 Brautigam, D.H., M.S. Gussenhoven, and D.A. Hardy (1991), A statistical study on the effects of IMF B_z and solar wind speed on auroral ion and electron precipitation, *J. Geophys. Res.* 96, 5525.

40.5.2 Hardy, D.A., M.S. Gussenhoven, R. Raistrick, and W.J. McNeil (1987), Statistical and functional representations of the pattern of auroral energy flux, number flux, and conductivity, *J. Geophys. Res.* 92, 12,275.

40.5.3 Hardy, D.A., M.S. Gussenhoven, and E. Holeman (1985), A statistical model of auroral electron precipitation, *J. Geophys. Res.* 90, 4229.

40.5.4 Redus, R.H., M.S. Gussenhoven, D.A. Hardy, and D.H. Brautigam (1988), Deviations from the average patterns of auroral ion precipitation, *Physics of Space Plasmas (1987)*, Vol. 7, edited by T. Chang, G.B. Crew, and J.R. Jasperse, Scientific Publishers, Inc.

40.6 Dates of Development, Authors, and Sponsors

40.6.1 Dates

1985–1991 Development of conductivity models.

40.6.2 Authors: D. H. Brautigam, M. S. Gussenhoven, D. A. Hardy, E. Holeman, W. J. McNeil, R. Raistrick, and R. H. Redus.

40.6.3 Sponsor: Air Force Research Laboratory/VSBS.

40.7 Model Codes and Sources

The model code for Hall and Pedersen conductivities is identical to that described in the “Auroral Electron and Ion Fluxes” model, section 41.

40.7.1 The simplest package of models is a set of Fortran subroutines for each species (electron; ion) and for each parameterized model (K_p ; B_z and V_{sw}), which contain the Epstein coefficients for the functional forms of the various computed quantities (integral number flux, integral energy flux, average energy, and conductivities). These subroutines return a specified average quantity for a given model parameter and magnetic coordinates (CGL, MLT). They are available on PC diskettes. Contact D. H. Brautigam, AFRL/VSBS, 29 Randolph Road, Hanscom AFB, MA 10731 (email: brautigam@plh.af.mil).

40.7.2 These subroutines (7.1) are embedded within AF-Geospace, where they may be run in conjunction with a number of other options via an interactively driven graphical interface. AF-Geospace currently runs on UNIX-based Silicon Graphics workstations, but is being ported to a Dec-Alpha workstation and will eventually run on Microsoft NT workstations. Contact G. P. Ginet, AFRL/VSBS, 29 Randolph Road, Hanscom AFB, MA 10731 (email: ginet@plh.af.mil).

41 Auroral Electron and Ion Fluxes

41.1 Model Content

Auroral particle (electron and ion) integral number flux, integral energy flux, and average energy are specified as a function of corrected geomagnetic latitude (CGL) and magnetic local time (MLT) for a range of magnetospheric conditions parameterized either by K_p or by IMF B_z and V_{sw} . From these statistical auroral flux maps, the number and energy flux precipitating over the entire auroral oval can be estimated for periods spanning weak to strong magnetic activity.

41.2 Model Uncertainties and Limitations

41.2.1 The individual statistical maps were constructed from anywhere between 0.2 and 3.8 million spectra (depending on the magnetospheric activity sort parameter), which were binned and averaged into a spatial grid (CGL \times MLT). By their very nature, statistical maps obscure the short-lived, small-scale-length features (Redus et al., 1988). Thus, these models are not expected to track the auroral particle precipitation throughout individual substorms with high precision, but they do provide a reasonable measure of the gross variations in the auroral oval in an average sense. Whether the B_z - V_{sw} maps resolve the short-lived, small-scale length features more successfully than do the K_p maps has never been investigated, although they are expected to because the sort parameters are more directly tied to solar wind–magnetospheric coupling, and the parameter space has a finer grid (30 B_z - V_{sw} maps vs. 7 K_p maps).

41.2.2 The steep gradient (with respect to CGL) in auroral precipitation flux at the time-dependent equatorward and poleward auroral boundary introduces an intrinsic difficulty in predicting fluxes along a specified orbit trajectory in proximity to such boundaries. Even though the hemispheric number and energy flux inputs may be well modeled, an uncertainty of 2° – 4° in magnetic latitude in the boundary location can mean up to an order of magnitude difference in local flux, depending on whether the trajectory is cutting through the oval or just skimming it.

41.3 Basis of the Model

41.3.1 This model is based on a compilation of statistical hemispherical maps of auroral ion and electron precipitation derived from measurements made by Air Force particle detectors flown primarily on the DMSP (and, to a lesser extent, P78-1) satellites under a wide range of magnetospheric conditions.

41.3.2 These statistical maps were created from particle flux databases, which were separated according to the magnetic activity index K_p for both electrons (Hardy et al., 1985) and ions (Hardy et al., 1989) and according to the z component of the interplanetary magnetic field (B_z) and the solar wind speed (V_{sw}) for both electrons and ions (Brautigam et al., 1991). For the K_p models, the separation resulted in seven intervals of K_p : $K_p = 0$, 0^+ , $K_p = 1^-$, 1 , 1^+ , etc., up to $K_p = 5^-$, 5 , 5^+ , and for $K_p \geq 6^-$. For the B_z - V_{sw} models, each map was defined by a discrete point in the parameter space defined by ordered pairs of $B_z = (-4.5, -2.2, -0.7, 0.7, 2.2, 4.5$ nT) and $V_{sw} = (346, 408, 485, 572, \text{ and } 677$ km/sec).

41.3.3 The various maps were all created using the same spatial grid defined by CGL and MLT. The high-latitude region was separated into 30 zones in CGL between 50° and 90° and 48 0.5-hr zones in MLT. The zones in latitude are 2° wide between 50° and 60° and between 80° and 90° ; they are 1° wide between 60° and 80° latitude. Although the nominal altitude of the DMSP satellites is 840 km, particle fluxes are mapped down the magnetic field lines to 110 km (base of the ionospheric E layer) before constructing the statistical maps.

41.3.4 In each spatial element and at each level of activity, the average flux value in each of the energy channels was determined. The resulting average spectra were extrapolated to 100 keV. The final spectra were integrated over energy to determine the average integral number flux and the average integral energy flux of the precipitating electrons and ions in each spatial element. The average energy was calculated by dividing the integral energy flux by the integral number flux.

41.3.5 Finally, these average quantities were fit to Epstein functions, with the tables of function coefficients published as a representation of the statistical maps. These quantities and the references

defining their representations are as follows: (1) K_p models (electrons): integral number and energy flux (Hardy et al., 1987); (2) K_p models (ions): average energy (McNeil and Brautigam, 1998), integral number, and energy flux (Hardy et al., 1987); and (3) B_z - V_{sw} models (electrons and ions): average energy, integral number, and energy flux (McNeil and Brautigam, 1998).

41.4 Model Input Parameters

There is a version of the auroral model that is driven by the magnetic activity index K_p , and one that is driven by a pair of parameters: the IMF B_z and solar wind speed V_{sw} . One source for these parameters is the web site <http://nssdc.gsfc.nasa.gov/omniweb>.

41.5 Publication References

41.5.1 Brautigam, D.H., M.S. Gussenhoven, and D.A. Hardy (1991), A statistical study on the Effects of IMF B_z and solar wind speed on auroral ion and electron precipitation, *J. Geophys. Res.* 96, 5525.

41.5.2 Hardy, D.A., W.J. McNeil, M. S. Gussenhoven, and D. Brautigam (1991), A statistical model of auroral ion precipitation: 2. Functional representation of the average patterns, *J. Geophys. Res.* 96, 5539.

41.5.3 Hardy, D.A., M.S. Gussenhoven, and D. Brautigam (1989), A statistical model of auroral ion precipitation, *J. Geophys. Res.* 94, 370.

41.5.4 Hardy, D.A., M.S. Gussenhoven, R. Raistrick, and W.J. McNeil (1987), Statistical and functional representations of the pattern of auroral energy flux, number flux, and conductivity, *J. Geophys. Res.* 92, 12,275.

41.5.5 Hardy, D.A., M.S. Gussenhoven, and E. Holeman (1985), A statistical model of auroral electron precipitation, *J. Geophys. Res.* 90, 4229.

41.5.6 Redus, R.H., M.S. Gussenhoven, D.A. Hardy, and D.H. Brautigam (1988), Deviations from the average patterns of auroral ion precipitation, *Physics of Space Plasmas* (1987), Vol. 7, edited by T. Chang, G.B. Crew, and J.R. Jasperse, Scientific Publishers, Inc.

41.6 Dates of Development, Authors, and Sponsors

41.6.1 Dates

1985–1998 Development of auroral models.

41.6.2 Authors: D. H. Brautigam, M. S. Gussenhoven, D. A. Hardy, E. Holeman, W. J. McNeil, R. Raistrick, and R. H. Redus.

41.6.3 Sponsor: Air Force Research Laboratory/VSBS.

41.7 Model Codes and Sources

41.7.1 The simplest package of models is a set of Fortran subroutines for each species (electron; ion) and for each parameterized model (K_p ; B_z and V_{sw}) that contains the Epstein coefficients for the functional forms of the various computed quantities (integral number flux, integral energy flux, average energy, and conductivities). These subroutines will return a specified average quantity for a given model parameter and magnetic coordinates (CGL, MLT). They are available on PC diskettes. Contact D. H. Brautigam, AFRL/VSBS, 29 Randolph Road, Hanscom AFB, MA 10731 (email: brautigam@plh.af.mil).

41.7.2 These subroutines (7.1) are embedded within AF-Geospace, where they may be run in conjunction with a number of other options via an interactively driven graphical interface. AF-Geospace currently runs on UNIX-based Silicon Graphics workstations but is being ported to a Dec-Alpha workstation and will eventually run on Microsoft NT workstations. Contact G. P. Ginet, AFRL/VSBS, 29 Randolph Road, Hanscom AFB, MA 10731 (email: ginet@plh.af.mil).

42 WBMOD Ionospheric Scintillation Model (NWRA), 1995

42.1 Model Content

North West Research Associates (NWRA) has developed an empirical model of the irregularities in F-layer plasma density, which produces radio-wave scintillation. Based mainly on direct measurement of intensity and phase scintillation, primarily from the Defense Nuclear Agency (DNA) Wide-Band Satellite Experiment, the scintillation model is incorporated in a computer program called WBMOD. Development of the model initially (Fremouw and Lansinger, 1981; Fremouw and Secan, 1984) was sponsored by DNA. Because of Wide-Band's sun-synchronous orbit and a limited number of observing sites, the early version of WBMOD did not fully reproduce the observed temporal and spatial variations of scintillation (Basu et al., 1988). Recently, the model was upgraded by ingesting high-latitude scintillation data from DNA's Hilat and Polar BEAR satellites and the time-continuous equatorial scintillation database of the Geophysics Directorate of Phillips Laboratory (PL/GD). These model upgrades (Secan and Bussey, 1994; Secan et al., 1995) have been executed by NWRA and were sponsored by PL/GD with the support of HQ Air Weather Service. In addition to scintillation observations, WBMOD incorporates a modified version of the phase-screen propagation theory of Rino (1979). For two-way propagation, the theory is augmented by the work of Fremouw and Ishimaru (1992). The irregularity model contains statistical descriptions of their anisotropy in geomagnetic coordinates and their spatial power spectrum, the latter characterized by means of an outer scale, a power-law spectral index, and the height-integrated power spectral density (psd), CkL, at a cross-field scale size of 1 km/cycle. The occurrence statistics of the most variable of these parameters, CkL, are modeled by means of a probability density function (pdf), the relevant moments of which are expressed as functions of geomagnetic latitude, longitude, local time of day, season, solar-cycle epoch, and planetary geomagnetic activity index. The irregularities are taken to drift with the background F-layer. For an operating scenario (location, time, operating frequency, etc.) specified by the user, WBMOD outputs signal-statistical parameters that quantify phase and intensity scintillation. The phase spectrum is characterized by its power-law spectral index p and its psd T at a fluctuation frequency of 1 Hz. The rms phase fluctuation σ_ϕ for a time interval specified by the user is computed as the square root of the integral of the spectrum. Intensity scintillation is quantified by the normalized (by the mean) standard deviation S_4 of power, which also is converted to a dB scintillation index.

42.2 Model Uncertainties and Limitations

42.2.1 The observations on which WBMOD is based were carried out at VHF, UHF, and L bands. The propagation theory that it incorporates is valid down to about 100 MHz (somewhat less at high elevation angles) and improves with increasing frequency.

42.2.2 The irregularities are characterized by a single-regime power-law spatial spectrum, although spectra with at least two power-law regimes are known to exist at both auroral and equatorial latitudes.

42.2.3 The high-latitude portion of the model has been well tested only at auroral latitudes, and deficiencies are likely in the polar cap. At auroral latitudes, testing has been without benefit of data from the Russian sector.

42.2.4 The model's description of the coupled seasonal and longitudinal dependence of equatorial scintillation may suffer from sparse data and incomplete understanding of the relevant geophysical drivers.

42.2.5 Versions 12, 13.00, and 13.01 output the SI index of Whitney et al. (1969) as an auxiliary (dB) intensity scintillation index. Since SI depends upon record length, the standard deviation of dB intensity is output instead of SI in version 13.02.

42.2.6 WBMOD is a climatological model. In view of the patchiness and day-to-day variability of scintillation, its outputs may differ considerably from measurements at a given place on a given day.

42.3 Basis of the Model

42.3.1 The model is based on multi-frequency scintillation measurements. The data were acquired at a variety of ground stations, which recorded scintillation of radio signals from low-orbiting and geostationary satellites.

42.3.2 The scintillation data were translated to turbulence strengths of the irregularities by means of the phase-screen theory for weak scattering from irregularities with a power-law spectrum (Rino, 1979). The turbulence strength of the irregularities is characterized by the height-integrated psd at a cross-field wave number corresponding to 1 km scale size. The irregularity spectrum is defined by an outer scale and a power-law spectral index. An empirical model of irregularity anisotropy and its variations is incorporated.

42.3.3 The global irregularity model is used to specify scintillation parameters. Transformation from spatial to temporal statistics is based on scan of the line of sight and appropriate models of ionospheric drift.

42.4 Database

42.4.1 The primary data employed are intensity and phase scintillation measurements at VHF, UHF, and L band (with an S-band phase reference) carried out at Poker Flat, AK; Stanford, CA; Ancon, Peru; and Kwajalein, Marshall Islands in the WideBand experiment.

42.4.2 More recently, data from the DNA HiLat and Polar BEAR Satellite experiments have been employed. Specifically, VHF and UHF phase (with an L-band reference) and intensity data recorded at Bellevue, WA; Tromso, Norway; Ft. Churchill, Manitoba; and Sondre Stromfjord, Greenland have been used.

42.4.3 The foregoing have been augmented with intensity measurements performed by PL/GD at L band on Ascension Island in the Atlantic and at VHF in Manila, Philippines, and Huancayo, Peru. Similar VHF data from Narssarsuaq, Greenland (Basu, 1975) have been applied to the question of seasonal variation at high latitudes.

42.5 Publication References

42.5.1 Basu, Sa., E. MacKenzie, and Su. Basu (1988), Ionospheric constraints on VHF/UHF communications links during solar maximum and minimum periods, *Radio Sci.* 23, 363.

42.5.2 Basu, Su. (1975), Universal-time/seasonal variations of auroral-zone magnetic activity and VHF scintillations, *J. Geophys. Res.* 80, 4725–4728.

42.5.3 Fremouw, E.J., and A. Ishimaru (1992), Intensity scintillation index and mean apparent radar cross section on monostatic and bistatic paths, *Radio Sci.* 27, 539–543.

42.5.4 Fremouw, E.J., and J.M. Lansinger (1981), *A computer model for high-latitude phase scintillation based on wideband satellite data from Poker Flat*, Defense Nuclear Agency, Washington, DC, Rept. DNA5686F.

42.5.5 Fremouw, E.J., and J.A. Secan (1984), Modeling and scientific application of scintillation results, *Radio Sci.* 19, 687–694.

42.5.6 Rino, C.L. (1979), A power-law phase-screen model for ionospheric scintillation: 1, weak scatter, *Radio Sci.* 14, 1135–1145.

42.5.7 Secan, J.A., and R.M. Bussey (1994), *An improved model of high-latitude F-region scintillation (WBMOD Version 13)*, Phillips Lab., Hanscom AFB, MA, Rept. PL-TR-94-2254.

42.5.8 Secan, J.A., R.M. Bussey, E.J. Fremouw, and Sa. Basu (1995), An improved model of equatorial scintillation, *Radio Sci.* 30, 607–617.

42.5.9 Whitney, H.E., J. Aarons, and C. Malik (1969), A proposed index for measuring ionospheric scintillations, *Planetary Space Sci.* 17, 1069–1073.

42.6 Dates of Development, Authors, and Sponsors

42.6.1 Dates

- 1981 Original high-latitude WMOD.
- 1984 Extension to equatorial latitudes.
- 1986 Extension to middle latitudes.
- 1994 Improvement at high latitudes.
- 1994 Improvement at middle latitudes.
- 1993, 1995 Improvements at equatorial latitudes.

42.6.2 Authors (principal): Edward J. Fremouw, NWRA President and Senior Research Scientist, and James A. Secan, NWRA Research Scientist.

42.6.3 Sponsors: Defense Nuclear Agency (now Defense Special Weapons Agency) of the U.S. Department of Defense, and Phillips Laboratory of the USAF Materiel Command.

42.7 Model Codes and Sources

The evolution of WBMOD traced herein refers to the “research” versions developed by NWRA under contracts from DNA and Phillips Laboratory. Users interested in obtaining a copy should address requests to J. A. Secan (email: jim@nwra.com) or E.J. Fremouw (email: ed@nwra.com) at NWRA, P.O. Box 3027, Bellevue, WA 98009, tel. 425/644-9660. NWRA has devised specialized versions for the USAF Air Weather Service. Parties interested in versions tailored for particular applications should visit <http://www.nwra.com>, or contact Mr. Secan or Dr. Fremouw.

43 PBMOD Time-Dependent Model of the Global Low-Latitude Ionosphere and Radio Scintillation

43.1 Model Content

The PBMOD ionospheric model from AFRL is a system of **Physics-Based MODEls** that describes the three-dimensional, time-dependent evolution of the low-latitude ionosphere on several different spatial scales: globally it provides the plasma density and composition at altitudes between 90 and 2000 km, and at finer scales it describes the development of fluid plasma turbulence within this region and the resulting radio scintillation. The numerical model of the ambient (global scale) ionosphere yields density distributions for electrons and several ion species (O^+ , H^+ , NO^+ , O_2^+ , N_2^+) as a function of latitude, longitude, and altitude on a pre-specified spatial grid at specified times. The system also includes models that evaluate the growth rate for the generalized Rayleigh-Taylor instability; perform evolutionary calculations of the self-consistent, nonlinear development of equatorial low-density plasma plumes/bubbles; and perform a phase-screen calculation to estimate the strength of amplitude and phase scintillation of radio signals passing through the turbulent structure.

Numerous physical and chemical processes are contained in the model, including field-aligned diffusion, cross-field electrodynamic drifts, thermospheric winds, ion production due to EUV radiation, and chemical and other collisional processes. The model uses the IGRF geomagnetic field model for an accurate depiction of the Earth's magnetic field geometry. Depending on the inputs, the global ionospheric model can describe different solar cycle, seasonal, and daily variations. It can describe the low-latitude effects of geomagnetic storm dynamics.

Built to be the forecast model in the C/NOFS (Communication and Navigation Outage Forecast System) Data Center, a demonstration of a potential operational system, the models employ robust numerical techniques, and are designed to be fault-tolerant of data dropouts and noise in the ingested data from the satellite and other sensors. One implementation of the model has been providing climatology-based forecasts of UHF and L-band scintillation every 6 hours since 2008 for the Space Environment Technologies CAPS web site (http://www.spacewx.com/CAPS_notice.html), with the only outages being those of the host computer. The models have been validated with *in situ* satellite data (CHAMP, DMSP, C/NOFS), ionosonde data, Jicamarca ISR data, JASON vertical TEC data, and SCINDA scintillation data.

43.2 Model Uncertainties and Limitations

43.2.1 To a large extent, the reliability of the calculated ionospheric parameters depends on the accuracy with which the global inputs have been specified. The ambient ionospheric model is particularly sensitive to the equatorial electric field (including both penetration and dynamo fields), but also depends on thermospheric winds, neutral densities, plasma temperatures, and plasma production rates.

43.2.2 The plasma plume model depends on the parameters in 2.1, and is additionally dependent on the choice of "seed" or initial perturbation for plume development.

43.2.3 The structuring of the plasma in the turbulent plumes does not feed back into the ambient model.

43.2.4 A Beowulf-class supercomputer (i.e., multiple processors) is needed for global simulations.

43.3 Basis of the Model

43.3.1 The ambient plasma density model calculates the O^+ and H^+ densities by solving the coupled ion momentum and continuity equations numerically using a Crank-Nicholson implicit finite differencing technique along closed geomagnetic field lines near the geomagnetic equator, in a code originally developed by D. N. Anderson in 1973 (LOWLAT). The flux tubes are allowed to convect through the neutral atmosphere in directions perpendicular to \mathbf{B} as a consequence of electric-field drift. The three-dimensional nature of the model is obtained by following many flux tubes of plasma while keeping track of their positions at all times. The model includes the effects of production by solar EUV radiation, loss through charge exchange with the neutral atmosphere and transport by $\mathbf{E} \times \mathbf{B}$ drift, ambipolar diffusion, and momentum exchange with the neutral atmosphere through collisions. The density of the molecular

ions NO^+ , O^+ , and O_2^+ are calculated under the chemical equilibrium assumption that production equals loss, without transport effects. Electric fields and plasma temperatures are specified *a priori* and are not calculated self-consistently.

43.3.2 The transport model for the mesoscale plumes requires the simultaneous solution of the nonlinear continuity and momentum equations with electric fields calculated self-consistently using the principle of current continuity. Transport processes parallel and perpendicular to the geomagnetic field are treated separately using an operator-splitting technique, with the LOWLAT algorithm from the ambient code for parallel transport, and a flux-corrected transport algorithm for the perpendicular motion. A Eulerian grid, typically of an altitude range of 1000 km and a similar East–West extent, defines the grid in the plane of the geomagnetic equator; transport along each field line is described down to altitudes of 90 km at the ends. From an initial, arbitrary density perturbation, the evolution of the F-region plasma is followed self-consistently, allowing low-density plasma plumes or bubbles to develop if the plasma is unstable to interchange instabilities. Numerous diagnostics, including snapshots of density and velocity, irregularity spectra, and airglow depletion images, are available.

43.3.3 The phase-screen calculation of the strength of radio scintillation relies on spectra of the total electron content integrated along the signal ray path through the turbulent ionosphere; extrapolation down to the Fresnel wavelength (sub-km) regime relevant for scintillation is necessary. The simple asymptotic behavior of amplitude scintillation when irregularities are strong permits extrapolation of the phase screen, resulting in a more general description.

43.4 Model Input Parameters

The ionospheric model requires several inputs. The main global inputs are the neutral densities, temperatures, and winds; the magnetospheric and equatorial electric field distributions and histories; the plasma temperatures; the plasma production rate; and the seed perturbation for the plume calculation. Typically, empirical or statistical models are used for these inputs. For storm simulations, the temporal variation of the magnetospheric and atmospheric inputs must be specified. Simple scaling with the interplanetary electric field (as provided by the solar-wind parameters measured by the sensors on the ACE satellite or forecast by a solar-wind model) can provide a rough estimate of the penetration field and thermospheric energy input in storm events. Alternatively, the model can be driven by parameters obtained from a run of TIE-GCM, the NCAR general circulation model, or another thermospheric model. Additionally, since PBMOD was designed as the ionospheric forecast model for the C/NOFS program, *in situ* or other measurements can also be used to specify or constrain the variation of the driving parameters of the model.

43.5 Publication References

43.5.1 Retterer, J.M., D.T. Decker, W.S. Borer, R.E. Daniell, and B.G. Fejer (2005), Assimilative modeling of the equatorial ionosphere for scintillation forecasting: modeling with vertical drifts, *J. Geophys. Res.* 110, A11307.

43.5.2 Retterer, J.M. (2005), Physics-based forecasts of equatorial radio scintillation for C/NOFS, *Space Weather J.* 3, S12C03.

43.5.3 Retterer, J.M. (2010), Forecasting low-latitude radio scintillation with 3-D ionospheric plume models: I. Plume model, *J. Geophys. Res.*, doi:10.1029/2008JA013839.

43.5.4 Retterer, J.M. (2010), Forecasting low-latitude radio scintillation with 3-D ionospheric plume models: II. Scintillation calculation, *J. Geophys. Res.*, doi:10.1029/2008JA013840.

43.5.5 Retterer, J.M., and M.C. Kelley (2010), Solar wind drivers for low-latitude ionosphere models during geomagnetic storms, *J. Atmos. Solar-Terr. Phys.*, doi:10.1016/j.jastp.2009.07.003.

43.6 Dates of Development, Authors, and Sponsors:

43.6.1 Dates

- 1997 D. N. Anderson LOWLAT code (1973) adapted for low-latitude ionosphere.
- 1998 Two-dimensional plasma bubble code written.
- 2001 PBMOD system concept organized.
- 2002 IGRF geomagnetic field model incorporated.
- 2004 Three-dimensional plasma bubble code developed.
- 2008 Coupling to TIE-GCM.
- 2010 Coupling to solar-wind models

43.6.2 Author: John M. Retterer (john.retterer@hanscom.af.mil or john.retterer@gmail.com).

43.6.3 Sponsors: Air Force Research Laboratory, Air Force Office of Scientific Research, National Aeronautics and Space Administration.

43.7 Model Codes and Sources

The model system is in the form of a set of Fortran codes, with libraries of Fortran, C, yacc, and lex helper routines, and a SQL database of geophysical parameters, all controlled by a set of UNIX shell scripts. It might not be user-friendly, and it is certainly not well documented, but it is logically organized, with an object-oriented Fortran style. Although the author may be able to accommodate runs on request for collaborative studies, the model is in the process of being deployed at CCMC, where users will be able to carry out runs on their own.

44 FIRST: Forecasting Ionospheric Real-Time Scintillation Tool (NOAA, CIRES)

44.1 Model Content

A real-time, VHF scintillation forecasting technique has been developed for low latitudes, at longitudes that have real-time F-layer height information available. The Forecasting Ionospheric Real-time Scintillation Tool (FIRST) automatically acquires h'F values near dusk (nominally 18:30–19:30 LT) in real time from ground-based ionosonde sounders and computes a forecast for the evening. Forecasts are made publicly available to portable devices and web browsers.

44.2 Model Uncertainties and Limitations

The model is designed to produce VHF scintillation likelihood forecasts on a day-to-day basis and was tested specifically for the Jicamarca, Peru and Kwajalein Atoll, Marshall Islands regions.

44.3 Basis of Model

The pre-reversal enhancement (PRE) of the vertical $\mathbf{E} \times \mathbf{B}$ drift is the dominant sunset process driving the height of the F-layer upward. In the Peruvian longitude sector, there is an excellent correlation ($R^2 \sim 0.91$) between the maximum PRE as determined by the height-rise-with-time of the 4 MHz (2×10^5 el/cm³) contour (observed by the Jicamarca ionosonde) and the ionosonde-observed h'F value at 19:30 LT. There exists a “threshold” value in h'F (19:30 LT), above which the nightly computed VHF scintillation activity index, THMS4, is greater than 1 and below which, THMS4 is less than 1. In addition, this h'F threshold value, $h'F_{thr}$, decreases with decreasing $F_{10.7}$ cm flux. The linear relationship between $h'F_{thr}$ and $F_{10.7}$ cm flux is given by:

$$h'F_{thr} (1930 \text{ LT}) = 1.08 \times F_{10.7} \text{ cm flux} + 200.3$$

Based on this relationship, a real-time forecasting technique has been developed for the Peruvian and Kwajalein Atoll longitude sectors.

The FIRST system automatically acquires h'F values between 18:30 and 19:30 LT in real time from the ground-based sounders at Jicamarca and the Kwajalein Atoll and computes a forecast for the evening. The forecast is coded as “Green,” “Yellow,” “Red,” or “Blue/Unknown” using the following rubric:

Status	h'F condition
Green	$h'F \leq (h'F_{thr} - 10)$
Yellow	$(h'F_{thr} - 10) < h'F < (h'F_{thr} + 10)$
Red	$h'F \geq (h'F_{thr} + 10)$
Blue	Unknown. A forecast couldn't be computed.

44.4 Database

44.4.1 Model input parameters

The FIRST system requires the F-layer height near dusk and $F_{10.7}$ cm radio flux.

44.4.2 Model output

The FIRST model forecasts the occurrence or non-occurrence of low-latitude scintillation activity in VHF/UHF bands. As outputs, the model provides scintillation likelihood (green, yellow, red) in a simple ASCII format.

44.5 Publication References

44.5.1 Anderson, D.N. (1973). A theoretical study of the ionospheric F-region equatorial anomaly, 2. Results in the American and Asian sectors, *Planet. Space Sci.* 21, 421–442.

44.5.2 Anderson, D.N., B. Reinisch, C. Valladares, C. Chau, and O. Veliz (2004), Forecasting the occurrence of ionospheric scintillation activity in the equatorial ionosphere on a day-to-day basis, *J. Atmos. Sol.-Terr. Phys.* 66(17), 1567–1572, doi: 10.1016/j.jastp.2004.07.010.

44.5.3 Redmon, R., D. Anderson, R. Caton, and T.W. Bullett (2010), A forecasting ionospheric real-time scintillation tool (FIRST), space weather, doi:10.1029/2010SW000582.

44.6 Dates of Development, Authors, and Sponsors

44.6.1 Dates: 2008–2010.

44.6.2 Authors: Rob Redmon, Dave Anderson, Ron Caton, Terry Bullett.

44.6.3 Sponsors: National Oceanic Atmospheric Administration, Cooperative Institute for Research in Environmental Sciences, Air Force Research Lab.

44.7 Model Codes and Sources

The model and its documentation are open source, and example implementations are available.

DRAFT--For Public Review Only--Dec 2013

45 Model of the Trough in the High-Latitude F-Layer

45.1 Model Content

MLAT/MLT boundaries occur in the high-latitude ionosphere that separates regions where there are macroscopic changes in F-layer electron density. These boundaries, which are often stable for many hours UT, are formed by the convection pattern and the auroral oval.

45.2 Model Uncertainties and Limitations

The model describes only f_oF_2 , so that h_mF_2 and the shape of the altitude profile must come from the parameterized USU model or from some empirical model. In addition, the model is uncertain about the merging of the afternoon trough with the mid-latitude ionosphere in the hours before midnight. A further uncertainty is the daytime trough in the morning sector from ~0600 to 1100 MLT, which is variable and poorly defined.

45.3 Basis of Model

45.3.1 This is an empirical model derived from data from a dense network of ionospheric sounders during winter at solar maximum.

45.3.2 The first part is a daytime trough in the afternoon sector. The equatorward boundary of this trough separates the high-density daytime F-layer from the depleted and disturbed F-region plasma. This is nighttime plasma that is transported sunward by the convection pattern. This trough is well defined and very persistent, extending as a spiral from about 1300 MLT until nearly midnight. The equatorward edge is the boundary of the convection pattern. At this edge, f_oF_2 decreases exponentially with increasing MLAT over a nominal range of 3° to a nominal minimum value 2.5 times smaller than at the edge. However, f_oF_2 remains constant over a range of 2° MLAT, where it is terminated by the auroral F-layer.

45.3.3 The second part is a post-midnight trough extending from midnight to dawn at nearly constant MLAT. This trough is defined by its minimum, which is the juncture between the normal nighttime mid-latitude F-layer that decreases with latitude and the auroral F-layer that increases with latitude to form the poleward trough wall. As defined from its minimum, the trough increases in f_oF_2 with increasing latitude as $\exp(L/3.7^\circ)$. It increases equatorward from the minimum with decreasing latitude as $\exp(L/16^\circ)$ with the mid-latitude F-layer. The location and value of the minimum are determined by the intersection of these two regions, which vary independently. If not measurable directly, they are given by the boundary of the auroral oval and of the mid-latitude F-layer, the latter given by the URSI coefficients.

45.4 Model Input Parameters

45.4.1 If not measurable directly, the equatorward edge of the afternoon trough is taken from the Heppner-Maynard model, and f_oF_2 at the equatorward edge, from the URSI coefficients.

45.4.2 If not measurable directly, the post-midnight trough minimum is given by the boundary of the auroral oval and of the mid-latitude F-layer by the URSI coefficients.

45.5 Publication References

45.5.1 Sojka, J.J., R.W. Schunk, and J.A. Whalen (1990), The longitude dependence of the dayside F-region trough: a detailed model-observation comparison, *J. Geophys. Res.* 95, 15,275.

45.5.2 Whalen, J.A. (1987), The daytime F layer trough observed on a macroscopic scale, *J. Geophys. Res.* 92, 2571.

45.5.3 Whalen, J.A. (1989), The daytime F layer trough and its relation to ionospheric-magnetospheric convection, *J. Geophys. Res.* 94, 17,169.

45.6 Dates of Development, Authors, and Sponsors

45.6.1 Dates: 1985–1990.

45.6.2 Author: J.A. Whalen.

45.6.3 Sponsor: Air Force Geophysics Laboratory.

45.7 Model Codes and Sources

This daytime trough is incorporated into the High Latitude Ionospheric Specification Model.

DRAFT--For Public Review Only--Dec 2013

46 GPS Eight-Coefficient TEC Model

46.1 Model Content

The GPS (or Klobuchar) TEC model was originally developed in the late 1970s to provide an estimate of the ionospheric range delay for single-frequency users of the Global Positioning System (GPS). Because of very severe restrictions on the amount of data that could be transmitted as part of the GPS navigation message, the model attempts to represent the global ionosphere using only eight coefficients. These coefficients were derived from the Bent model and are functions of time of year and solar activity (represented by $F_{10.7}$). Despite the model's computational simplicity, it performs remarkably well, with a root mean square (RMS) error of about 50%.

For a specified location, line of sight, time of day, day of the year, and solar activity level ($F_{10.7}$), the model provides the ionospheric slant TEC (in terms of the group delay at 1.57542 GHz).

46.2 Model Uncertainties and Limitations

The most obvious limitation of the model is its reliance on only eight coefficients to represent the global ionosphere. It makes no attempt to model the equatorial anomaly or the highly dynamic high-latitude ionosphere.

46.3 Basis of the Model

The GPS Eight-Coefficient Model was obtained by performing least-squares fits to vertical TEC computed from the Bent model. Since the Bent model's own coefficients are provided at 10-day intervals throughout the year, the GPS model was organized in the same way. The diurnal variation is described as a half-cosine (actually calculated by its truncated Taylor series) for the daytime TEC and a constant value for the nighttime TEC. The amplitude and period of the half-cosine are each described by a cubic equation in geomagnetic latitude (accounting for the eight coefficients broadcast in the GPS navigation message).

The conversion from vertical TEC to slant TEC is accomplished by multiplication by an obliquity factor that assumes a constant ionospheric height of 350 km. Conversion from the geodetic coordinates of the ionospheric intersection point to the geomagnetic coordinates required by the model is accomplished using approximate formulae.

46.4 Model Input Parameters

As implemented in a typical single-frequency GPS receiver, the inputs are the universal time (UT), the user's approximate location in geodetic coordinates, the azimuth and elevation of the line of sight, and the eight coefficients broadcast in the GPS navigation message. When used as a standalone model, it also requires the day of the year and solar activity level ($F_{10.7}$). The standalone model can provide vertical TEC and slant TEC, as well as vertical and slant group delay.

46.5 Publication References

46.5.1 Klobuchar, J.A. (1986), Design and characteristics of the GPS ionospheric time delay algorithm for single frequency users, *Proceedings of PLANS '86*, Las Vegas, NV, pp. 280–286.

46.5.2 Klobuchar, J.A. (1987), Ionospheric time-delay algorithm for single frequency GPS users, *IEEE Transactions on Aerospace and Electronic Systems* AES-23(3), 325–331.

46.5.3 Spilker, J.J. (1996), GPS navigation data, *Global Positioning System: Theory and Applications*, Vol. I, edited by B.W. Parkinson and J.J. Spilker, AIAA, Reston, VA, pp. 121–176.

46.6 Dates of Development, Authors, and Sponsors

46.6.1 Date: Late 1970s.

46.6.2 Author: John R. Klobuchar.

46.6.3 Sponsor: Air Force Geophysics Laboratory (AFGL), which is now a part of the Air Force Research Laboratory (AFRL).

46.7 Model Codes and Sources

Although the mathematical formulae of the model have been published in the references cited above, the tables of the eight coefficients for each 10-day period and each level of solar activity are not publicly available. A master set is maintained at AFRL and at the GPS Control Segment, which broadcasts the appropriate coefficients as part of the GPS navigation message.

DRAFT--For Public Review Only--Dec 2013

47 The CPI TEC Model

47.1 Model Content

The CPI TEC model for single-frequency GPS users was developed to replace the GPS Eight-Coefficient Model (Klobuchar Model). The CPI model is actually a three-dimensional model of the ionosphere similar to PIM but with additional environmental parameters, specifically a set of longitude-dependent parameters describing the equatorial vertical drift and thermospheric winds that control much of the day-to-day variability of the ionosphere.

The model takes advantage of the enormous computing power available in even handheld devices now available. The model provides slant TEC (in terms of the group delay at 1.57542 GHz) along the lines of sight to GPS satellites.

47.2 Model Uncertainties and Limitations

Although capturing more of the spatial structure of the ionosphere than the GPS Eight-Coefficient Model, the accuracy of the model is dependent on timely measurements of the equatorial vertical drift (for low latitudes) and/or the thermospheric winds (for mid latitudes). The model does not attempt to capture the dynamic state of the high-latitude ionosphere.

47.3 Basis of the Model

Like its cousin PIM, the CPI GPS model is a parameterization of diurnally reproducible runs of the AFRL Global Theoretical Ionospheric Model (GTIM). Unlike PIM, however, the geophysical parameters include not only solar activity, but also the equatorial vertical drift (which drives the formation of the equatorial anomaly) and the thermospheric winds (which control much of the variability of the mid-latitude ionosphere).

The output of GTIM is represented by an expansion in terms of Empirical Orthonormal Functions (EOFs) derived from a representative subset of the complete set of GIM runs. The coefficients of this orthonormal expansion are themselves represented by simple functions of solar activity, equatorial drift, and thermospheric winds.

The conversion from vertical TEC to slant TEC is accomplished by integrating model electron density along the line of sight rather than applying an obliquity factor to the vertical TEC. Although the obliquity factor works well at mid latitudes, it can be very inaccurate in the equatorial anomaly or anywhere there are large spatial gradients.

47.4 Model Input Parameters

The model requires the date and time (UT) and the location of the observer, the solar activity level, and the equatorial drift and thermospheric wind parameters for the longitude of the user. If drift and wind parameter values are not available, the model uses climatological estimates.

47.5 Publication References

47.5.1 Daniell, R.E., L.D. Brown, and R.W. Simon (1996), A new, improved ionospheric correction algorithm for single frequency GPS receivers, *Proceedings of ION GPS-96*, Institute of Navigation, Alexandria, VA, pp. 635–640.

47.5.2 Daniell, R.E., L.D. Brown, and R.W. Simon (1997), Performance comparisons between the current and a new prototype single frequency ionospheric correction algorithm, *Proceedings of the 53rd Annual Meeting*, Institute of Navigation, Alexandria, VA, pp. 101–106.

47.6 Dates of Development, Authors, and Sponsors

47.6.1 Dates: 1996–1998.

47.6.2 Authors: R. E. Daniell, L. D. Brown, and R. W. Simon.

47.6.3 Sponsors: Computational Physics, Inc. (CPI) under a Small Business Innovation Research (SBIR) contract with the Air Force Research Laboratory.

47.7 Model Codes and Sources

Under the terms of the SBIR program, the model is a proprietary product of CPI, although the government retains certain rights to license the software. Others may contact CPI to obtain licensing information: Robert E. Daniell Jr., Computational Physics, Inc., Suite 202A, 240 Bear Hill Road, Waltham, MA 02154-1026, tel. 781-487-2250, FAX 781-487-2290 (email: daniell@cpiboston.com).

DRAFT--For Public Review Only--Dec 2013

DRAFT--For Public Review Only--Dec 2013